CHARACTERIZATION OF THE NEURAL CODEBOOK IN AN INVERTEBRATE SENSORY SYSTEM

by

Zane Nathan Aldworth

A dissertation submitted in partial fulfillment
of the requirements for the degree

of

Doctor of Philosophy

in

Neuroscience

MONTANA STATE UNIVERSITY
Bozeman, Montana

August 2007

APPROVAL

of a dissertation submitted by

Zane Nathan Aldworth

This dissertation has been read by each member of the dissertation committee and has been found to be satisfactory regarding content, English usage, format, citations, bibliographic style, and consistency, and is ready for submission to the Division of Graduate Education.

Dr. John P. Miller

Approved for the Department of Cell Biology and Neuroscience

Dr. Thomas E. Hughes

Approved for the Division of Graduate Education

Dr. Carl A. Fox

STATEMENT OF PERMISSION TO USE

In presenting this dissertation in partial fulfillment of the requirements for a doctoral degree at Montana State University, I agree that the Library shall make it available to borrowers under rules of the Library. I further agree that copying of this dissertation is allowable only for scholarly purposes, consistent with “fair use” as prescribed in the U.S. Copyright Law. Requests for extensive copying or reproduction of this dissertation should be referred to ProQuest Information and Learning, 300 North Zeeb Road, Ann Arbor, Michigan 48106, to whom I have granted “the exclusive right to reproduce and distribute my abstract in any format in whole or in part.”

Zane Nathan Aldworth

August 2007

This thesis is dedicated:

to my wife, Clara Bodelón,
for persevering with me on this rather long journey
and providing love and support all along the way;

to my parents, Jeff Aldworth and Marilou Turrentine
for instilling in me a love of knowledge
and sense of wonder for the natural world;

to my Grandfather William Aldworth
who concluded his adventure in this world
with encouragement to me to *finish my thesis already*!

I hope you are all as proud of this work
as much as I am grateful for your help in accomplishing it.

ACKNOWLEDGEMENTS

I am indebted to a great number of people, and I do not have the space here to thank all to the extent that they deserve, so I will be brief.

First and foremost, I would like to thank my advisor John Miller. I am and remain grateful for the opportunity to work with him, and for the mentoring, both professional and personal, which he has provided in the ensuing years.

I have benefited enormously from the work Gwen Jacobs has put into neuroscience at MSU, as the original chair of the Department, as co-director of the CCB, and, most importantly, as co-PI of the NSF-IGERT grant in CBS.

My co-advisor Tomas Gedeon has acquainted me with the finer points of math, and has provided useful insight from outside the bubble. Thanks to Alex Dimitrov- most of the work in this thesis is traceable to his ideas. Thanks also to Graham Cummins, who asks difficult questions and helps find the answers.

My work would not have been possible without the financial support I received from NSF-IGERT program, and the Phil Kopriva and Gary Lynch foundations.

Additionally, I am grateful to the members of the CCB. I'm especially grateful for the many adventures spent with Shih-Cheng Yen, Siew-Peen Chong, Rodrigo and Erica Salazar, Troy and Jessica McKeehan, Michael and Kate Patterson, John Bender, Erich Staudacher, Jonathan and Aditi Baker, and Travis Ganje.

Finally and most importantly, thank you to my family and my beautiful wife Clara, to whom this dissertation is dedicated. Words are not enough to express my gratitude.

TABLE OF CONTENTS

PROLOGUE: THE VIRTUES OF SIMPLICITY 1
ORGANIZATION OF THE THESIS 3

1. THE CERCAL SYSTEM 6

Evolutionary History 6
Anatomy and Physiology of the System 10
The Cercus 10
Afferent Projections to the Terminal Abdominal Ganglion 12
Connectivity within the TAG 14
The Thoracic Ganglia 19
Projections in the Brain 24
Descending Input 26
Role of the Cercal System in Escape Behavior 27
Predation and Parasitism 27
Predation Signals in the Environment 28
Initiation of Escape 29
Escape Elicited by Auditory Behavior 31
Other Cercally-Mediated Behaviors 32
Initation of Defense and Touch-Elicited Escape 32
Flight 34
The Problem of Self-Motion 34
The Cercal System and Stridulation 35
Cricket Song 35
Effect of Air Particle Displacement on Male Singing 36
Cercal Reception of Song 37
Importance of the 30 Hz Component in Phonotaxis 38
Analogy to Signaling in *Phaeophilacris spectrum* 39
Cautionary Note 40
Discussion of Cercal System Form and Function 40

2. REVIEW OF APPROACHES TO THE NEURAL CODING PROBLEM 43

Tuning Curves 43
White Noise, Kernels, Stimulus Reconstruction, and Information Rates 48
Quantization Methods 63

3. NEURAL PRECISION AND 'DEJITTERING' 69

Abstract 69
Introduction 70

TABLE OF CONTENTS – CONTINUED

Materials and Methods 72
Preparation 72
Electrophysiology 73
Calculation of 'Dejittered' Mean Stimulus Waveform 73
Calculation of Shift Time from a Distance Measure 76
Convergence Criteria 78
Calculation of Information Rates 78
Results 79
Illustration of the Problem Using a Thought Experiment, Formulated as a Simulation 79
Time Scale of the Stimulus-to-Spike Latency Jitter in a Sensory Interneuron 82
Dejittering a Sample of Spike-Conditioned Stimulus Waveforms 85
Functional Significance of the Dejittered Mean Waveforms 89
Sensitivity of the Technique to the Value of σ_{t0} Used for the Calculations 93
Inter-Animal Variability of the Dejittered Mean Stimuli and σ_t for this Type of Interneuron 94
Calculation of the Information Rate for IN10-3 Using a Direct Method 99
Discussion 100
Refinement of Conventional Techniques 100
Implications for the Assessment of Temporal Precision 102
Factors Contributing to Stimulus-to-Spike Timing Jitter 103
Other Related Measures of Spike Jitter 104
Implications for Kernel-Based Analyses of Information Encoding Rates 105
Reappraisal of Encoding by This Four-Cell Group of Cricket Cercal Interneurons 106

4. TEMPORAL CODING 108

Abstract 108
Introduction 108
Materials and Methods 109
Preparation 109
Stimulation 110
Electrophysiology 111
Histology 112
Identification of Doublet Events 112
Response-Conditioned Stimulus Models 113
Likelihood Test 114

TABLE OF CONTENTS – CONTINUED

iSTAC Analysis 115
Results 116
Simulation of Distinct Stimulus-Conditioned Spike Interactions 116
Measurement of Pattern Variability 120
Modeling of Pattern-Conditioned Stimuli 122
Consistency of Measure Across Population of Animals 123
Quantification of Difference in Synthetic and Data-Based Models 126
Discussion 129
Temporal Coding Hypotheses 129
Burst vs Tonic Spiking 130

5. ITERATIVE REFINEMENT 132

Abstract 132
Introduction 132
Materials and Methods 135
Preparation 135
Electrophysiology 135
Stimulation 136
Response-Conditioned Stimulus Models 137
Refinement of Stimuli 138
Discrimination Test 140
Results 142
Probability of Eliciting Responses 142
Distinction in Selectivity of Responses to Imbedded Stimuli 144
Temporal Precision of Models 145
Changes in Models Over Iterations 146
Refinement Improves Discriminability of Stimuli 148
Changes to Global Structure of Stimuli 149
Discussion 150
Refinement of Models 150

BIBLIOGRAPHY 152

LIST OF TABLES

Table Page

1.1 Position of projecting air movement-sensitive interneurons in the TAG across othopteran species 16

1.2 Position of air movement-sensitive nGIs in the TAG of three species of crickets 17

2.1 Comparison of linear and direct estimates of information rates in various sensory systems 61

LIST OF FIGURES

Figure Page

1.1 Phylogenetic relationship of cricket and other insect species with cerci 7

1.2 Ten cercal systems and the insects that possess them 8

1.3 Scanning electron micrographs of cricket cerci 11

1.4 Distribution of directional sensitivities of filiform hairs 12

1.5 Projection of afferent axons to terminal ganglion 13

1.6 Morphology of air movement-sensitive interneurons in the terminal ganglion 16

1.7 Projections of the GIs in the thoracic ganglia of crickets and related orthopterans 21

1.8 Air particle displacement-sensitive neurons originating in the thoracic ganglia of crickets and cockroaches 22

1.9 Projection of the GIs in the brain of crickets and related orthopterans 25

1.10 Morphology of local brain neurons in the cricket 25

1.11 Structure of the calling song of *Acheta domesticus* 37

2.1 Directional tuning curve for interneuron 10-2a 44

2.2 Directional tuning curves for vGIs and dGIs 47

2.3 Stimulus reconstruction and coherence measures 53

2.4 Failures of the linear reconstruction approach 59

2.5 Example of quantization analysis in the case of two stimulus-response classes 65

3.1 A thought experiment to define the jitter problem, using simulated recordings 80

LIST OF FIGURES – CONTINUED

Figure Page

3.2 An experiment to illustrate the jitter problem, using a mechanosensory interneuron 84

3.3 Illustration of the dejittering algorithm 86

3.4 Characteristics of a dejittered mean stimulus 88

3.5 Dependence of the dejittered mean shape and σ_{tf} on σ_{t0} 94

3.6 Composite average stimulus waveforms for a sample of seven cells from class 10-3a 96

3.7 Composite average stimulus waveforms for a sample of seven cells from class 10-2a 97

3.8 Comparison of the composite average dejittered mean stimulus waveforms for seven examples of each of the cell classes 10-3a and 10-2a 98

4.1 Three models of spike-spike interaction in a doublet pattern 119

4.2 Spike-spike interactions in doublet patterns recorded in cricket interneurons 121

4.3 Building and testing of models of stimuli associated with doublet spiking patterns 124

4.4 T-test for log-likelihood distributions 125

4.5 iSTAC analysis of difference between data-based and synthetic models of stimuli associated with doublet spiking patterns 128

5.1 Schematic of iterative enrichment for a Gaussian white noise stimulus.....140

5.2 Probabilities of eliciting responses 143

5.3 Temporal jitter of elicited responses 146

5.4 Change to eigenspectra of models 147

LIST OF FIGURES – CONTINUED

Figure Page

5.5 Discrimination ability of models 148

5.6 Changes to global statistics of stimuli 150

ABSTRACT

An outstanding problem in neuroscience is to describe the relationship between various stimulus sources in the environment and how they are represented by patterns of activity in nervous systems, a problem generically referred to as 'neural coding'. Most previous methods developed to address this problem have assumed a linear relationship between environmental stimuli and neural responses, and generally relied on measures of the mean state of the environment preceding neural activity to characterize the stimulus-response transformation. The goal of this thesis is to develop new methods of characterization that extend earlier work, and to demonstrate the utility of these new methods through application to an invertebrate sensory system.

All applications of the methods developed in this thesis were carried out in the cercal system of crickets. The cercal system mediates the detection and analysis of low velocity air currents, and is implemented around an internal representation of air current direction that demonstrates the essential features of a continuous neural map. The stimulus feature selectivity, timing precision and coding characteristics of two bilateral pairs of primary sensory interneurons of the cercal system were characterized using three novel techniques. First, estimates of the cells' feature selectivity that take the natural variance in stimulus-response latency (i.e., spike 'jitter') into account were derived. Second, the cells' stimulus-response relationship was probed for specific non-linear aspects that could constitute 'temporal' encoding. Third, an iterative stimulation paradigm was used to test and refine the predictions of the cercal system's stimulus selectivity.

Compared to earlier characterization of this system, these new analytical procedures yield significantly different estimates of the stimulus feature selectivity of these cells. A 'code book' for the stimulus-response characteristics of these cells is presented, with emphasis on demonstrating instances where a cell represents different stimuli with distinct spike 'code-word' patterns.

PROLOGUE: THE VIRTUES OF SIMPLICITY

¿Será demasiado ambicioso esperar que, por lo menos con relación a ciertos centros sensoriales o a determinados mecanismos de reacción nerviosa, los invertebrados, y sobre todo los insectos, ofrezcan algún criterio interpretativo del sistema nervioso complicadísimo de los vertebrados superiores?

Santiago Ramón y Cajal

The ability of the nervous systems of animals to translate information about the environment into patterns of electrical activity, and to further translate those patterns into behavioral action is one of the great triumphs of evolution. Study of the precise mechanisms involved in these transformations falls under the general term 'neural coding', the study of which currently consumes the efforts of several thousand research teams worldwide. Arguably the most vibrant subfield of this area of research is the study of coding in mammalian vision: how photons impinging on the surface of the retina give rise to humankind's most dominant form of perception. While the potential benefits of progress are easily realized by both scientists and non-scientists alike, researchers in the field face a monumental challenge: the issue of complexity. ~A billion neurons in visual cortex each making synaptic contact with potentially thousands of other cells, all occurring several brain areas away from behavioral access via perceptual reporting can bury the traditional neurophysiologist and his trusty electrode under the crushing weight of combinatorics. It is important to emphasize that great progress has been made in our understanding of coding in the vertebrate visual

system through the use of single-cell recording techniques, and our knowledge will undoubtedly continue to be greatly augmented by the current trends towards tetrodes, massive electrode arrays, and fMRI studies. However, an alternate route of discovery remains open to those who crave simplicity: the study of neural coding in invertebrate sensory systems.

In addition to the orders-of-magnitude reduction in the number of neurons per sensory system, investigations in invertebrates offer several other advantages over queries in their chordate counterparts. Neurons in invertebrates are frequently re-identifiable not only within a population of conspecifics, but also across closely related species, allowing researchers to probe variability in structure-function relationships in a manner that simply isn't available in vertebrates. Similarly, the genomic sequencing of model organisms such as *Drosophila melanogaster* and *C. elegans*, the ease with which animals can be 'trained' to report perception, and the abundance of relatively large neuronal processes providing accessibility to techniques such as laser ablation and voltage clamping *in vivo* allows for studies which can elegantly relate biophysical minutia with behavior.

It is with this mindfulness of the virtues of simplicity that the author has sharpened his intracellular electrode and set to discovering what he could of neural coding in a humble insect sensory system.

ORGANIZATION OF THE THESIS

The body of this thesis is divided into six chapters, with two chapters devoted to broadly introducing the experimental system as well as previous methods used in the study of neural coding, three chapters detailing new methods for studying neural coding, and a final chapter concluding the thesis.

In chapter one I describe the air particle displacement-sensitive cercal sensory system of the cricket *Acheta domesticus* (formerly *Gryllus domesticus*) and other closely related orthopteran insects, detailing the anatomy of the system and its known role in behavior. I do this with the intent that later neurophysiological results pertaining to solution of the neural coding problem can be interpreted in the greater context of the animal's natural environment, as well as what behaviors are ethologically relevant within that environment.

In the second chapter I briefly discuss select approaches to the problem of neural coding, highlighting when these methods have been applied to the cercal system and what knowledge of the system's function was gleaned from these experiments. Collectively these methods have formed a template for extracting information on neural coding from diverse animal models, and it is with the effort to both extend and refine these methods that this thesis will be concerned. In the proceeding chapters I resume the discussion from these preceding sections, namely how the methodologies previously applied to the neural coding problem can be 'tweaked' in order to more fully describe what aspects of environmental

stimuli are encoded in neural activity.

Chapter three focuses on the impact that the known variability in stimulus-response latency has on an experimenter's ability to describe the ensemble of stimulus that drives spiking in single neurons. I detail how 'kernel'-based methods such as stimulus reconstruction conflate the questions of 'What caused a neuron to spike?' and 'When did such an event occur?' I describe a method that disentangles these fundamentally distinct questions, and then demonstrate its usage in projecting interneurons 10-2a and 10-3a of the cricket cercal sensory system.

In chapter four I explore the implications of temporal coding in single neurons. I look at the temporal constraints restricting the use of a temporal coding scheme from both above and below. In particular I demonstrate that cells are capable of responding to identical presentations of a stimulus with precise temporal patterns of activity even in the presence of 'jitter' in the stimulus-response latency. I further show that such short temporal patterns of activity in interneurons 10-2a and 10-3a represent stimuli distinct from that which could be predicted by independent consideration of the individual spikes in the firing patterns. I propose that these cells utilize a temporal code in such situations. This can be considered a refinement of general reverse-reconstruction techniques, in which it is generally assumed that the single spike is the only indivisible response codeword. I show that a more accurate description of the coding scheme takes into account two response codewords: the isolated single spike and short (<5

msec ISI) two-spike bursts. Finally I show how this analysis provides a useful limit for those wishing to employ quantization techniques to analyze various temporal patterns of spikes.

In chapter five I detail a novel method for stimulus optimization that takes advantage of our knowledge of the coding schema of interneurons 10-2a and 10-3a. First I show how models of the stimulus selectivity of a neuron can be tested in real-time while recording from the cell. I then show how iterative applications of this methodology can refine the model, leading to improved predictive power. I apply this method to the cricket cercal system, and relate which of the changes to the model of stimulus selectivity lead to improvements in performance.

Chapter six summarizes the collective work of this thesis, and suggests how to proceed in future experimentation.

THE CERCAL SYSTEM

Evolutionary History

The cercal sensory system is common to many taxa of the class insecta, and has been studied in diverse species from primitive insects such as the thysanurans (Edwards and Reddy, 1986) to many of the species of orthopteran insects, including cockroaches (Pumphrey and Rawdon-Smith, 1937; Roeder, 1948; Dagan and Parnas, 1970), stick insects (Rice and Webb, 1975), grylloblatids (Edwards and Mann, 1981, Cell Tissue Res, 217, 177-88), mantids (Ball and Stone, 1982; Boyan and Ball, 1986), locusts (Seabrook, 1970; Boyan et al., 1989a), katydids (Shen, 1983), cave crickets (Schrader, 2000), wood crickets (Coolen et al., 2005; Dangles et al., 2006), phalangopsidans (Kämper and Dambach, 1979; Heinzel and Dambach, 1987), and several species of field crickets (Pumphrey and Rawdon-Smith, 1936; Bentley, 1975; Gnatzy, 1978; Kämper and Dambach, 1981; Kanou et al., 2006). The phylogenetic relationship of these animals is shown in figure 1.1, while the morphology of a selection of these diverse species is shown in figure 1.2.

Cercal systems predate the origin of insects and are still found in many wingless hexopods, both of the class insecta (i.e. firebrats and silverfish, see figure 1.2 A) and of the class parainsecta (such as diplurans). These arthropods are thought to closely resemble (and are phylogeneically related to) the very first

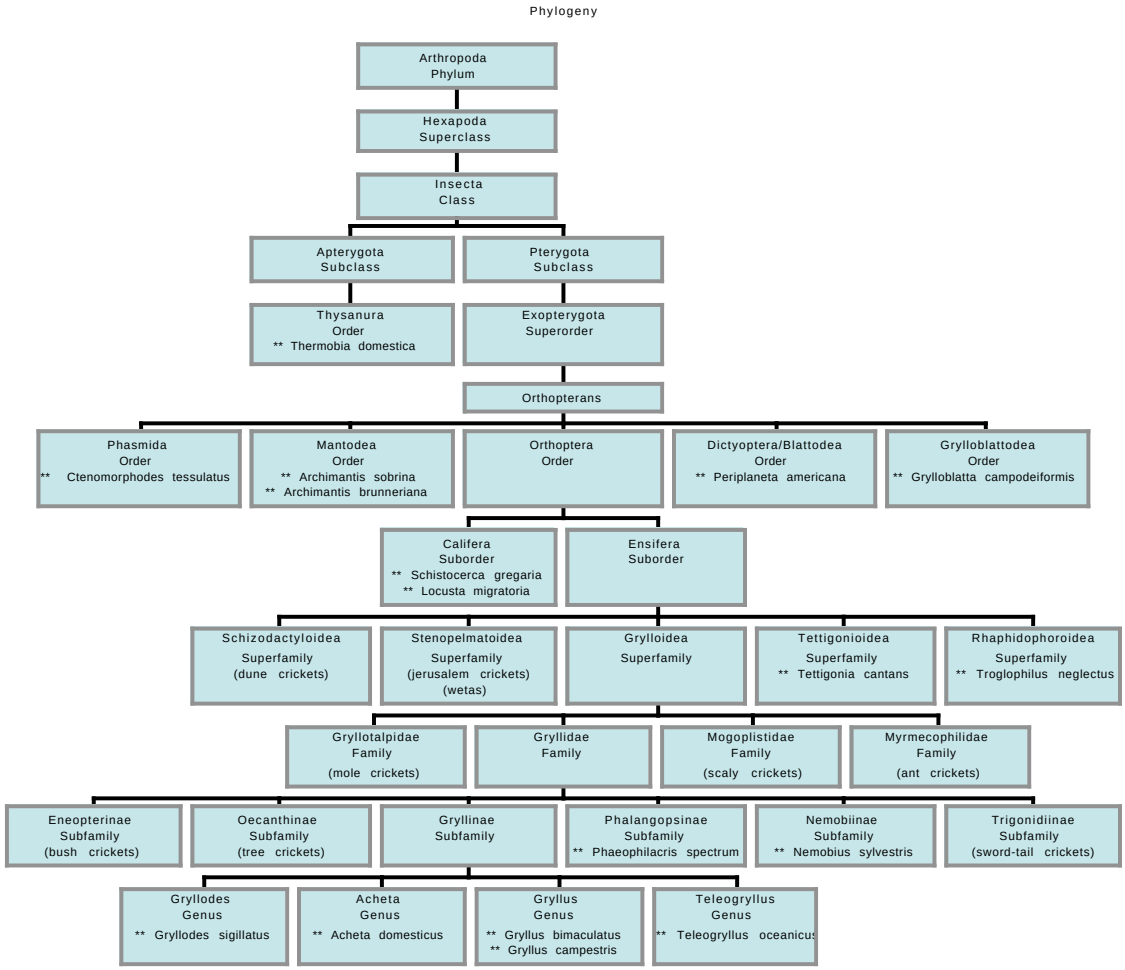

Figure 1.1. Phylogenetic relationship of cricket and other insect species with cerci. Species for which the cercal systems have been studied are indicated with a **. Note- proximity within horizontal layers does not denote relatedness.

insects from the Devonian Era (Edwards and Reddy, 1986). The cercal systems of these species are immediately recognizable as homologues of their counterparts in the orthopterans, containing structures such as filiform hairs, afferent projections into the terminal abdominal ganglion, and synaptic connections with giant interneurons which projects to more anterior nervous centers (Edwards and Reddy, 1986).

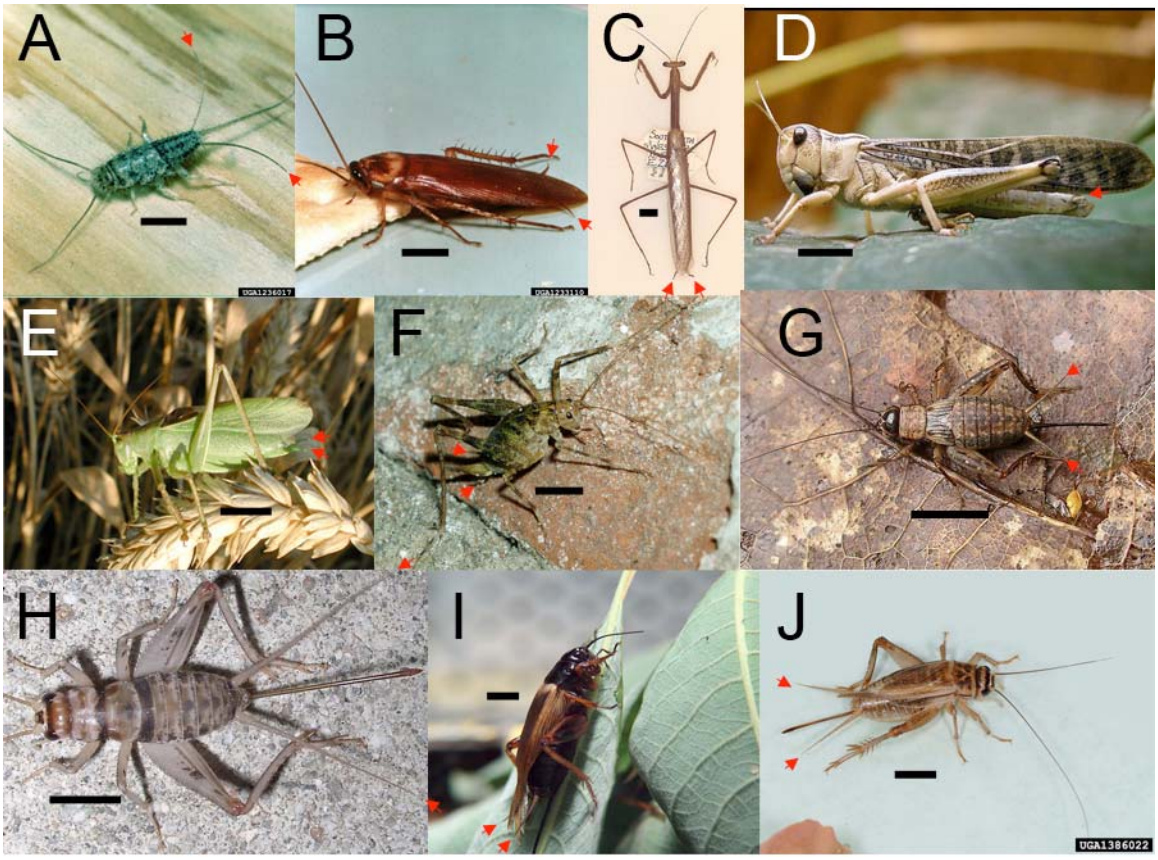

Figure 1.2. Ten cercal systems and the insects that possess them. Red arrows indicate posterior end of cerci, scalebars: 5 mm. A, the firebrat *Thermobia domestica* (Insecta: Thysanura), from Clemson University - USDA Cooperative Extension Slide Series, Bugwood.org. B, the American cockroach *Periplaneta americana* (Insecta: Dictyoptera), from Clemson University - USDA Cooperative Extension Slide Series, Bugwood.org. C, the mantid *Archimantis sobrina* (Insecta: Mantodea), from Natarsha Zilm, Agriculture Western Australia, agspsrv34.agric.wa.gov.au. D, the desert locust *Locusta migratoria* (Insecta: Orthoptera), from Jonathan Hornung, commons.wikimedia.org. E, the bush cricket/kadydid *Tettigonia cantans* (Insecta: Orthoptera), from G.-U. Tolkiehn, commons.wikimedia.org. F, the cave cricket *Troglophilus neglectus* (Insecta: Orthoptera), from P Kocárek, www1.osu.cz/orthoptera/druhy/tro_neg.htm. G, the wood cricket *Nemobius sylvestris* (Insecta: Orthoptera), from Frank Stavenuiter, species.wikimedia.org. H: the tropical house cricket *Gryollodes sigillatus* (Insecta: Orthoptera), from gypsumwolf, flickr.com. I: the field cricket *Gryllus bimaculatus* (Insecta: Orthoptera), from Sami Vuori, commons.wikimedia.org. J: the house cricket *Acheta domesticus* (Insecta: Orthoptera), from Joseph Berger, Bugwood.org.

While fossil evidence indicates that cerci were present on the original pterygotes (and probably earlier in the original apterygotes), they seem to have declined in importance in later radiations, becoming absent in the holometabolus

insects (those which undergo metamorphoses that include larval and pupal stages before adulthood). Comparative morphological studies show that the giant interneurons that ascend from the terminal ganglion to more anterior nerve centers in the more primitive insects were replaced in holometabolus insects by giant neurons descending from the brain and with input originating in the optic lobes. This indicates a change in escape behavior accompanying the advent of metamorphosis- more primitive animals relied on the air particle displacement-sensitive cercal system to drive predator evasion, while more modern adaptations such as flight increased the prominence of visually mediated escape behavior (Edwards and Reddy, 1986).

Orthopterans seem to represent a zenith in cercal development, with the most complex of all cerci occurring in the Gryllidae family (true crickets, compare figure 1.2 G-J with B-F) (Edwards and Reddy, 1986). Orthopterans diverged from other insects over 300 million years ago in the Carboniferous period, and crickets diverged from the other orthopterans in the mid-Permian period, appearing to have evolved very little since then (Walker and Masaki, 1989). This represents an curious occurrence, as many of the selective pressures and pre-adaptive elements which led to the disappearance of cercal systems in the more advanced insects (such as flight) are present in varying extents in the cricket. An interesting avenue of research, which will be addressed somewhat in the following sections of this chapter, is to examine to what extent the cerci of crickets have been co-opted to fit new ecological and behavioral niches as

opposed to how well they perform in their ancestral role of eliciting escape response.

Anatomy and Physiology of the System

The Cercus.

In crickets the cercal system is responsible for several sensory modalities, including acceleration due to gravity, touch sensitivity, and the detection of low frequency air movement in the animal's direct proximity. This thesis will focus principally on the latter modality, and when not otherwise specified, will refer to the cercal system of species from the family *Grillidae* (such as *Acheta domesticus* or *Gryllus bimaculatus*).

The sensory organ is composed of the cerci: two antennae-like appendages extending from the posterior of the insect. The proximal base of the right cercus of *Acheta domesticus* is shown in figure 1.3 A. In the cricket each cercus is covered with four different varieties of sensors: deeply inserted bristle (trichoid) hairs which mediate touch sensitivity (figure 1.3 C, b1 and b2) (Murphey, 1985); club-shaped, freely articulating clavate hairs which mediate detection of acceleration due to gravity (figure 1.3 B, e.g. # 40 60 80 90; C, e.g. # 64, 65 70, 83) (Murphey et al., 1980; Sakaguchi and Murphey, 1983); freely articulating filiform hairs which sense the near-field particle displacement (figure 1.3 C, f, and figure 1.3 D-F)(Palka et al., 1977); and campaniform sensilla, which activate when the cuticle surrounding the filiform hair sockets is deformed, thereby

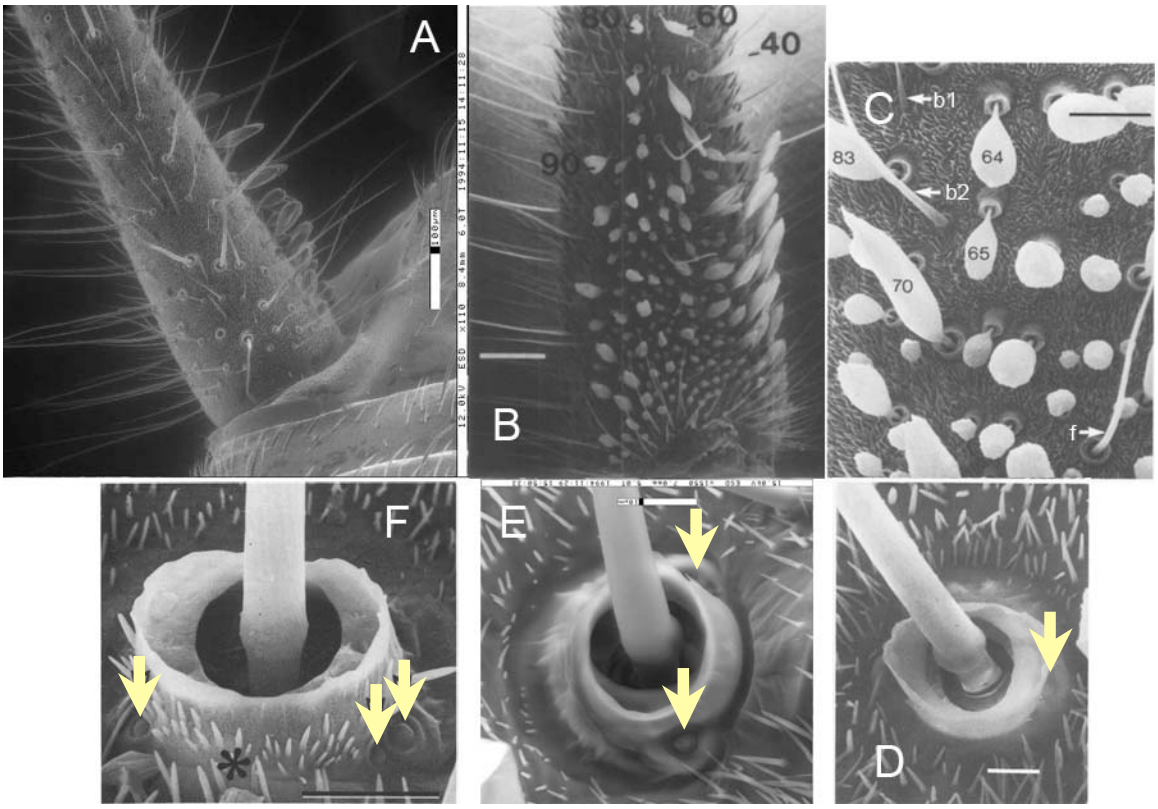

Figure 1.3. Scanning electron micrographs of cricket cerci. A, dorsal scan of right cercus of *A domesticus*. B, closer picture of cercus, showing details of filiform and clavate hairs (numbered). C, Partial scan showing the clavate sensilla (numberered), the filiform sensilla (f), and the bristle or deeply inserted trychoid sensilla (b1 and b2). F, E, and D, micrographs of filiform base and socket. In D-F the campaniform sensilla are visible (arrows). A and E modified from (Osborne, 1997); B modified from (Murphey, 1981); C and D modified from (Murphey, 1985); F modified from (Heusslein and Gnatzy, 1987).

extending the dynamic range of the filiform hairs (arrows in figure 1.3 F) (Dumpert and Gnatzy, 1977), see figure 1.3. Air particle displacement detection is mediated by the approximately 750 filiform hairs (Palka et al., 1977; Bentley, 1975), each of which is constrained to move along a single axis of motion within the animal's horizontal plane (Edwards and Palka, 1974). Hairs with similar directional selectivity are arranged in columns running longitudinally along the cercus, with hairs sensitive to air movement transverse to the long axis of the

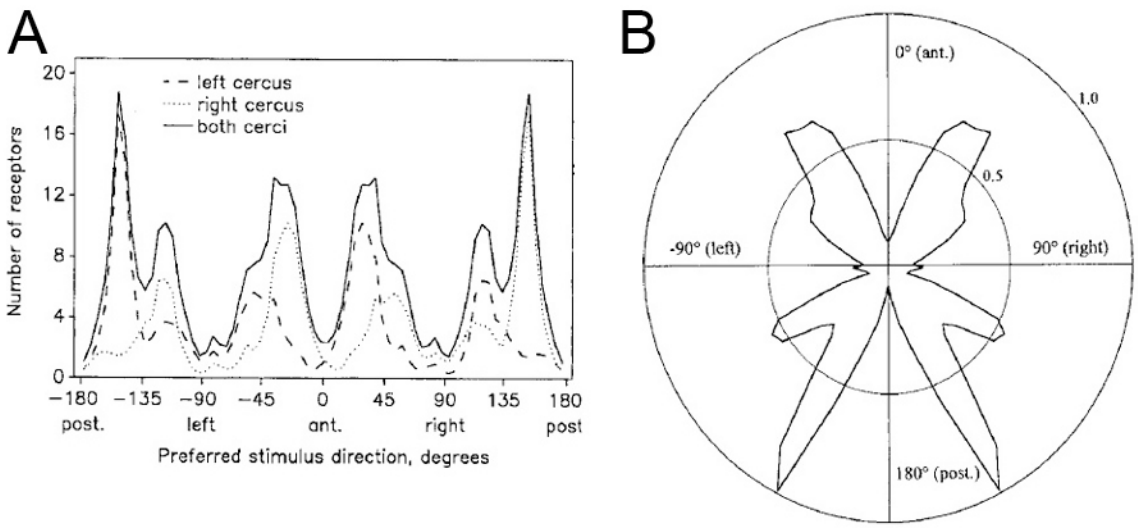

Figure 1.4. Distribution of directional sensitivities of filiform hairs. A, Histogram of directional selectivity of hairs on the left cercus (dashed line), right cercus (dotted line), and sum from both cerci (solid line). B, Polar representation of summed data from A. Modified from (Landolfa and Jacobs, 1995).

cerci generally being located on the dorsal and ventral surfaces, and hairs sensitive to air movement along the longitudinal axis being located on the lateral surfaces (Palka et al., 1977). The transverse-longitudinal classification can be refined to at least 13 different subtypes, each with a slightly different preferred axis of motion that together span the full 360º of horizontal space surrounding the cercus (Landolfa and Jacobs, 1995; Paydar et al., 1999) (figure 1.4). Hairs range in length from approximately 30 to over 1500 microns, with resonance characteristics of the hairs determined by hair length (Shimozawa and Kanou, 1984b; Shimozawa and Kanou, 1984a; Osborne, 1997). Attached to each filiform hair is a single afferent neuron (Gnatzy, 1978)- movement of the hair in one direction along its axis of motion provides excitatory currents to the afferent, while movement in the opposite direction inhibits it (Bacon and Murphey, 1984).

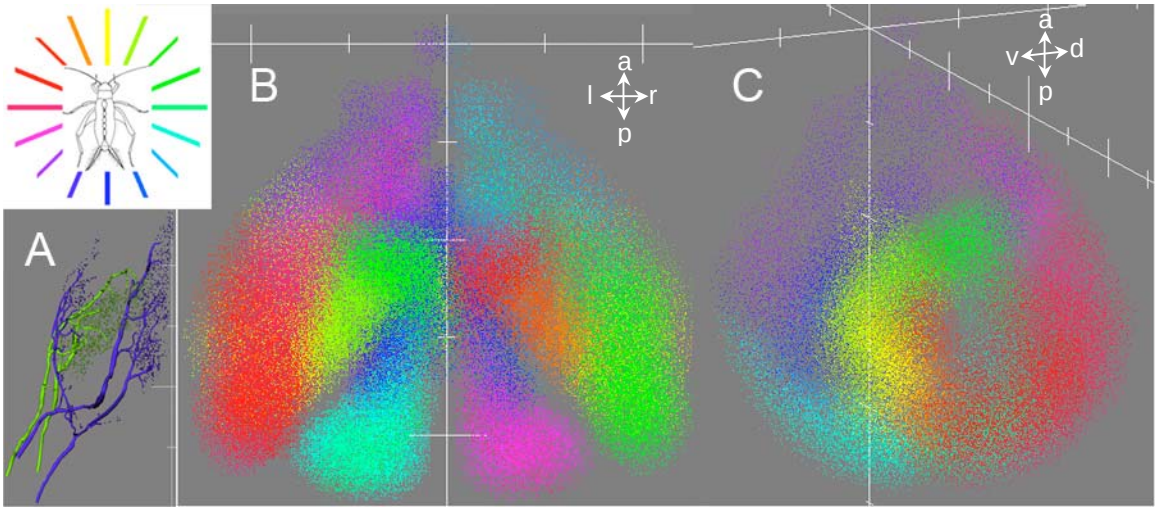

Figure 1.5. Projection of afferent axons to terminal ganglion. A, Three-dimensional reconstruction from the TAG of axonal arborizations for two afferents with distinct directional selectivities (inset shows color code for directional selectivity relative to animal). Sites of varicosities (likely regions of synaptic contact) are shown as dots. B, Dorsal view of varicosities from all filiform afferents of the cerci as they occupy volume in the terminal ganglion. Two continuous maps of directional space are visible, one in each of the left and right hemiganglia. C, Ventrally rotated sagittal view of cercal glomerulus of the left hemiganglion, showing the three-dimensional structure of the map (left is out of the page). Abbreviations: a- anterior, p- posterior, l- left, r- right, v- ventral, d- dorsal.

Afferent Projections to the Terminal Abdominal Ganglion.

The axons of the sensory afferents project into the terminal abdominal ganglion (TAG) of the cricket, which is formed by the fusing of embryonic ganglia innervating the 7^{th}-11^{th} abdominal body segments in the cricket (Jacobs and Murphey, 1987). The projections of these sensory axons terminate in the posterior region of the TAG known as the cercal glomerulus (Bacon and Murphey, 1984), and, except for one known class of receptors ('X hairs', Murphey and Lemere, 1984) are confined to the hemiganglion ipsilateral to the cercal nerve containing the axons (Palka et al., 1977). The spatial organization of afferents with similar directional sensitivity is maintained in the projection from

cercus to TAG, meaning that the axonal arborizations of the afferents from the two cerci form two mirror symmetric maps of directional space within the cercal glomerulus (Bacon and Murphey, 1984; Jacobs and Nevin, 1991; Jacobs and Theunissen, 1996). A reconstruction of the axonal arborizations of two afferents as they project into the TAG is shown in figure 1.5 A, while the maps of directional space formed by these projections are shown in figure 1.5 B-C.

Connectivity within the TAG.

In the TAG the afferents form synaptic connections with an estimated 200 bilaterally symmetric pairs of air particle displacement-sensitive local interneurons (at least 36 of which have been identified) and an estimated 32 bilaterally symmetric pairs of air particle displacement-sensitive projecting interneurons (21 of which have been identified- see tables 1.1 and 1.2) (Baba et al., 1995; Mendenhall and Murphey, 1974; Jacobs and Murphey, 1987; Baba et al., 1991; Kohstall-Schnell and Gras, 1994). The somas of both local and projecting interneurons are grouped into three distinct clusters within each neuromere of the TAG, and these clusters form a set of homologues which serially repeat in each of the neuromeres (Jacobs and Murphey, 1987). This repeating structure provides for a convenient system of nomenclature for naming the interneurons: for both local and projecting interneurons the cells are first given a number designation indicating the neuromere which contains the cell's soma (i.e. 7, 8, 9, 10, or 11 in crickets), followed by either a letter (local interneurons) or number (projecting interneurons) which indicates the cluster

containing the soma- L/1 for the lateral cluster within the neuromere, V/2 for the ventral cluster, and D/3 for the dorsal cluster (Jacobs and Murphey, 1987; Baba et al., 1995).

In addition to the air particle displacement-sensitive projecting interneurons, several interneurons innervated by afferents in the bristle neuropil have been described, including 7-1a, 7-1b, 7-1z, and 8-1c from (Murphey, 1985; Jacobs and Murphey, 1987) and probably nGI 13 from (Baba et al., 1991). While it is possible to elicit responses in these cells from air particle displacement stimuli (personal observation), they will not be considered in subsequent discussion in this thesis.

Local interneurons fall into two general classes: local non-spiking (LNIs) and local spiking (LSIs); projecting interneurons can be divided into two classes: giants (GIs, a group approximately 10-15 pairs of bilaterally symmetric neurons, (Edwards and Palka, 1974), see figure 1.6 for morphology, and table 1.1 for comparisons of GIs across orthopterans) and non-giants (nGIs, an amorphorous grouping of at least 10 bilaterally symmetric pairs of neurons, some of which are variously described as GIs or nGIs (Kämper, 1984; Baba et al., 1991; Kohstall-Schnell and Gras, 1994), see table 1.2 for naming and position within the TAG). While all four classes of interneuron (LNIs, LSIs, GIs, and nGis) appear to receive input from the afferents, there is also lateral connectivity within the interneuron layer: local non-spiking interneurons have excitatory connections with both varieties of projecting interneurons; LSIs and LNIs connect with each

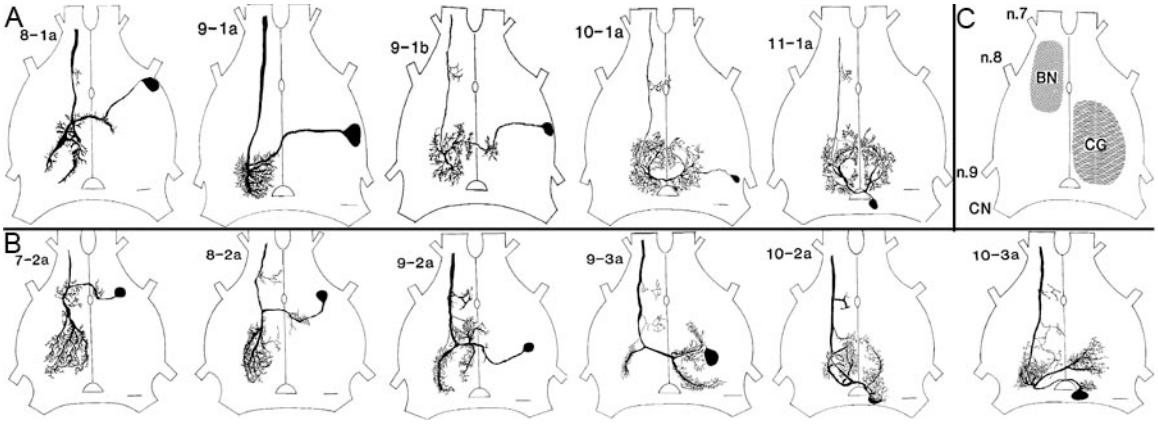

Figure 1.6. Morphology of air movement-sensitive interneurons in the terminal ganglion. A, Camera lucida drawings of dendritic structure and morphology of five neurons belonging to the vGI class in the TAG. Cells 7-1a, 7-1b, and 8-1c belong in the ventral group but belong to the touch-sensitive bristle-hair system. Interneuron 8-1b has also been excluded, though it likely mediates responses to air particle displacement. B, Camera lucida drawing of five largest dGIs. Interneuron 7-2a (and likely 8-2a) is sensitive to acceleration due to gravity as well as air particle displacement stimuli (Sakaguchi and Murphey, 1983; Kämper, 1984). C, scaled drawing of TAG showing the relative positions and sizes of the right cercal glomerulus (CG) and the left bristle neuropil (BN). Both regions have mirror-symmetric homologues in the contralateral hemiganglion. The CG roughly corresponds with the map of directional space from figure 1.5, and contains input both from the filiform and clavate hairs (Murphey, 1981). Scale bars: 50 microns. Modified from (Jacobs and Murphey, 1987).

Neuro -mere	Cluster	*Acheta domesticus*	*Tettigonia cantans*	*Locusta migratoria*	*Periplaneta americana*	*Archimantis sobrina*
7	2	7-2a	*	*	*	
8	1	8-1a		nGI 7	GI-1, GI-3	1,2
	2	8-2a				
9	1	9-1a, 9-1b	GI 1, GI 2, GI 3	GIN 1, nGI 1	GI-2	3
	2	9-2a	GI 4	GIN 2	GI-5	4
	3	9-3a	GI 5	nGI 17, nGI 19		5
10	1	10-1a		nGI 13		
	2	10-2a	GI 7	GIN 3, nGI 14	GI-6	7,8,9
	3	10-3a	GI 6		GI-7	6
11	1	11-1a			GI-4	10,11
	2	**		GIN 4		

Table 1.1. Position of projecting air movement-sensitive interneurons in the TAG across othopteran species. *A domesticus* and *P americana* data from (Jacobs and Murphey, 1987), *T cantans* from (Shen, 1983), *L migratoria* data from (Boyan et al., 1989a; Boyan et al., 1989b) and *A sobrina* data from (Boyan and Ball, 1986). Note- position in the same neuromere or cluster in different species does not necessarily imply homology. * Neuromere 7 does not fuse with the TAG of bush crickets, locusts or cockroaches. ** Neuromere 11 in crickets is not completely formed, and consequently does not contain neuron clusters 2 or 3.

A domesticus	*G bimaculatus*	*G campestris*	Neuromere	Cluster
8-1b†	nGI 3*,	8-1b**	8	1
NN1¬	nGI 1*	NN1**	8	1
8-2a†	nGI 15*, 8-2a‡	8-2a**	8	2
-	nGI 2*	-	8	2
-	nGI 9*	-	8	2
9-1b†¬	nGI 16*	9-1b**	9	1
-	nGI 6*	-	9	1
-	nGI 4*	-	9	2
-	nGI 8*	-	9	2
-	nGI 11*	-	9	2
-	nGI 7*	-	9	3
10-1a†	nGI 12*	10-1c**	10	1
-	nGI 10*, AS1‡	-	10	2
11-1a†, 11-1c¬	nGI 5*, 11-1a‡	11-1c**	11	1
-	nGI 14*, AS2‡	-	11	1

Table 1.2. Position of air movement-sensitive nGIs in the TAG of three species of crickets. * from (Baba et al., 1991) ‡ from (Kohstall-Schnell and Gras, 1994), ** from (Kämper, 1984), ¬ from (Vedenina et al., 1998), † from (Jacobs and Murphey, 1987)

other and are theorized to be reciprocally inhibitory (Baba et al., 1995). All monosynaptic connections between afferents and the projecting interneurons appear to be excitatory. Some interneurons do receive ‘cross’ inhibition when afferents projecting to the glomerulus contralateral to the interneurons’ axon are stimulated, but this inhibitory pathway is thought to be polysynaptic (Matsumoto and Murphey, 1977; Palka and Olberg, 1977; Tobias and Murphey, 1979; Levine and Murphey, 1980; Jacobs et al., 1986), probably mediated by the local interneurons. Gross directional selectivity of the projecting interneurons can be predicted by consideration of the excitatory afferent input only (Cummins et al., 2003).

The air particle displacement-sensitive cells most commonly referred to as giants include INs 7-2a, 8-1a, 8-2a, 9-1a, 9-1b, 9-2a, 9-3a, 10-2a, 10-3a, 10-1a,

10-2a, 10-3a, and 11-1a. These cells can be differentiated into two separate groups: the ventral giant interneurons (vGIs, figure 1.6 A), which have axons ascending the abdominal nerve cord through the ventral intermediate tract (VIT) in the connectives and whose somas originate in the first cluster of their respective neuromeres, and the dorsal giant interneurons (dGIs, figure 1.6 B), which have their axons ascending through the dorsal intermediate tract (DIT) and somas originating from clusters two and three (Edwards and Palka, 1974; Jacobs and Murphey, 1987) (see also tables 1.1 and 1.2). vGIs have their somas in cluster one of their respective neuromeres, while dGIs come from cluster two and three. These two groups have distinct functional roles in the cockroach cercal system (Daley and Delcomyn, 1980), and preliminary analysis indicates a similar functional distinction in crickets (Hirota et al., 1993).

In addition to studies on the giant interneurons, several studies have tried to examine the anatomy and physiology of some of the non-giant interneurons, but there does not seem to be a standardized way of distinguishing between the two groups. (Mendenhall and Murphey, 1974) describe the giants as the seven largest cells in the connective anterior to the TAG (7-1a, 8-1a, 9-1a, 9-2a, 9-3a, 10-2a, and 10-3a), which have somas with diameters of 31-71 microns and axon diameters of 7-28 microns. In contrast, (Edwards and Palka, 1974) describe the GIs as 10 pairs of bilaterally symmetric interneurons with axons in the ascending connective whose diameters fall between between 20 and 40 microns. Note that both of the above studies were carried out in the same species, *Acheta*

domesticus, making the discrepancy in ranges of reported diameters all the more striking. (Baba et al., 1991) describe the nGIs of *Gryllus bimaculatus* as having soma diameters of 10-45 microns and axon diameters of 4-9 microns (excluding their labeling of IN 9-1b as an nGI). Both these ranges overlap the sizes of the giant interneurons described by Mendenhall and Murphy. It's important here to emphasize that the distinction between giant and non-giant is rather fuzzy, and that there is a continuum of soma and axon sizes amongst the air particle displacement-sensitive neurons (see figure 1.7 D). In this thesis the use of the term 'giant interneurons' will be restricted to the 11 cells pictured in figure 1.6, though as mentioned this is an arbitrary distinction. For the sake of completeness, table 1.2 details all of the other identified air particle displacement sensitive ascending neurons from studies in the cricket species *A domesticus*, *G bimaculatus*, and *G campestris*, as well as detailing alternative naming of some of the cells which have been studied.

The Thoracic Ganglia.

From the TAG the projecting interneurons send their axons to the thoracic ganglia and brain, which form the subsequent processing centers in the abdominal nerve cord. While it has been shown that action potentials from the axons of the GIs reach at least to the metathoracic ganglion (Gozani and Miller, 1994), the shape of their branching structure in subsequent ganglia is poorly understood. Two separate efforts at characterizing the anatomy of GI projections in the meso- and metathoracic ganglion, (Mendenhall and Murphey, 1974), in

adult *A domesticus* and (Hirota et al., 1993) in 3rd instar *G bimaculatus*, came to relatively contradictory conclusions. The former study showed branches extending both medially and laterally from the axons of GIs 8-1a and 9-1a (the medial giant interneuron, MGI, and lateral giant interneuron, LGI, respectively, figure 1.7 A), while the latter study found only medial branching in the homologous cells (figure 1.7 B, the two left-most cells). This discrepancy could be an important one, as the authors of the latter paper assert that the lack of any lateral branching in the vGIs could potentially restrict their role in motor responses to air particle displacement stimuli. The authors further made extracellular recording of activity in the 5th nerve root of the mesothoracic ganglion, and the 3rd nerve root of the metathoracic ganglion (innervating flight and leg muscles, but which do not contain the fast tibia extensors that control jumping) in adult animals while simultaneously stimulating individual neurons from the dorsal and ventral groups intracellularly, finding that stimulation of the vGIs never led to spiking in these two nerve roots, while stimulation in all of the dGIs did lead to spiking activity in the nerve roots. Conversely, in a third study (Kanou et al., 1985) the motor neurons of the 4th and 5th nerve roots of the mesothoracic ganglion were excited by activity correlated with the vGIs and inhibited by activity correlated with the dGIs. None of the studies showed any evidence for GI arborizations crossing the midline in the thoracics.

In addition to the possibility that the GIs synapse directly with motoneurons in the thoracis, several studies have shown that local interneurons in the thoracics

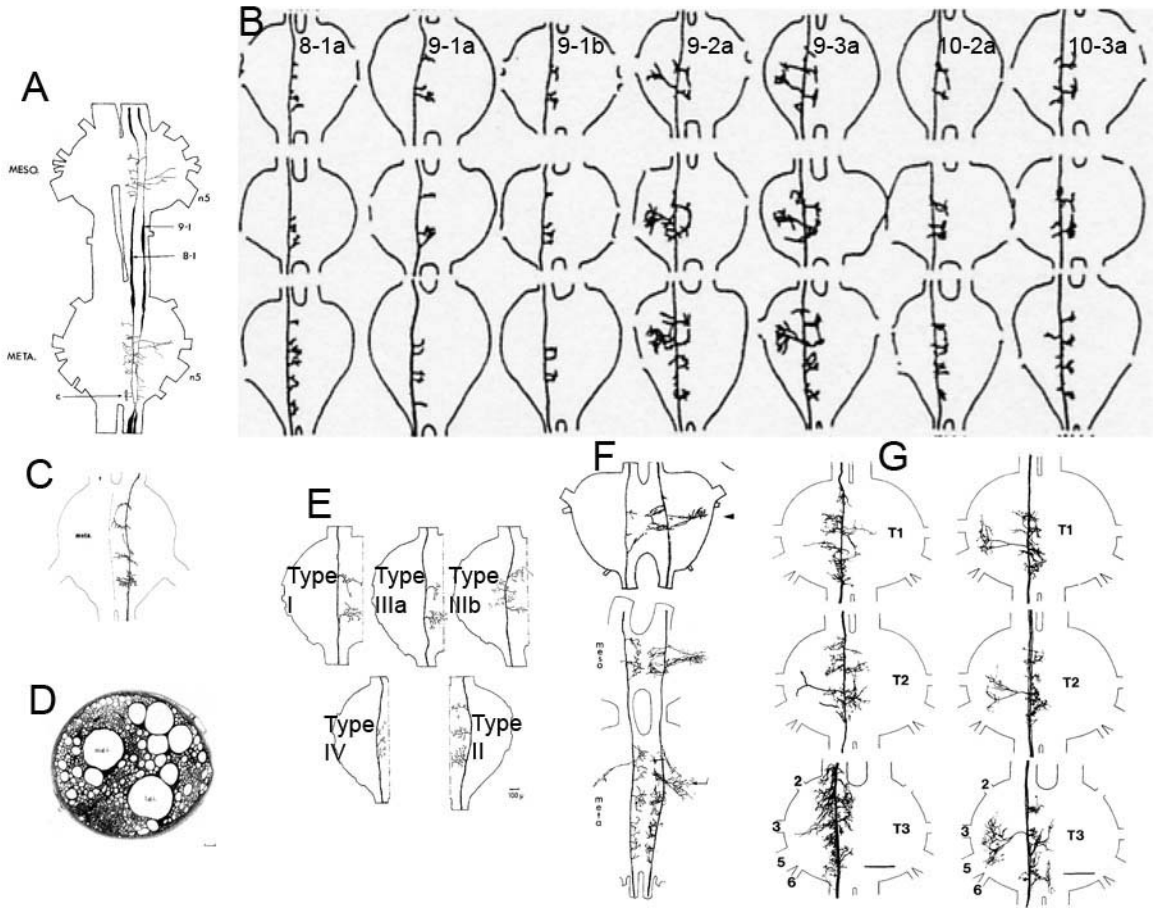

Figure 1.7. Projections of the GIs in the thoracic ganglia of crickets and related orthopterans. A, GIs 8-1a and 9-1a in the meta- and mesothoracic ganglia of adult *A domesticus*, modified from (Mendenhall and Murphey, 1974). B, vGIs and dGIs in the meta- (lower), meso- (middle), and prothoracic ganglia (upper) of 3rd instar *G bimaculatus*, modified from (Hirota et al., 1993). C, GI 7-2a in the metathoracic ganglion of *A domesticus*, modified from (Sakaguchi and Murphey, 1983). D, transverse section of abdominal nerve cord anterior to TAG, showing relative sizes of GI axons, with medial to the left and lateral to the right. vGI 8-1a is labeled as m.g.i. medial giant interneuron, and vGI 9-1a is labeled l.g.i. (lateral giant interneuron). vGI 9-1b is known to be the intermediately-sized axon immediately superior and lateral to l.g.i. Axons for 10-1a and 11-1a are unidentified. dGI axons 9-2a, 9-3a, 10-2a, and 10-3a are the four large axons visible in the dorsal lateral region. dGIs 7-2a and 8-2a are assumed to be among the intermediately-sized axons immediately ventral and medial relative to the rest of the dGIs. Scale bar 10 microns, modified from (Edwards and Palka, 1974). E, projections of GIs in the meta- (type II) and prothoracic (types I, IIIa, IIIb, and IV) ganglia of the adult bush cricket *T cantans*. From (Shen, 1983). F, all four identified GIs of the locust *L migratoria* in all three thoracic ganglia. GI 1 lies on the left of the tract, while GIs 2-4 are grouped together on the right. From (Boyan et al., 1989a). G, thoracic projections of the dorsal (left) and ventral (right) GIs of the cockroach *P americana*, modified from (Collin, 1985). Scale bar: 200 microns.

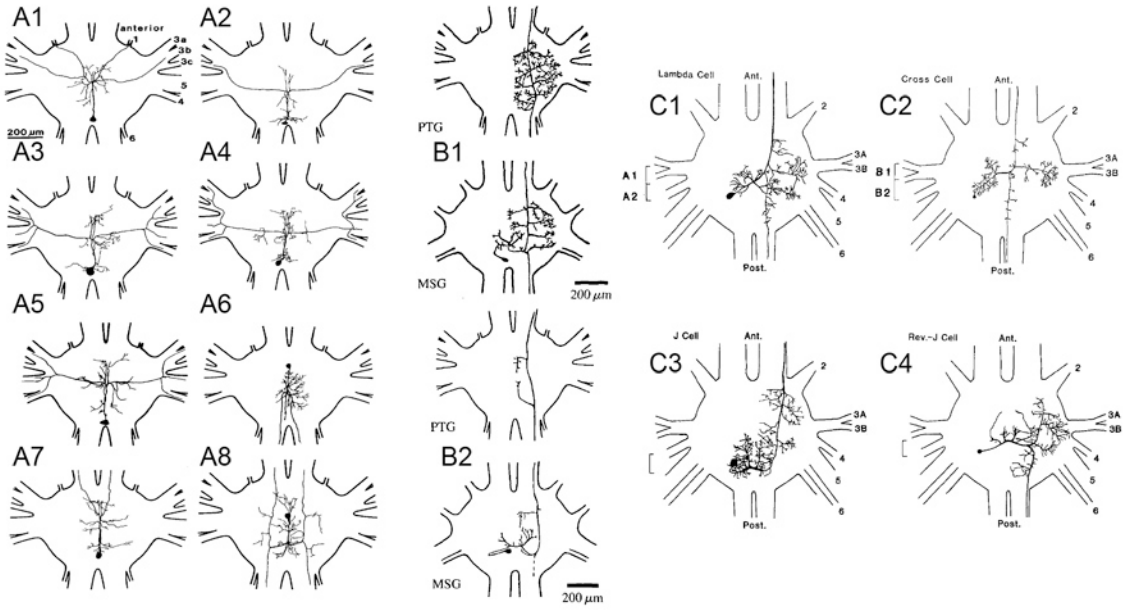

Figure 1.8. Air particle displacement-sensitive neurons originating in the thoracic ganglia of crickets and cockroaches. A, air particle displacement-sensitive dorsal-unpaired median (DUM) neurons of the prothoracic ganglion of *G bimaculatus*, modified from (Gras et al., 1990). DUM neurons fall into three morphological and physiological classes: DUMa (A1-A5), DUMb (A6-A7), and DUMc (A8). B, morphology in the prothoracic (upper) and mesothoracic (lower) ganglia of two types of air particle displacement-sensitive interneurons originating in the mesothoracics of *G bimaculatus*, modified from (Hörner, 1992). C, Four classes of air particle displacement-sensitive interneurons originating in the metathoracic ganglion of *P americana*, modified from (Ritzmann and Pollack, 1986).

as well as intersegmental neurons with somas in the thoracics are modulated by cercal stimulation (Hörner et al., 1989; Gras et al., 1990; Hörner, 1992)). Several of the local dorsal unpaired median (DUM) neurons as well as the intersegmental neurons are shown in figure 1.8 A and B. Although the DUM neurons send axons out the segmental nerves towards the leg muscles, it is unlikely that they are solely responsible for muscle contraction, but rather are likely to modulate the strength of contraction via octopaminergic action on the motoneurons (Gras et al., 1990). In the case of the cricket it is not known if the GIs synapse directly on

the motoneurons of the thoracics (though note the regions of overlap figure 1.8 A and B with figure 1.7 A and B), whether they are completely mediated by the local interneurons, or whether they innervate the motoneurons through a combination of mono- and polysynaptic mechanisms. The delay between stimulation and action potentials in the DUM neurons is consistent with the timing of descending activity in the brain (Gras et al., 1990).

In the cockroach *P americana* both anatomy and physiology of the GI-thoracic circuitry is better understood. The dGIs and the vGIs (as well as a 3rd, unidentified group of axons in the median ventral tract, tentatively identified as non-giant air particle displacement-sensitive cercal interneurons) both arborize to a greater extent both laterally and medially than their homologues in the cricket, and show considerable overlap with the dendrites of fast and slow levator and depresser motoneurons in the metathoracic ganglion (Collin, 1985) (see figure 1.7 G). Initial experiments in the system showed that several of the motoneurons in the metathoracic ganglion have firing activity which is highly correlated with firing from the dGIs, but are not very correlated with firing in the vGIs (Ritzmann and Camhi, 1978). However, further experiments have shown that activity in the vGIs could elicit short-latency, subthreshold excitatory potentials in a specific population of thoracic interneurons, the TI-As, and that this same group of interneurons in turn excited motoneurons (Ritzmann and Pollack, 1986; Westin et al., 1988; Ritzmann and Pollack, 1988; Ritzmann and Pollack, 1990). The synaptic connectivy is mediated through a ventral dendritic projection common to

group TI-A (Casagrand and Ritzmann, 1991). It has also been shown that TI-As are the sites of convergence for several modalities and pathways that effect motor output, both descending and ascending (Ritzmann et al., 1991). The morphology of these cells resembles somewhat the intersegmental thoracic interneurons of the cricket- compare figures 1.8 B and C.

Projections in the Brain.

In the cricket *G bimaculatus* ((Hirota et al., 1993), figure 1.9 A), the bush cricket *T cantans* ((Shen, 1983), figure 1.9 B), and in the locust *L migratoria* ((Boyan et al., 1989a), figure 1.9 C) the air particle displacement-sensitive giants all project to a relatively localized region in the lateral posterior protocerebrum, probably in the lateral accessory lobes (Burrows, 1996)- see figure 1.9. Many of the air particle displacement-sensitive intersegmental neurons originating in the thoracic and unfused abdominal ganglia of crickets and locusts also arborize in these regions (Hörner et al., 1989; Gras et al., 1990; Pfluger, 1984). These areas as well as the mushroom bodies have been shown to be regions of multimodal convergence, receiving inputs from air particle displacement-receptive units on the both the cerci and antenna, as well as visual information (Hörner and Gras, 1985; Schildberger, 1984a). Several of these are shown in figure 1.10 B.

Not surprisingly, these areas are also loci for information processing in the auditory pathway- local brain neurons called BNCs (brain cell neurons) have extensive arborizations in the posterior lateral protocerebrum and mushroom

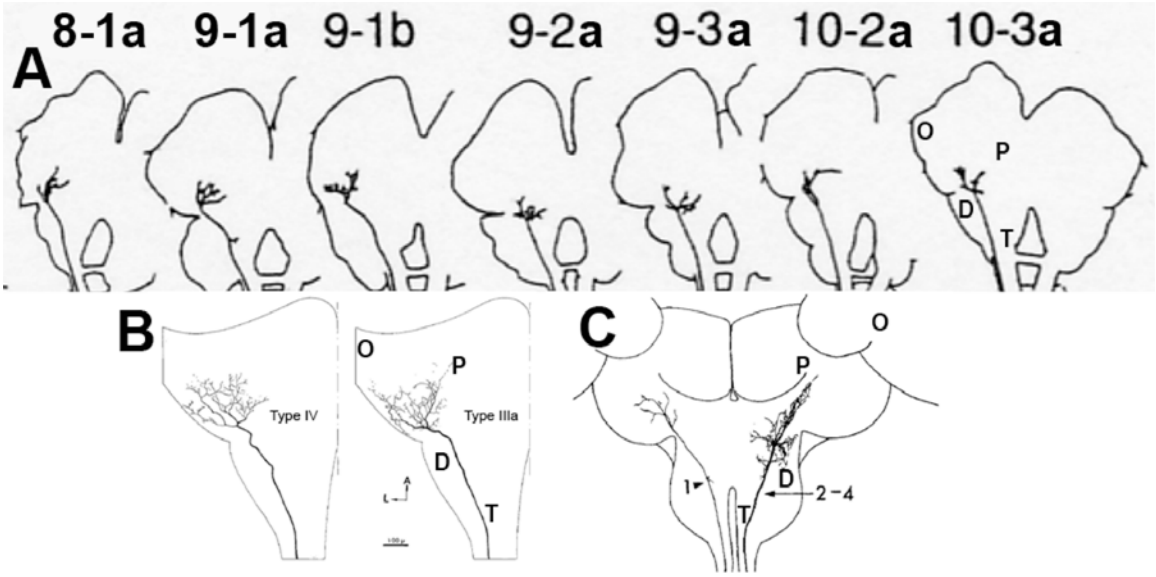

Figure 1.9. Projections of the GIs in the brain of crickets and related orthopterans. A, Dorsal view of projections of cells (from left to right) 8-1a, 9-1a, 9-1b, 9-2a, 9-3a, 10-2a, 10-3b into the brain of 3rd instar *G bimaculatus*, modified from (Hirota et al., 1993). B, Dorsal view of projections of Type IV (left) and Type IIIa (right) giant interneurons in the brain of *T cantans*, modified from (Shen, 1983). C, Dorsal view of projections of giant interneurons 1 (left) and 2-4 (right) into the brain of the locust *L migratoria*, modified from (Boyan et al., 1989a). Abbreviations: O, optic stalk; P, protocerebrum; D, deutocerebrum; T, tritocerebrum.

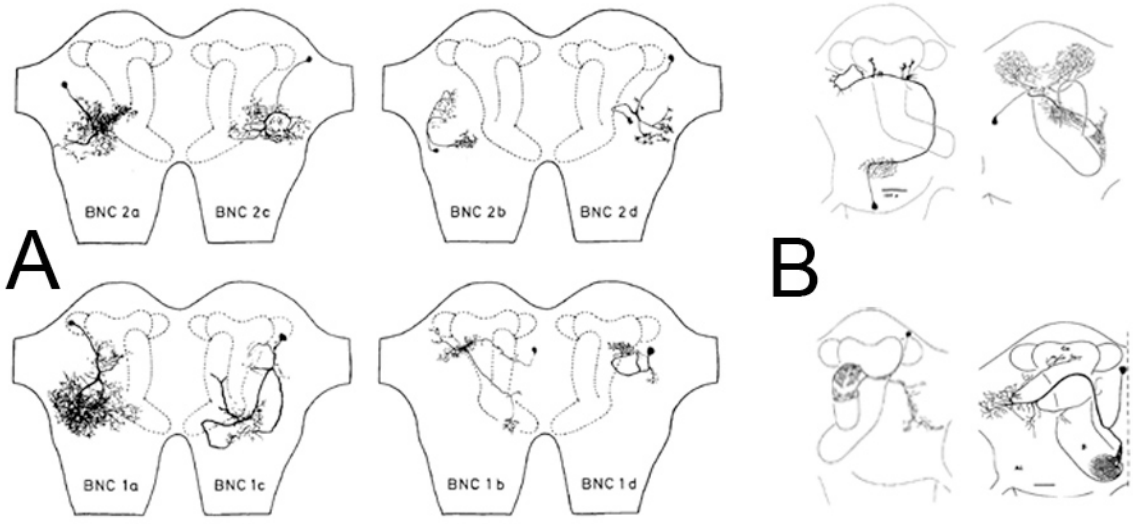

Figure 1.10. Morphology of local brain neurons in the cricket. A, 8 neurons involved with auditory processing, belonging either to Brain Neuron Class 1 or 2 (BNC 1 or 2), modified from (Schildberger, 1984b). Outlines of the mushroom body complex are stippled. B, 4 neurons with multimodal sensitivities, including cercal stimulation, modified from (Schildberger, 1984a).

bodies, and are thought to make synaptic connections with both ascending neurons from the auditory areas of the prothoracic ganglia and descending neurons which are implicated in motor activity such as phonotaxis and predator evasion (Schildberger, 1984b; Hörner and Gras, 1985; Schildberger et al., 1989). Some BNCs are band selective specifically to the syllable repetition rate of the cricket's calling songs (Schildberger et al., 1989)- see section on calling songs below. Eight of the BNC neurons are shown in figure 1.10 A- note the overlap with the brain projections of the air particle displacement-sensitive giant interneurons in figure 1.9 as well as the movement sensitive cells associated with the mushroom bodies in figure 1.10 B.

Descending Input.

Air particle displacement-sensitive neurons are known to descend from both the brain (Hörner and Gras, 1985; Staudacher, 2001), and thoracic ganglia (Gras et al., 1990) to the rest of the abdominal nerve cord, but the role of these efferent input has not been conclusively demonstrated. There is some evidence in the form of lesioning experiments that descending input carries inhibits the ascending giants, specifically the ventral giants. This could possibly be a strategy to suppress spurious signals from self motion, thereby effectively raising the threshold for air particle displacement-evoked escape behavior during locomotion or grooming behavior (Murphey and Palka, 1974; Belosky and Delcomyn, 1977). However, it has also been shown (Orida and Josephson, 1978) that these descending pathways were not required to have inhibition

during walking, and experiments on a single vGI of mantids showed no difference in response to air particle displacement before and after lesioning of the ascending connective (Boyan and Ball, 1986).

Experiments in cockroaches reiterated that descending neurons inhibited the ventral GIs during locomotion, and also showed that dorsal internurons were excited at the same tim (Daley and Delcomyn, 1980; Libersat et al., 1989). Cockroach experiments also showed that precise control of directionality in escape movements were degraded after cutting the connectives from the brain (Keegan and Comer, 1993; Schaefer and Ritzmann, 2001). The results of Orida and Josephson indicating that descending input are not necessary and that inhibition was increased after lesion of the ascending connectives could not be repeated in cockroaches, and in fact it has been suggested that their results were due to the fact that they used extracellular recording methods to monitor the excitation, so that they saw the activity of both vGIs and dGIs (Daley and Delcomyn, 1980).

Role of the Cercal System in Escape Behavior

Predation and Parasitism.

Crickets are an evolutionarily successful group of insects, having arisen over 270 million years ago. Success at reproduction however has marked them as a plentiful and stable source of nourishment for a large variety of other animals (Walker and Masaki, 1989). In the wild crickets are known to be eaten by bats

(Moiseff et al., 1978), arachnids (Rovner, 1980; Dangles et al., 2006), mantids (Reitze and Nentwig, 1991), and rodents (Anjum et al., 2006), among many other species. The stridulatory behavior of male crickets has especially marked them out, as the auditory systems of vertebrate such as cats allow them to phonotax to the singer along with the cricket's potential mates (Walker, 1964). Cricket stridulation has even driven a single species of the otherwise deaf flies to evolve an ear physiologically similar to that of the cricket itself (Robert et al., 1992). In addition to outright predations, several species parasitize crickets, including the behavior-altering nematode *Paragordius tricuspidatus* (Ponton et al., 2006) as well as the classical nemesis of *Acheta domesticus*, the digger wasp *Liris niger* (Steiner, 1968). Many of these predators and parasites attack crickets with sudden ballistic movements, and these generate signals in the air around the crickets. The cercal system is often able to detect these signals and in turn trigger an escape behavior, allowing the cricket (or cockroach) to live to reproduce another day.

Predation Signals in the Environment.

The air particle displacement signatures of potential predators principally come in two varieties, air movements due to a lunging or ballistic attack (such as a toad tongue-strike or the lunge of a spider or shrew), or oscillatory air movement due to non-attack movements of the animal, such as the wingbeat of a predatory wasp as it forages. In a pair of studies, Tautz and Markl showed that airborne signals due to flying wasps were concentrated in a frequency band

between 150 and 165 Hz, and generated air particle velocities as high as 2 mm/sec at distances up to 0.5 meters (Markl and Tautz, 1975; Tautz and Markl, 1978), which puts them in the range of frequencies and velocity amplitudes detectable by the cercal system (Shimozawa and Kanou, 1984b). Crickets usually respond to detection of a flying wasp by freezing in place, a highly effective defense as wasps apparently use motion cues during foraging (Steiner, 1968). In contrast, a wasp on the ground (a much more immediate threat to a cricket) produces air signals mostly concentrated below 10 Hz, and with amplitudes as large as 2 cm/sec in the immediate vicinity of the wasp (Gnatzy and Kämper, 1990). The strike of a toad's tongue was determined to reach threshold for sensitivity of the cockroach cercal system (3 mm/sec) when the toad was just 12 cm (and ~100 msec) away from the insect (Camhi et al., 1978). These give a range of spectral characteristics, velocity profiles, and latencies to which crickets and cockroaches are required to react.

Initiation of Escape.

The best known and most studies behavioral reaction to air particle displacement movement in crickets and cockroaches is escape behavior (Bentley, 1975; Kanou et al., 1985; Hörner et al., 1989; Camhi et al., 1978; Ritzmann et al., 1980), In cockroaches this consists of a rapid turn 58 ms after stimulation followed by a quick run (Camhi and Tom, 1978), while in crickets the response could either be a turn ~80 msec after stimulation, a jump approximately ~90 msec after stimulation, or a combined turn (~50 msec post stimulus) and

jump (~190 msec post stimulus) (Tauber and Camhi, 1995; Gras et al., 1994). Stimulation amplitudes as low as 35-50 cm/sec could trigger escape movement (Gras and Hörner, 1992; Gras et al., 1994; Baba et al., 1997), Both Crickets and cockroaches turn to orient themselves almost 180º away from the air particle displacement source, and in crickets the escape mode (turn, jump, or turn & jump) was influenced by the direction relative to the cricket (anterior stimuli were less likely to elicit jumping than posterior-directed stimuli) (Tauber and Camhi, 1995; Kanou et al., 1999; Camhi and Tom, 1978). Additionally, while the latency, speed and duration of cricket escape movements were relatively invariant under different stimulus conditions, the *probability* of eliciting escape running was dependant on the behavioral state of the animal- crickets that were already walking were much more likely to respond with escape movements than cricket which were stationary (Gras and Bartels, 1999), though with strong enough amplitudes stimuli almost always elicited escape behavior (Baba et al., 1997).

In cockroaches the escape circuit is better understood. Both vGIs and dGIs send their axons to groups of thoracic interneurons. However, the vGIs have a shorter latency, and are believed to be responsible for simultaneous initiation of the escape movement and inhibition of the dGIs (Plummer and Camhi, 1981; Camhi and Nolen, 1981), but see (Mizrahi and Libersat, 1997). Relatively weak vGI to thoracic connectivity is overcome by the broad directional sensitivity of the vGIs and convergent input onto the thoracics, allowing the vGIs to sum their output. After initiation of escape movement descending input inhibits the vGIs,

which also releases the dGIs from their inhibition. At this later stage in the escape response the dGIs, with their greater directional sensitivity become responsible for the fine control of the direction of escape (Plummer and Camhi, 1981; Camhi and Nolen, 1981).

Although the exact mechanism of signal transduction in the cricket is not known, several of the necessary components from the cockroach circuit seem to be missing, including differential dGI-vGI response latency and vGI-mediated dGI inhibition.

Escape Elicited by Auditory Stimuli.

Although it is not directly related to the cercal system, it is worth mentioning the escape system associated with the auditory system, which has a few parallels with the cercally-mediated escape behavior. Flying crickets exhibit a stereotyped evasive response when presented with stimuli in the ultrasound range, such as that used by echolocating bats (Moiseff et al., 1978). Reception of this ultrasound stimulus is via the tympanal structures on the forelegs of crickets, from where the signal is passed along to the prothoracic ganglion by auditory afferent fibers. From the prothoracic ganglion the signal ascends to the brain via Interneuron 1 (Int-1, also described by Schildberger as AN-2) (Moiseff and Hoy, 1983; Schildberger, 1984b), where it then arborizes into several areas of the protocerebrum which also contain the anterior terminations of the air particle displacement-sensitive giant interneuron system (see figures 1.9 and 1.10). The precise postsynaptic sites for the signal in the brain are not known,

but the circuit in the brain is not very large, as the signal can be measured with short latency from Int-1 in the prothoracic ganglion to the longitudinal dorsal muscles which control the wings (Pollack et al., 1989). As well as triggering evasive responses (negative phonotaxis), the auditory system is also primarily responsible for positive phonotaxis in the case of a female cricket localizing a stridulating male (Nolen and Hoy, 1986). This might also parallel the cercal system, as it is thought that the cercal system might mediate positive phonotaxis in the near field (see section on the cercal system and stridulation, below). If this is the case, then it is possible that both cercal and auditory inputs converge in the brain, where they could take advantage of the same circuitry to either approach a stridulating conspecific or flee a predator. Anatomical and physiological evidence of multimodal convergence support this hypothesis (see section on cercal projections to the brain, above).

Other Cercally-Mediated Behaviors

Initiation of Defense and Touch-Elicited Escape.

Predation attempts do not always evoke an evasive response from crickets- the (relatively) muscular hindlegs of the cricket can be used to lethal effect on smaller predators such as the digger wasp *Liris niger* and wolf spiders (Steiner, 1968; Rovner, 1980; Gnatzy and Heusslein, 1986; Baba et al., 1997). Anti-predator kicks are usually observed in response to high-intensity stimuli such as air particle displacement ~> 2 meters per second, or direct touching of the filiform

hairs (Dumpert and Gnatzy, 1977). This behavior is mediated by the campaniform sensilla, which become active when nearby filiform hairs contact the cuticular wall of their socket, thereby deforming the cuticle in the immediate vicinity. Campaniform sensilla arborize in the ventral and anterior portions of the terminal ganglion, as well as in the sixth abdominal ganglion (Heusslein and Gnatzy, 1987). These areas are closely associated with the bristle neuropil, another sensory system that is sensitive to touch (Murphey, 1985). It is probable that the afferents from these two sets of sensilla act on the same sets of ascending interneurons, namely INs 7-1a, 7-1b, 7-1z, 8-1c, and NGI 13 (Murphey, 1985; Jacobs and Murphey, 1987; Baba et al., 1991), although to my knowledge a behavioral role for these INs has not yet been demonstrated.

A closely related system is the touch-initiated escape circuit of the hindwing of crickets. Touching, pinching, or bending the hindwing elicits escape actions such as running, turning, and jumping (Hiraguchi and Yamaguchi, 2000). These actions are mediated through mechanosensors on the wings themselves, which send afferent information to the metathoracic ganglion (Hiraguchi et al., 2003). In the thoracic ganglia of cockroaches, the same neuronal group which mediates the escape response due to activity of the vGIs also responds to tactile stimuli (Ritzmann and Pollack, 1994; Pollack et al., 1995), which again implies that the separate touch-sensitive and air particle displacement-sensitive modalities converge to take advantage of the same machinery for eliciting behavior.

Flight.

Perhaps related to its role in escape behavior, the cercal system is capable of initiating flight in crickets (Hirota et al., 1993). Crickets are reluctant flyers, and this behavior is somewhat difficult to elicit. Stimulation (at least in the form of intracellular injection into single cells) needs to be to the dGIs, and needs to occur while the cricket's legs are not in contact with a substrate. Initiation of flight by the dGIs was first studied in cockroaches, where it seems to be better developed (Ritzmann et al., 1980; Ritzmann et al., 1982; Libersat et al., 1989), and has also been studied in locusts (Boyan and Ball, 1989) and mantids (Boyan and Ball, 1986).

In addition to initiating flight, the cercal system seems to have a role in helping orient the animals during flight, though this has only been studied in cockroach and locust preparations (Fraser, 1977; Boyan and Ball, 1989). In addition to their cerci, locusts also use facial setae (another mechanosensory receptor) to initiate and control flight, and it seems probable that the cercal and setae systems converge in the brain and so represent two separate sensors mediating the same behavior through similar pathways (Camhi, 1969).

The Problem of Self-Motion.

Constant velocity walking effectively produces constant air movement over a cricket's body (and in particular its cerci), and leg motions themselves create turbulent air flow that can be detected by cercal filiform hairs (Kohstall-Schnell and Gras, 1994). How animals deal with reafference is a question that has been

addressed in several studies in both crickets and cockroaches (Murphey and Palka, 1974; Kohstall-Schnell and Gras, 1994; Delcomyn, 1977; Daley and Delcomyn, 1980; Camhi and Nolen, 1981; Plummer and Camhi, 1981). The consensus view seems to be that the vGIs are inhibited by descending input during motion, while dGIs actually increase their sensitivity due to excitatory input from anterior ganglia. In the case of the dGIs lesion studies were used to implicate that the descending excitation came from motor units, rather than sensory input (Daley and Delcomyn, 1980).

The Cercal System and Stridulation

Cricket Song.

There have been several implications that the cercal system might be involved in the reception of air movement due to stridulatory signals, though relatively little in the way of behavioral evidence (Kämper and Dambach, 1981; Kämper, 1984; Kämper and Dambach, 1985). Nevertheless, it is worth the time to examine the temporal structure of cricket songs and to review the evidence for reception of the temporal properties of the songs by the interneurons of the cercal system.

Male crickets generate songs by repeatedly closing their two raised forewings, with the sound itself being produced by the rubbing of a file on the upper wing along a scraper of the lower wing (Bennet-Clark and , 1989). Each closing movement creates a single unit of the song, called a syllable (see figure

1.11). In chirping crickets such as *A domesticus*, several syllables are grouped together into a secondary unit known as a chirp. The syllable exists in the song as an amplitude modulation of a carrier frequency, with each cycle generated by the impingement of a single tooth from the file on the scraper (Bennet-Clark and , 1989).

In Acheta domesticus the modal values for the calling song are 20 Hz for the syllable repetition rate, with 2-3 syllables per chirp (10-7 Hz chirp rate, respectively), all modifying a 4-5 kHz carrier frequency (Stout et al., 1983). Calling songs from males in our laboratory colony were determined to have a syllable repetition rate of 20.38 Hz, almost exclusively 2 syllables per chirp, and a carrier frequency of 4.7 kHz, although noise in the recordings made the determination of these values difficult (see figure 1.11 A).

Effect of Air Particle Displacement on Male Singing.

One of the first demonstrations of a role for the cercal system in song behavior was that a weak air current can reset the motor behavior underlying singing when a puff of air was applied during the silent period between chirps (Dambach et al., 1983). The original interpretation of this phenomenon is that the cerci of the singing male were stimulated by the movement of his own wings while singing, and that this provided propioceptive feedback to the male enabling him to monitor his own song. Additionally, an increase in the amplitude of the air particle displacement stimulus on the cercus leads to cessation of singing altogether, with the male lowering his wings (Hedwig, 2000). At least the latter

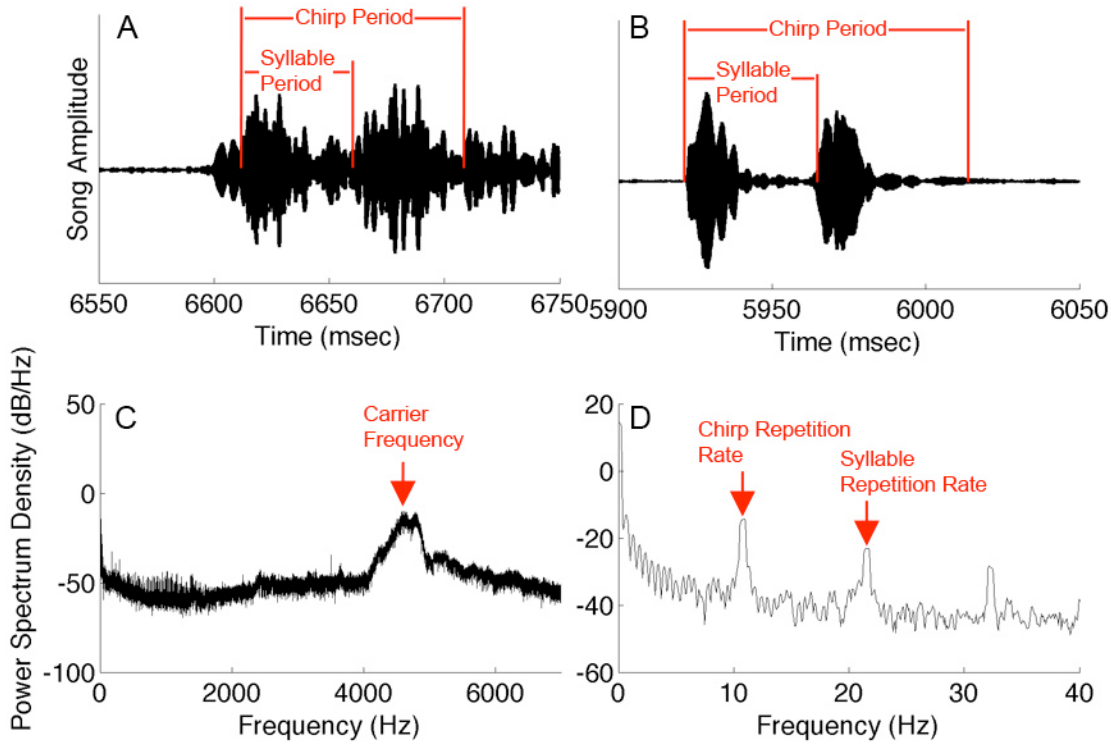

Figure 1.11. Structure of the calling song of *Acheta domesticus.* A, 150 msec sample of calling song for an *A domesticus* male from our laboratory colony, recorded at 22º C. Sample contains a single chirp with two separate syllables. B, 150 msec sample of calling song for an *A domesticus* male from collection at buzz.ifas.ufl.edu/index.htm, recorded in Alachua County, FL at 26.5°C. Syllable period is approximately 43 msec, chirp period is approximately 92 msec. C, power spectra of full 29 sec recording from B. Carrier frequency is approximately 4.74 kHz. D, Expanded power spectra from C, showing frequencies under 50 Hz. Modes corresponding with the chirp repetition rate and syllable repetition rate occur at 10.84 Hz and 23.15 Hz, respectively.

behavior seems to be centrally controlled by cercal input reaching up to the brain before being sent back down to the motor units of the thoracics.

Cercal Reception of Song.

As well as males being able to sense air movement due to their own singing, it is possible that females can also sense air particle displacement due to stridulating males. In several studies approaching this topic, it was found that females could indeed detect air signals due to stridulation from as far away as 15

cm in the lab. From this distance the air particle displacement amplitudes at the female's cerci are as low as 0.03 mm/sec (Kämper and Dambach, 1981; Kämper, 1984; Kämper and Dambach, 1985). Physiological correlates of reception to the air particle displacement generated by stridulation were recorded in the GIs both extra- (Kämper and Dambach, 1981) and intracellularly (Kämper, 1984). Additionally, in unpublished work it was shown that females phonotaxing towards a stridulating male accelerated when within ~20 cm of the caller, perhaps due to the increased directional acuity of the cercal system in comparison with the cricket's auditory system (Dambach and , 1989; Schildberger et al., 1989; Miller et al., 1991).

Importance of the 30 Hz Component in Phonotaxis.

An interesting corollary to the theory that the cercal system might mediate detection of a singing male by a phonotaxing female comes from studies of the relative importance of various components of calling songs in female phonotaxis. It has been shown that the single most important component of a male's song in phonotaxis of *G campestris* is the syllable repetition rate at 30 Hz- the same frequency to which Kämper and Dambach showed that the cercal system is most sensitive. (Weber et al., 1981; Thorson et al., 1982; Loher et al., 1989; Weber et al., 1989; Schildberger et al., 1989). In a similar set of studies in *G bimaculatus and A domesticus*, (Doherty, 1985) and (Stout et al., 1983), confirmed the work of Weber and colleagues, albeit they also showed that other components of the song could also have a strong effect on phonotaxis. Worth mentioning here is

the fact that for *A domesticus* the syllable repetition rate is 20 Hz, while in both species of *Gryllus* it is 30 Hz- see figure 1.11 D, so this section could equivalently be titled “The Importance of the *20* Hz Component” in as far as it pertains to *A domesticus*. It is also advantageous here to recall from figures 1.9 and 1.10 the very close association of the anterior termini of the air particle displacement-sensitive GIs with the BNC in the protocerebrum, as well as the convergent areas of air particle displacement-sensitive and sound-sensitive neurons in the thoracics, which ultimately act on the motoneurons involved in phonotaxis as well as air particle displacement- and sound-mediated escape behavior. This anatomical as well as physiological evidence at least leaves open the possibility that the cercal system is involved in mediating phonotactic behavior.

Analogy to Signaling in *Phaeophilacris spectrum*.

Analogous to the apparent reception of air particle displacement due to song behavior in stridulating crickets (and actually preceding and inspiring those studies), it has been shown that the non-stridulating phalangopsidan *Phaeophilacris spectrum* uses air movement exclusively for intra-specific communication. This is done for both male-male and male-female communication, and is accomplished by forward flicks of the male wings in order to produce vortices (males of this species lack files and scrapers on their wings, rendering stridulation impossible). These signals are then transduced through the air particle displacement-sensitive machinery in the cercus and terminal abdominal ganglion (Kämper and Dambach, 1979; Heinzel and Dambach, 1987;

Heidelbac et al., 1991).

Cautionary Note.

Although it is tempting to believe that reception of calling songs is in part mediated by the cercal system, it is worth noting that there is no behavioral experiment which corroborates this theory (other than the unpublished work of Dambach, (Dambach and , 1989)). In fact, the work of Pollack and colleagues (Pollack et al., 1998) came up with a negative result- crickets of the species *T oceanicus* were tested in various ways for a cercal role mediating mating behavior. It turned out that for a male to successfully initiate copulation with his courtship song, neither the females cerci, nor the air currents produced by the male were necessary. Although this does not preclude a role for the cerci in phonotactic (as opposed to copulatory) behavior, it is an important point to keep in mind when considering what roles the air particle displacement-sensitive cercal system might play in behavior beyond the well-stereotyped escape response.

Discussion of Cercal System Form and Function

The emerging picture of the cercal system and its associated behaviors is fairly complex. Air particle displacement directed at the cerci can elicit at least 14 distinct responses, including evasion, flight, offensive reactions, scanning, freezing, and various reactions during male stridulation, and response can depend on the behavioral state of the animal as well as the context of the

environment (Baba et al., 1997). In addition to air particle displacement stimuli, the cercal system is responsible for mediating behavior related to orientation relative to gravity as well as a variety of touch and chemotactic sensations (Sakaguchi and Murphey, 1983; Murphey, 1985; Heusslein and Gnatzy, 1987).

Appropriate for a structure responsible for such a diverse array of behavior, the physiological and morphological characteristics of the cercal system are equally complex. Although dendritic structure of interneurons can account for a wide variety of their response properties, interneurons which should solely mediate touch and gravity sensitivity also have directionally sensitive to air particle displacement (e.g. INs 7-1a and 7-2a respectively, personal observation). Information processing in the TAG is not only feed-forward from the afferents, but also extensively lateral within the local interneuron populations, and includes significant effects from descending input. Differences in behavior between walking and standing can drastically alter the firing rates of the ascending interneurons, and information from those interneurons is generally fed into centers of multimodal convergence where they combine with further mechanoreceptive, olfactory, visual, and especially auditoy input.

Finally, while many of the gross elements of the cercal system are consistent across orthopteran species, evolution has provided a striking diversity in form, physiology, and behavioral function among the different cercal systems that have been studied.

Although this intricacy somewhat dampens the ideal of the ‘simple’

invertebrate sensory systems (and complicates analysis!), it also allows for much richer experiments, with proportionally richer insight into the functioning of complex biological systems as a potential reward.

REVIEW OF APPROACHES TO THE NEURAL CODING PROBLEM

Tuning Curves

For the purposes of this thesis, neural coding is defined as the mapping between stimuli in the environment and their representation in patterns of electrical activity in the nervous system. The earliest efforts toward discovering the nature of these mappings stretch back over 80 years to the work of Adrian and colleagues on stretch receptors in the leg muscles of frogs (Adrian and Zotterman, 1926). They employed what is now known as the tuning curve technique- a stimulus is presented to the nervous system in which a single parameter can be systematically varied over the course of several trials. For each presentation of the stimulus with a specific value of the parameter of interest, an output of the nervous system is measured, generally a count of the number of action potentials in a small window of time during or after the stimulus presentation. Other tuning curve metrics include the time to the first discriminable response, or, inversely, the mapping is reported as the minimum value of a stimulus parameter that elicits *any* activity in the nervous system. Solving the neural coding problem is then just reduced to determining the input-output relationship defined by the function relating the values of the stimulus parameter to the measured output of the cell. An example of such a relationship- the directional tuning curve of interneuron right 10-2a from *A domesticus*- is shown in figure 2.1.

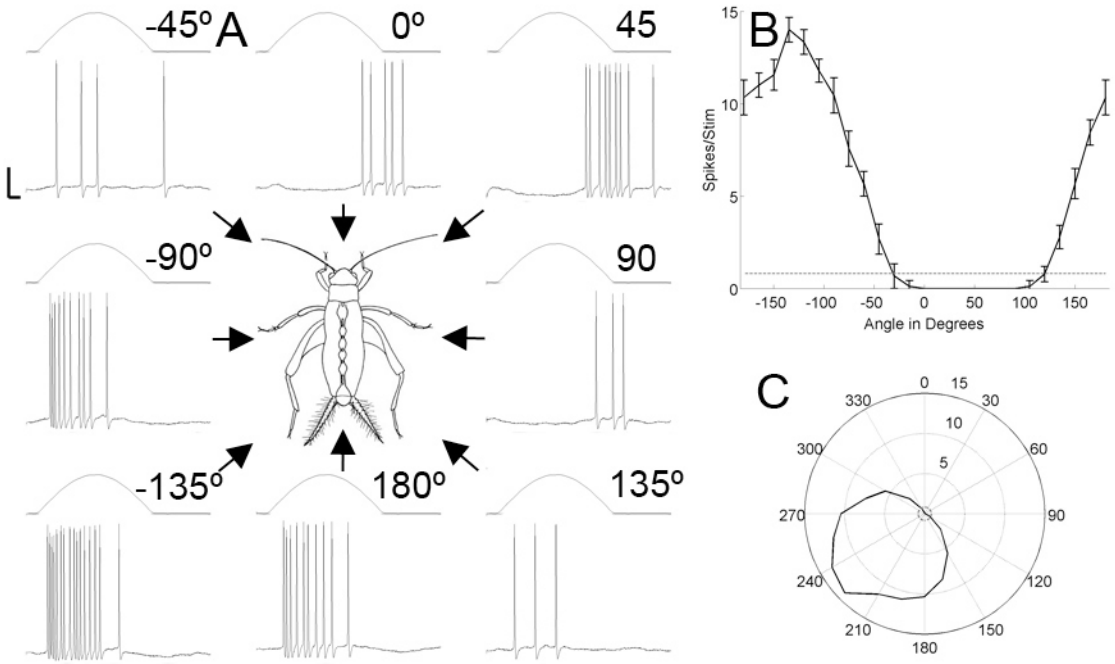

Figure 2.1. Directional tuning curve for interneuron 10-2a. A, single puffs of air from eight different directions relative to the cricket (top traces) elicit various patterns of spiking activity (bottom traces) in an interneuron of class R10-2a. Scale bar: x- 10 msec, y- 875 mm/sec (stimulus)/10 mV (intracellular membrane potential). B, to generate the tuning curve the same cell from A was presented with ten stimuli from each of 24 different directions in the horizontal plane (15º separation between samples). The number of spikes elicited in the 60 msec window following stimulus onset were counted for each trial, and mean and standard deviation across trials is shown as a function of stimulus direction. The spontaneous firing rate of the cell was also determined, and the gray dotted line shows the expected number of spontaneous spikes in a 60 msec window. Note that stimuli from angles -15º to 105º inhibit the firing activity of this cell below the spontaneous rate, which can also be seen as a slight hyperpolarization in the membrane potentials of A. C, the mean values from B, plotted in polar instead of cartesian coordinates.

Although simple to use, the method relies on two rather strict set of assumptions. First, it is assumed that a single, generally static parameter of the stimulus is important for the nervous system. This can be a problem when the nervous system actually depends on a dynamic stimulus, or a stimulus which can not be easily parameterized. Second, the choice of how the response is measured necessarily requires a strong assumption about the nature of the code

itself- usually that the information about the stimulus is completely contained in the firing rate.

In spite of its limitations, the tuning curve methodology has enjoyed wide use as a tool in neuroscience, for instance being used in the work on information processing in the visual system that eventually garnered David Hubel and Torsten Wiesel the Nobel Prize in Physiology and Medicine. The method has been extensively used to demonstrate the directionality of the cercal system, beginning with the use of directional oscillatory sound stimuli (Tokareva and Rozhkova, 1973; Edwards and Palka, 1974; Palka et al., 1977; Palka and Olberg, 1977), and later being refined to stimuli consisting of single puffs of air (Westin et al., 1977; Tobias and Murphey, 1979; Westin, 1979; Bacon and Murphey, 1984; Bodnar et al., 1991; Baba et al., 1991; Baba et al., 1995; Kolton and Camhi, 1995).

In an elegant set of experiments, the contribution of individual dendrites (and their presynaptic afferent and local interneuron populations) to the emergent directional tuning of interneurons was elucidated by means of killing various dendrites using photoablation techniques and then measuring the consequent changes in the cells' tuning curves (Miller and Jacobs, 1984; Jacobs and Miller, 1985; Jacobs et al., 1986; Jacobs and Miller, 1988; Bodnar et al., 1991).

In another set of experiments, it was shown that two bilateral pairs of interneurons (DGIs 10-2a and 10-3a) formed a functional unit capable of detecting air particle displacement at moderate velocities from all 360º of space

in the horizontal plane (Miller et al., 1991; Theunissen and Miller, 1991). Similarly, by statistically sampling the cercal afferent population, Landolfa and colleagues were able to determine the directional sensitivity of the entire afferent array (Landolfa, 1992; Landolfa and Miller, 1995; Landolfa and Jacobs, 1995) (figure 1.4). These population-level tuning curves have in turn led to theoretical work on how neural coding is implemented in populations of neurons, both in interneurons (Salinas and Abbott, 1994; Butts and Goldman, 2006) and the afferents (Ergun et al., 2007).

These studies spanned the system from the receptor level through the local and projecting interneurons of the terminal abdominal ganglia, though most of the studies with air particle displacement stimuli (rather than oscillatory sound stimuli) focused on GIs 10-2a and 10-3a. For the sake of completeness, average tuning curves elicited by air particle displacement stimuli for 222 cells (127 of whose morphology was confirmed by staining) from classes 8-1a, 9-1a, 9-1b, 10-1a, 7-2a, 8-2a, 9-2a, 9-3a, 10-2a, and 10-3a are shown in figure 2.2. vGI 11-1a was never recorded from in over 500 recordings, but has been reported to be sensitive to multiple stimulus directions and especially stimuli with angular velocity (i.e. vortices, Kämper, 1984; Baba et al., 1991, labeled as 11-1c in the former and NGI-5 in the latter study). Panel 2.2 C shows the peak directions for all of the giant interneurons with unimodal tuning (compare with the directionality of the afferent layer in figure 1.4).

As detailed in (Miller et al., 1991), the four INs composed of left and right 10-

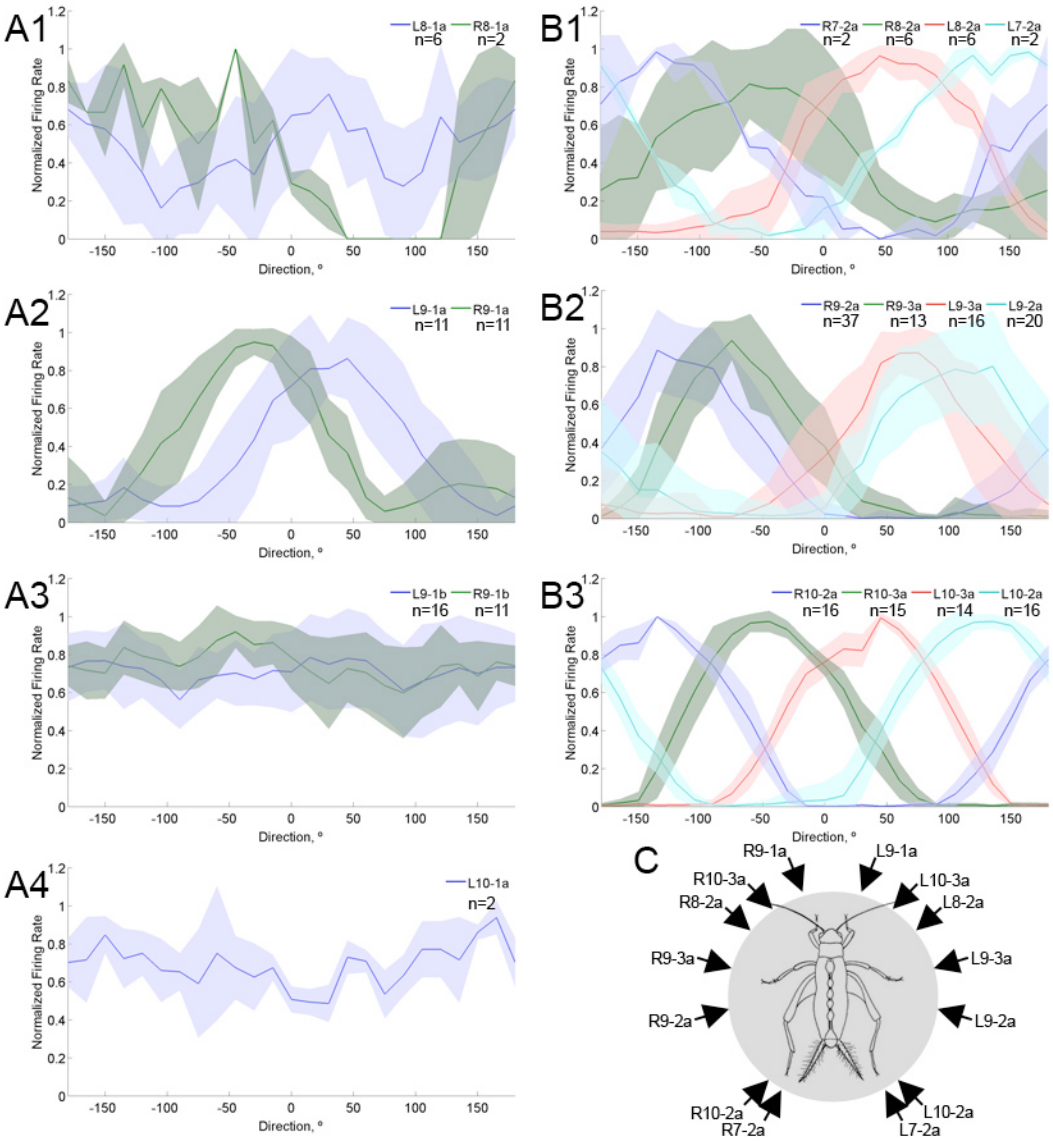

Figure 2.2. Directional tuning curves for vGIs and dGIs. A, Mean Cartesian tuning curves for interneurons with axons in the ventral group, with amplitude normalized to maximal firing rate. The shaded background represents ± 1 STD across the populations of specified neurons. A1, 8-1a (MGI); A2, 9-1a (LGI); A3, 9-1b; A4, 10-1a. B, Mean Cartesian tuning curves for dGIs, grouped into potential functional units (data format as in A). B1, 7-2a & 8-2a; B2, 9-2a & 9-3a; B3, 10-2a & 10-3a. C, representation of peak directional selectivity of all GIs with unimodal directional tuning in relationship to the cricket.

2a and left and right 10-3a form a functional unit sensitive to low velocity air displacement from all 360º of directional space in the horizontal plane (figure 2.2

B3). It has been speculated that INs 9-2a and 9-3a may form a second such functional unit sensitive to higher velocities of air movement (Miller et al., 1991). The data in figure 2.2 B2 confirms that the opposing pairs of this quartet (i.e. R9-3a and L9-2a, L9-3a and R9-2a) do indeed lie on the same axis within the horizontal plane, but also shows that such a functional unit would have a range of restricted sensitivity in the regions from -50º to 50º and from 150º to 150º due to the non-uniform spacing of the peak sensitivities (see (Theunissen and Miller, 1991)). GI 7-2a (and probably GI 8-2a) receives input from the clavate hairs and so is sensitive to acceleration due to gravity (Sakaguchi and Murphey, 1983), but here and in other studies (Kämper, 1984; Kohstall-Schnell and Gras, 1994) it was also found to respond to air particle displacement at sufficiently large stimulus levels. Along with 8-2a, 7-2a has directional tuning such that the two pairs of cells could form yet another functional unit, sensitive to very high intensity air particle displacement (figure 2.2 B1).

White Noise, Kernels, Stimulus Reconstruction & Information Rates

A second approach to the coding problem is the ‘white noise’ approach of Wiener, popularized for use in neuroscience by Marmarelis and colleagues (Wiener, 1958; Marmarelis and Naka, 1972). The goal in this methodology is to try and predict the output of a potentially nonlinear system to a stochastic input signal, usually gaussian white noise (GWN). The prediction is accomplished by taking a series expansion of the form:

$$y(t) = \sum_{n=0}^{\infty} G_n\left[h_n, x(t)\right] \tag{2.1}$$

where $x(t)$ is the input signal, $y(t)$ is the output signal (e.g. a neural spike train, or time series of membrane potential in the case of non-spiking cells), h_n are the basis functions ('Wiener kernels'), and G_n are orthogonal functionals. In neuroscience only the first three terms in the expansion are generally used, taking the following form:

$$G_0 = h_0 \tag{2.2}$$

$$G_1 = \int_0^{\infty} h_1(\tau)(t-\tau)d\tau \tag{2.3}$$

$$G2 = \int_0^{\infty}\int_0^{\infty} h_2(\tau_1,\tau_2)(t-\tau_1)(t-\tau_2)d\tau d\tau - P\int_0^{\infty} h_2(\tau,\tau)d\tau \tag{2.4}$$

where P is the power density spectrum of $x(t)$. The kernels themselves can be expressed in the following form, assuming GWN input:

$$h_0 = \langle y(t) \rangle \tag{2.5}$$

$$h_1(\tau) = \frac{1}{P}\langle y(t)(t-\tau) \rangle \tag{2.6}$$

$$h_2(\tau_1\tau_2) = \frac{\langle \{y(t) - h_0\}(t-\tau_1)(t-\tau_2) \rangle}{2P^2} \tag{2.7}$$

where $\langle . \rangle$ denotes the average over time.

The 'white noise approached' (named after the stimulus most commonly used) has been used extensively in neuroscience, providing a useful (if simple) model for the signal transduction from stimuli to neural responses.

Simplifications to the model include replacement of the second and higher order terms with cascade models including a thresholding non-linearity (Bryant and Segundo, 1976; Chichilnisky, 2001; Simoncelli et al., 2004; Paninski et al., 2004), as well as other methods (such as spike-triggered covariance) which are aimed at reducing the dimensionality of the input system (de Ruyter van Steveninck et al., 1988; Sharpee et al., 2004; Schwartz et al., 2006; Pillow and Simoncelli, 2006; Fairhall et al., 2006).

The white noise approach was first used to study the cercal system in experiments on the afferent layer and local non-spiking interneurons of the cockroach (Kondoh et al., 1991a, Kondoh et al., 1991b). For the afferent layer the first and second order kernels together provide a very good fit to experimental data, while in the local interneuron the first and second order filters combined only describe about half of the neural response (the contribution of the second order filter in this case is negligible), following a general trend of greater computational complexity in layers farther removed from the sensor periphery.

Traditional white noise analyses offer a substantial improvement over conventional tuning curve approaches, both in terms of the complexity of the stimulus that can be used as well as its descriptive power in modeling spiking behavior. However, among its shortcomings were difficulties in dealing with non-linearities involved in spike generation and quantitative comparisons between experiment and prediction. In a novel solution to these issues Bialek and colleagues approached the problem from the organism's viewpoint. Rather than

trying to model the *encoding* problem (i.e., how stimuli get transduced to neural output), their method addresses *decoding*: trying to estimate the stimulus that elicits a specific spike train (Bialek et al., 1991; Rieke et al., 1997). Although the math is essentially the same (in this case the neural response becomes the input variable, while the 'output variable' that is being estimated is the stimulus), many systems that have highly non-linear encoding can be decoded using only first-order linear kernels (Rieke et al., 1997). This approach enables elements of information theory to be brought into the analysis, allowing differences between stimulus and estimates to be quantified in terms of bits (Shannon, 1948; Cover and Thomas, 1991).

Since its inception this new approach (termed 'reverse reconstruction' to denote its inversion of the more traditional white noise analyses) has been widely used to investigate coding in the first two layers of the cercal system. In work in conjunction with Bialek and colleagues during the development of the reverse reconstruction methodologies, mechanical stimulation of the cercal hairs with band-passed GWN (150 Hz bandwidth) elicited spiking activity in the 150 Hz range, which could be decoded to obtain up to 300 bits per second about the stimulus (Warland et al., 1991). This is equivalent to being able to answer two 'yes or no' questions about the stimulus in a single period of the highest frequencies present, simply by observing the spike train). Results from other reverse reconstruction-based investigations in the cercal system include: a study of frequency sensitivity to broadband (10-400 Hz) stimuli showing that the four

cell ensemble of left and right 10-2a and 10-3a have identical frequency tuning, concentrated in the 10-50 Hz range (Theunissen et al., 1996); a similar study showing differential frequency tuning between afferents innervating different length filiform hairs, with the afferents that innervate shorter hairs being sensitive to higher frequency stimuli while the afferents associated with the longest hairs approximately match the frequency tuning of GIs 10-2a and 10-3a (Roddey and Jacobs, 1996); a study showing stochastic resonance in GIs 10-2a and 10-3a near their threshold detection level (Levin and Miller, 1996); a study of the effects of adaptation on coding in the projecting interneurons, which showed a decrement in the stimulus-response coherence above 70 Hz after adaptation to a broadband white noise stimulus (Clague et al., 1997); and finally a study showing combined directional and frequency tuning for the four cell ensemble of 10-2s and 10-3s stimulated with two-dimensional white noise, which confirmed earlier speculation on how these cells code for these stimulus parameters (Girish, 1998).

The version of reverse reconstruction methodology derived in (Theunissen et al., 1996) is demonstrated on data from INs 10-2a and 10-3a in figure 2.3. The reconstruction kernel in the frequency domain, $H(f)$, is obtained from a simultaneous recording of 10-200 Hz band-passed GWN air particle displacement and neural response (figure 2.3 A lower and upper panels, respectively) according to:

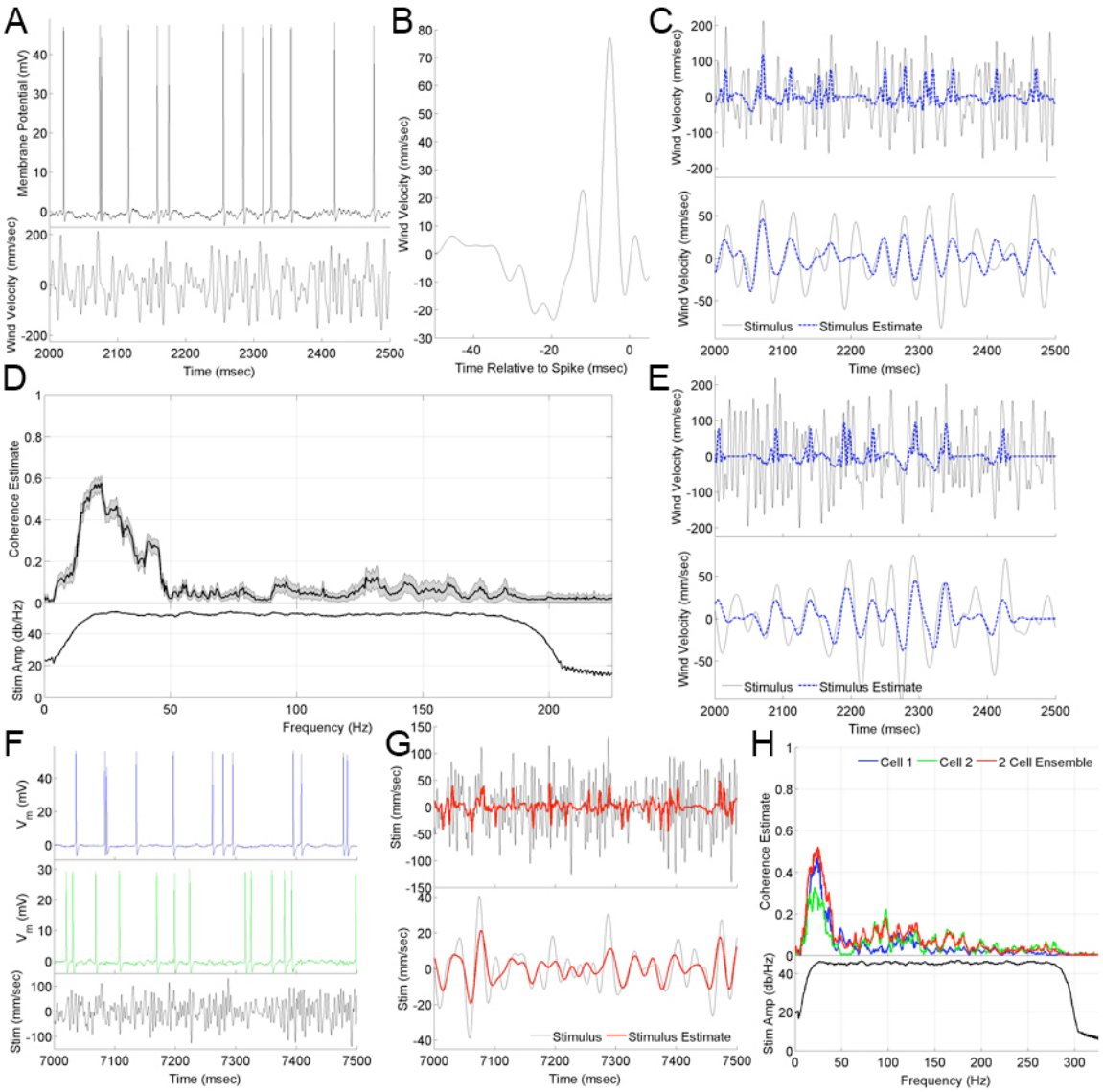

Figure 2.3. Stimulus reconstruction and coherence measures. A, 500 msec of recording of 10-200 Hz band-passed Gaussian White Noise (RMS=73 mm/sec) stimulation (lower panel and elicited response (upper panel) in an R10-2a (same cell as in figure 1.12). B, linear kernel obtained from full 100 seconds of simultaneously recorded stimulus and response data. C, stimulus from panel A (black) and best linear estimate obtained from stimulus reconstruction using kernel in B (dashed blue line). The upper panel shows the full stimulus and stimulus estimate, lower panel shows both after low-pass filtering below 50 Hz. D, upper panel- stimulus-response coherence mean (black line) ± 1 STD (gray background), calculated over 10 repeats of stimulus. D, lower panel- power spectra of stimulus (upper and lower panels calculated from data in panel A). E, stimulus reconstruction using kernel from panel B on a test data set where the stimulus was drawn from the same statistical distribution as the stimulus in A (upper and lower panels same convention as in C). F, 500 msec of simultaneous recording of R10-2a (blue, not the same cell as panel A) and L10-3a (green) in response to a 10-300 Hz band-passed Gaussian White Noise stimulus (lower trace, RMS=43 mm/sec).

Figure 2.3 continued. G, estimated reconstruction of stimulus in F using combined kernel from R10-2a and L10-3a (upper and lower panels same convention as in C and E). H, upper panel- coherence curves form data in F obtained using only cell R10-2a (blue), only cell L10-3a (green), and both cells together as a functional unit (red). H, lower panel- power spectra of stimulus from panel F.

$$H(f) = \frac{\langle R^*(f)S(f)\rangle}{\langle R(f)R^*(f)\rangle} \tag{2.8}$$

where $R(f)$ and $S(f)$ of denote the fourier transforms of the neural response and the stimulus, respectively, and R^* represents the complex conjugate of R. In the case of spiking neurons the response function in the temporal domain is generally reduced to a binary function where a value of 1 indicates a spike occurred at time t, and a value of 0 indicates no spiking activity at that time. Note that equation 2.8 is equivalent to the fourier transform of the first order Wiener Kernel (eqn 2.6), with the response as the input variable and the stimulus as the output variable. The reconstruction kernel in the temporal domain, $H(t)$, is obtained from $H(f)$ through an inverse fourier transform (figure 2.3 B). The kernel is then used to obtain an estimate of the stimulus waveform through convolution with the response function in the temporal domain:

$$S_{est}(t) = \int H(\tau)R(t-\tau)d\tau \tag{1.9}$$

The estimate of the stimulus can then be compared with the actual stimulus (figure 2.3 C, upper trace). In practice the cell's ability to reconstruct the stimulus is restricted to a smaller bandwidth than that of the stimulus itself. In this case much of the difference between stimulus and stimulus estimate is due to the stimulus bandwidth which is higher (or lower) than what the neuron can follow. In

this case, visualization of the difference between the stimulus and stimulus estimate at the frequencies relevant to the cell can be accomplished by filtering both (figure 2.3 C, lower trace).

A compact description of the error in the stimulus reconstruction in the frequency domain is the gain function:

$$g(f) = \frac{S_{est}(f)}{\left[S(f) + N(f)\right]} \tag{2.10}$$

where $N(f)$ is the effective noise in the reconstruction. Equation 2.10 is a valid measure for reconstructions where kernels of any order are used. In the case of the linear reconstruction (only the first order kernel is used) employed in figure 2.3, the gain function is equivalent to the magnitude squared coherence function shown in figure 2.3 D:

$$\gamma^2(f) = \frac{\langle S(f)R^*(f)\rangle\langle S^*(f)R(f)\rangle}{\langle S(f)S^*(f)\rangle\langle R(f)R^*(f)\rangle} \tag{2.11}$$

Both of these equations show, on average, how well a frequency in the stimulus estimate matches a frequency in the original stimulus, on a 0 to 1 scale. Coding accuracy can then be described in units from information theory by using Shannon's equation for capacity in a Gaussian information channel and the relationship between gain/coherence and the signal-to-noise ratio from equation 2.10:

$$I(R,S) = \int \log_2\left[\frac{S(f) + N(f)}{N(f)}\right] df = -\int \log_2\left[1 - \gamma^2(f)\right] df \tag{2.12}$$

This will provide an accurate lower bound estimate on the information rate

between stimulus and response, provided assumptions about the Gaussian nature of the stimulus, response and noise terms are all accurate (Cover and Thomas, 1991; Rieke et al., 1997; Shannon, 1948; Theunissen et al., 1996). In the case of the cell in figure 2.14 D, the lower bound on the information rate was determined to be 36.6 ± 1.9 bits/second.

In theory, estimating the stimulus from the same data set that was used to build the filter can be subject to the problem of overfitting the model to the data. Since the coherence function always effectively uses the same model and test data, this could potentially be a problem. In figure 2.3 E a distinct stimulus from the one that was used to estimate the filter function (but drawn from the same Gaussian distribution) was used in the reconstruction. Here the quality of the reconstruction is approximately the same whether or not the test stimulus is the same as that used to build the filter, indicating that overfitting the kernel was not a concern (compare 2.3 C and E).

In many cases cells have a directional selectivity, and so can only effectively reconstruct the positive (or negative, depending on convention used) portions of the stimulus. This can be seen by observation of the kernel function in figure 2.3 B, where most of the power in the kernel lies above zero, and in the reconstructions in the top panels of 2.3 C and E. One method of taking this into account for reconstruction analysis is to half-wave rectify the stimulus before comparing it to the reconstruction. Another way to get around this problem is to consider pairs of neurons with opposite directional sensitivities as a functional

unit, rather than single neurons. In the case of GI 10-2a, the contralateral 10-3a cell has the exact opposite tuning, and so a functional unit consisting of both cells can be used to reconstruct the entire stimulus waveform. Figure 2.3 G and H shows the reconstruction and coherence function from a simultaneously recorded right 10-2a and left 10-3a. The reconstructions capture both the sharp positive and sharp negative aspects of the original stimulus, and the coherence of the combined unit is larger than the coherence of either individual cell.

The use of the coherence method to measure stimulus-response fidelity led to a new criteria for examining how well a specific reconstruction compared with an optimal model (Haag and Borst, 1997), (Girish, 1998). In the case of linear stimulus reconstruction this involves comparing the coherence function between stimulus and response with the square root of the coherence function between two responses elicited by separate presentations of an identical stimulus. In the case of a purely linear system, the coherence function will match the square root of the response-response coherence. The degree to which there is a difference between the two curves indicates the non-linearity of the system. In the case of reconstructions of greater than first order, the gain function (eqn 2.10), should be used, in which case the resulting interpretation is an indication of whether or not higher order kernels should be used in the analysis (the analysis already assumes non-linearity by having kernels of higher than first order).

The intuitive rational for using the square root of the response-response coherence (rather than just the response-response coherence) is that in order to

find two responses related to a single stimulus through reconstruction in a completely linear system, two reconstructions would need to be performed (a reverse reconstruction to go from one response to the stimulus, and a forward reconstruction to go from that stimulus to a second sample of the response). Each transformation step would be subject to independent additive noise, and so would be doubly degraded by noise relative to a single reconstruction. A mathematically rigorous derivation of the method is presented in section 1.6 of (Girish, 1998).

The difference between the square root of the RR coherence and the reconstruction gain provides an indication of how much better an optimal model could do than the current model. In the case of reverse reconstruction with the linear (first order) filter, this difference gives an idea of how much better the reconstruction could become by adding in an 'optimal' number of higher order kernels (without explicitly describing how many filters would be needed). This method has been applied to cells in the fly visual system (Haag and Borst, 1997), to the electric sense organ of electric fish (Chacron, 2006), to cat retinal ganglion cells (Passaglia and Troy, 2004), to cricket auditory neurons (Passaglia and Troy, 2004), and to the afferent layer of the cricket (Roddey et al., 2000). In the latter case it was shown that for high stimulus intensities the linear model was not an accurate representation of neural encoding. The method is applied to GIs 10-2A and 10-3a (n = 40 cells) in figure 2.4A. Note the gap between the SR and √RR coherence estimates at frequencies between ~30 and ~125 Hz, indicating

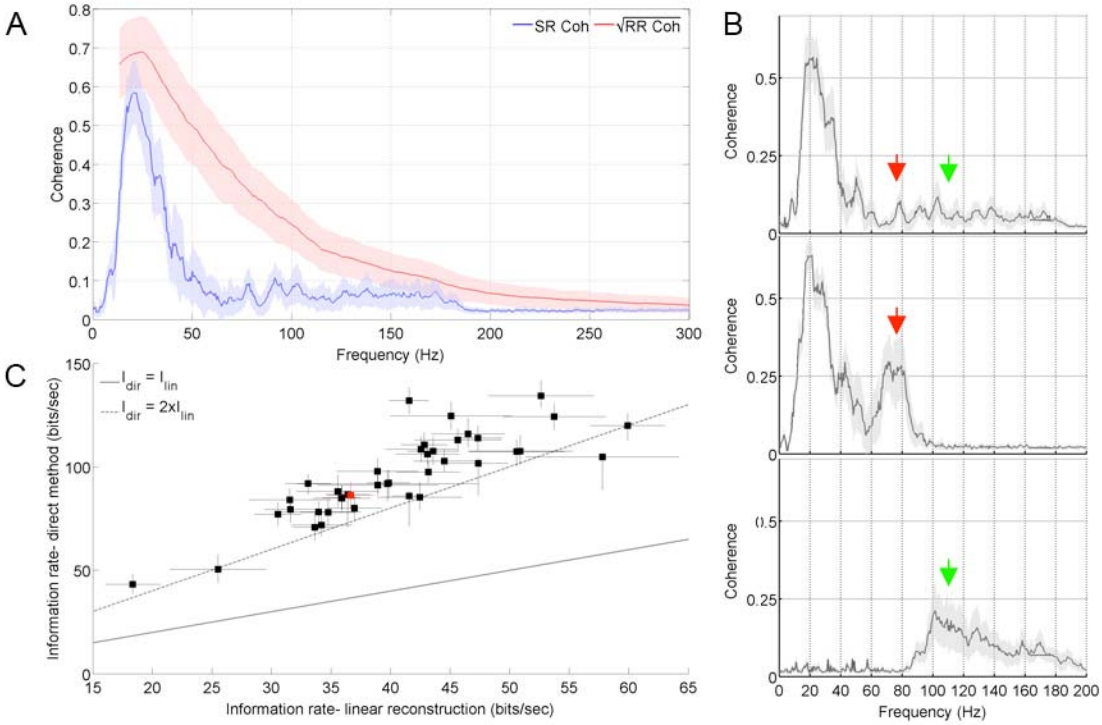

Figure 2.4. Failures of the linear reconstruction approach. A, comparison of stimulus-response (blue) and √response-response (red) coherencies. Dark lines represent coherence curves averaged across n = 40 cells, bands represent ± 1 STD of ensemble. B, Non-linearities associated with different bandwidth of stimulation. Top panel, SR coherence to 0-200 Hz band-passed GWN; middle panel, SR coherence to 10-100 Hz stimulation; bottom panel, SR coherence to 100-200 Hz stimulation. Curves represent mean ± 1 STD across population of 17 cells. A perfectly linear system would encode each frequency separately- here responses to ~70 Hz stimulation (red arrow) and ~115 Hz stimulation (green arrow) are significantly altered depending on the presence or absence of higher or lower frequency stimuli, respectively. C, comparison of information rates from stimulus reconstruction and direct method measurements in the dGIs. Error bars on linear reconstruction information estimate are STD across trials, error bars on direct method estimate represent 95% confidence intervals from bayesian parameter estimation, based on method of (Kennel et al., 2005). Information of neuron from figure 2.3 A-E is shown in red.

that a linear model does not adequately account for the information available in the response power spectra at these frequencies.

Another method of analysis which considers the stimulus-conditioned response variability is the 'direct method' estimate of the mutual information

between the stimulus and response (de Ruyter van Steveninck et al., 1997), (Strong et al., 1998). Recall that in the estimate of mutual information introduced earlier (equation 2.12), several criteria had to be met before the estimate became an accurate lower bound on the mutual information. The direct method avoids these issues by calculating the information in a manner that makes many less assumptions. The direct method calculates information based on the difference between unconditional and conditional entropies as derived in (Shannon, 1948):

$$I(R,S) = H(R) - H(R \mid S) \tag{2.13}$$

where $H(R)$ measures the (discrete) entropy of the response:

$$H(R) = \sum_r P(r)\log_2\left(P(r)\right) \tag{2.14}$$

and $H(R|S)$ measure the discrete entropy of the response conditioned on the stimuli:

$$H(R \mid S) = \left\langle \sum_r P(r \mid s)\log_2\left(P(r \mid s)\right) \right\rangle_s \tag{2.15}$$

where $\langle . \rangle_s$ denotes the average over all stimuli. While conceptually much simpler, the direct method is subject to biases due to trying to estimate probabilities based on the finite data available in an experiment. Several methods to adjust for these biases exist (Victor, 2002), (Paninski, 2003), (Nemenman et al., 2004), (Kennel et al., 2005), (Shlens et al., 2007), and this sort of methodology has been robustly applied to data in neuroscience. In the case where the stimulus used is Gaussian, the estimates of mutual information can be compared between direct method and reconstruction-based calculations. Such a comparison has

Preparation	Inf Method	Inf Rate	Inf Ratio	Reference
Fly H1*	Rev Recon	64 b/s	2.5**	(Bialek et al., 1991)
	Direct	81 b/s		(de Ruyter van Steveninck et al., 1997)
Salamander Retina	Rev Recon	3.2 b/s	~3	(Warland et al., 1997)
	Direct	~9.6 b/s		(Meister and Berry, 1999)
Cat Retina‡	Rev Recon	61.1/62.2 b/s	1.4/1.8	(Passaglia and Troy, 2004)
	Direct	82.5/109.2 b/s		
Cat Thalamus	Rev Recon	~1 b/spike	3-4	(Reinagel et al., 1999)
	Direct	~3-4 b/spike		(Reinagel and Reid, 2000)
Macaque MT	Rev Recon	5 b/s	2.5	(Buracas et al., 1998)
	Direct	12.5 b/s		
Fish ELL†	Rev Recon	14.7/25.2 b/s	1.6/2.1	(Chacron, 2006)
	Direct	23.1/52.9 b/s		
Cricket Cercal INs	Rev Recon	41.1±7.8 b/s	2.3±0.1	Figure 1.15c
	Direct	96.7±19.8 b/s		

Table 2.1. Comparison of linear and direct estimates of information rates in various sensory Systems. * The estimate of information rate from linear reconstruction for H1 was actually based on an artificial left/right pair, while the direct method estimate was for a single neuron. The ratio of direct estimate/linear reconstruction estimate was based on one-half of the linear reconstruction, as estimates from such artificial pairs tend to double the information estimate from a single cell (Theunissen et al., 1996). ‡Cat Retinal cells were split into four physiological categories- on and off X cells, and on and off Y cells. In this table the four categories were summarized by two numbers, with on and off X cells lumped into one category (numbers on the left), and on and off Y cells placed in a second category (numbers on the right). †The electric fish ELL was stimulated with two different, behaviorally-relevant stimulus geometries: local geometry corresponding to prey signals (numbers on the left), and global geometry corresponding to conspecifics signaling (numbers on the right).

been performed on the forty GIs from figure 2.4 A, with the results shown in figure 2.4 C, and summarized in table 2.1. Note that in almost every case in figure 2.4 C, the estimate from the direct method is at least twice that of the estimate based on reconstruction, and that across the forty cells the average ratio is well above 2. This indicates that on average the stimulus-reconstruction approach is failing to account for over half of the information about the stimulus that is available in the spike train. This includes information due to correlations in

temporal patterns of the response, which are ignored in linear reconstruction methods. For the data in figure 2.4 C, a linear regression was performed. The regression coefficient and a ± 95% confidence interval are shown in table 2.1, along with data from experiments comparing the information estimates from these two methods in several other systems. Note that the ratio between the two information estimates are fairly consistent across a wide variety of animals and sensory modalities, with values ranging from 1.5-3, meaning that linear estimates miss about 33-67% of the information available in the spike trains.

This last metric begins to address a controversy that has embroiled the field of neural coding for years- the distinction between temporal and rate coding. Generally speaking, a temporal code exists in a neural system when higher frequency (and shorter ISI) neural patterns represent lower frequency stimuli (Theunissen and Miller, 1995). Conversely, rate coding (specifically, linear rate coding) exists when the frequencies in the response are matched to the frequencies in the stimulus. This last characteristic is assumed in linear reverse reconstruction, consequently when direct method information estimates match estimates from linear reverse reconstruction, it can be deduced that the coding involved is purely linear. Unfortunately, the reverse (that differences between direct method and linear reconstruction estimates implies temporal coding) does not hold, as there are other potential categorizations of coding such as non-linear rate codes (Borst and Theunissen, 1999; Buracas et al., 1998; Passaglia and Troy, 2004).

Quantization Methods

A final set of analyses for neural coding is the quantization methodology, as derived and applied to neuroscience separately by Tishby and colleagues (Tishby et al., 1999; Slonim and Tishby, 2000; Schneidman et al., 2001; Friedman et al., 2001; Slonim et al., 2002), and Dimitrov and colleagues (Dimitrov and Miller, 2001; Dimitrov et al., 2001; Dimitrov et al., 2003; Gedeon et al., 2003; Parker and , 2003; Mumey et al., 2004; Gedeon et al.). In this methodology the response and stimulus space are clustered into a reduced reproduction set in such a way so as to retain as much of the information between the two spaces as possible. This is done through minimization of a distortion measure (D_I for the method of Dimitrov and colleagues, $\mathcal{L}$ for the 'Information bottleneck' method of Tishby and colleagues), which quantifies how much of the mutual information between the response space R and the stimulus space S is lost due to clustering into N classes (N is less than the actual dimensionality of the response, which in principle is unkown):

$$D_I(R,R_N) = I(S;R) - I(S;R_N) \tag{2.16}$$

and:

$$\mathcal{L}\left[p(r_N \mid r)\right] = I(R;R_N) - \beta I(S;R_N) \tag{2.17}$$

Minimization of the distortion function guarantees that the information between the clustered response and stimulus will be maximal given the constraints of data available. Optimizations and implementations for these methods can be found in

the above references.

One of the advantages of this method is that no assumptions about the coding scheme are made implicitly in the formulation of the problem, and so the stimulus-response clusters can be related through e.g. a linear rate code, a non-linear rate code, or a temporal code. The combination of minimal assumptions and maximal information makes quantization approaches potentially very powerful.

The quantization methodology is somewhat similar to the metric space and related approaches developed by Victor and colleagues (Victor and Purpura, 1996), (van Rossum, 2001), in that in both cases temporal patterns of spike activity and stimuli are jointly clustered, though in the metric space approach the clustering of the stimulus space is explicitly performed by the researcher during the experiment, while the response space is clustered according to a temporal precision parameter which determines how closely related are two response sequences.

In figure 2.5 the quantization method from (Dimitrov et al., 2003) was applied to a set of forty GIs from classes 10-2a and 10-3a (same data sets used in figure 2.4). Responses for figure 2.5 A-D were chosen to be 10 msec patterns of spikes beginning with a spike at time 0 with any subsequent activity in the following 10 msec, and being preceded by at least 10 msec of silence in the cell prior to t=0. Single spike patterns were excluded from the analysis. For panel E a second quantization was performed on each cell, with everything the same

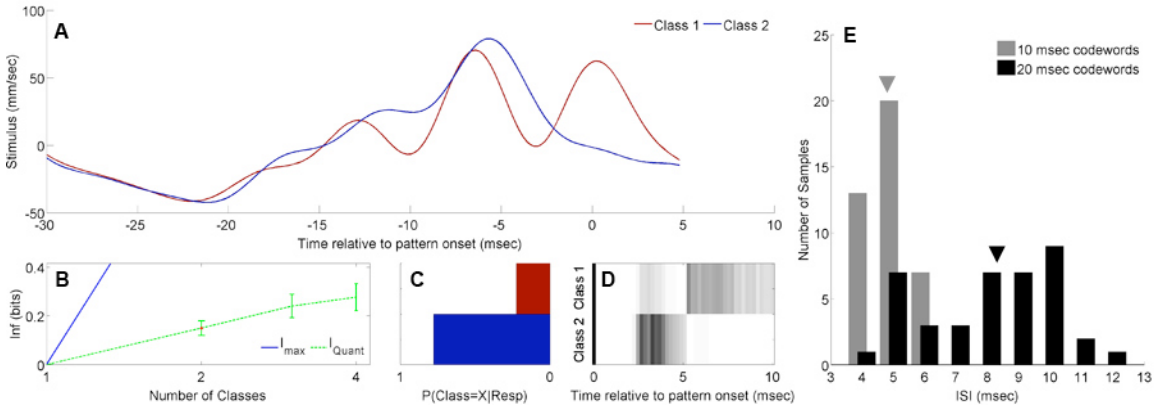

Figure 2.5. Example of quantization analysis in the case of two stimulus-response classes. A, the average stimuli associated with the two different response classes. B, estimate of mutual information recovered through quantization for this cell, as a function of the number of classes. The blue line shows the theoretical maximum for the information, $I_{max}=\log_2(\text{number of classes})$. Notice that the uncertainty in information increases with the number of classes, so that the information recovered from four classes is not significantly greater than the information recovered from three. C, relative probability of occurrence of class 1 (red) and class 2 (blue). D, the class conditioned response histogram, showing the probability of finding a spike at time t, conditioned on belonging to class 1 (upper panel) or class 2 (lower panel). Probability is denoted by the color axis, with p=0 in white and p=.15 in black. By design all responses have p(spike|t=0) = 1, which has been truncated here to allow more contrast for the other probabilities. Note that most short doublet responses (ISI < 6 msec) fall in class 2, while most longer doublet (and many triplet) responses fall in class 1. E, analysis for where division between class 1 and class 2 lies for an ensemble of 40 cells. The bars in gray represent analysis in which the response pattern length is set to 10 msec (as in panel D), for the bars in black it is set to 20 msec. Arrows denote median ISI for division between classes across population. Data in panels A-D from same cell as figures 2.1 and 2.3 A-E; ensemble data in panel E from same datasets as for figure 2.4 A & C.

except that the relevant response space used was all the 20 msec patterns preceded by 20 msec of silence. The stimuli associated with these response patterns was taken to be the 30 msec of the stimulus preceding the onset of the response pattern, and extending 5 msec into the 10 msec pattern. This corresponded to the times when the mean response-conditioned stimulus was non-zero. The response and the stimuli were sampled at 5 kHz precision. The stimulus covariance was reduced to a common model, and the vertex search optimization algorithm was used. Figure 2.5 A-D show the results from a single

cell, for the 10 msec response patterns and a quantization scheme to two classes. The output response spaced (panel D) can be described as all doublets over 5 msec ISI (class 1), and all short doublets under 5 msec ISI (class 2). Triplet patterns were spread through both classes, but occurred much less often than the doublets. The value of 5 msec corresponded with an inflection point in the ISI histogram immediately following the set of 'bursty' spikes which ride on the edge of the hard refractory period (data not shown). The mean stimulus waveform associated with the short doublet class (panel A) was a single large sinusoidal pulse with an maximal amplitude of 80 mm/sec occurring approximately 6 msec prior to the first spike of the pattern. The mean stimulus for the longer doublet class is similar to two copies of a somewhat smaller waveform offset in time by about 6.5 msec. The short doublet dominated the response space, comprising about 75% of all responses excluding single isolated spikes (panel C). Of the approximately 0.75 bits of response entropy in the two-class case, the quantization was able to recover about 0.15 bits of mutual information (panel B). Over the ensemble of 40 cells, the division point between short and long doublet classes was remarkably consistent, with a mean ± 1 std value of 4.9 ± 0.6 msec for the case of the 10 msec response patterns (panel E). However, when the response space was expanded to 20 msec, the location of the break was longer and more variable across the population (8.0 ± 2.2 msec).

One might expect that in quantization analysis the division between short and longer doublets might remain consistent across values of the response-codeword

length parameter. It is worth ending the chapter with a brief diversion to cogitate on a possible reason for why this is not the case in the preceding figure. Consider a neural encoder which employs two different channels for information transfer: a feature detector which represents large stimuli in the environment with a stereotyped burst, and a linear rate encoder which behaves according to the assumptions of linear stimulus reconstruction listed above. For any two impulse stimuli that are farther apart than the characteristic burst frequency of the first channel, the cell would respond with a two spikes, with the time between them corresponding to the time between occurrences of the impulses. This channel would be able to represent a range of such pairs of impulse stimuli, restricted only by the characteristic burst ISI in the short inter-stimulus limit, and the temporal uncertainty in spike generation in response to each stimulus pulse (see chapter 2). Note that this is a simplified model of how relay cells of vertebrate LGN, pyramidal cells of the ELL of electric fish, and auditory neurons ON1 and AN2 of the cricket are all thought to function (Reinagel et al., 1999; Lesica and Stanley, 2004; Alitto et al., 2005; Oswald et al., 2004; Chacron, 2006; Oswald et al., 2007; Doiron et al., 2007; Marsat and Pollack, 2004; Marsat and Pollack, 2006).

A naïve quantization analysis performed to the two-class level on this model cell could, in principal, simply divide the response completely on the basis of the reconstruction channel, provided that the information to be extracted based on clustering (for instance) 5-10 ms inter-stimulus intervals from 10-15 ms intervals

was greater than the information which could be extracted from clustering them both separately from the bursting channel. In this case the relatively shorter ISIs corresponding to short duration between stimulus pulses would be grouped into one class, and the set of longer ISIs corresponding to the reconstruction channel into the second class, with the burst-mode response being lumped into one of these two channels according to which average class stimulus was most similar to the large stimuli which elicit the bursts. The parameter for the length of the response codeword pattern could be increased, in which case the division point for the breakdown between the two classes would also lengthen, as maximization of information between the stimulus and response clusters would be attained by roughly dividing the response space of the reconstruction channel in half, with the bursting channel being thrown in wherever it fit best.

From an engineering standpoint this would be a good thing- the quantization method would be effectively doing its job of agnostically maximizing information by combining the two response channels. From a biological standpoint however, this would be unsatisfying, as the encoding mechanisms leading to the burst channel could arise from interesting network or cellular dynamics that would be worth studying. Also the output of the channel could be important when studying the animal in a behavioral context, as the stimuli that elicit bursts could be caused by predators, prey, mates, or other items of ethological relevance. We will revisit this topic in chapter four, where I derive an objective measure which could allow two such channels to be separated prior to quantization analysis.

NEURAL PRECISION AND ‘DEJITTERING’

Abstract

What is the meaning associated with a single action potential in a neural spike train? The answer depends on the way the question is formulated. One general approach toward formulating this question involves estimating the average stimulus waveform preceding spikes in a spike train. Many different algorithms have been used to obtain such estimates, ranging from spike-triggered averaging of stimuli to correlation-based extraction of ‘stimulus-reconstruction’ kernels or spatio-temporal receptive fields. We demonstrate that all of these approaches miscalculate a neuron’s stimulus feature selectivity. Their errors arise from the manner in which the stimulus waveforms are aligned to one another during the calculations. Specifically, the waveform segments are locked to the precise time of spike occurrence, ignoring the intrinsic ‘jitter’ in the stimulus-to-spike latency. We present an algorithm that takes this jitter into account. ‘Dejittered’ estimates of a neuron’s feature selectivity are more accurate (*i.e.*, provide a better estimate of the mean waveform eliciting a spike) and more precise (*i.e.*, have smaller variance around that waveform) than estimates obtained using standard techniques. Moreover, this approach yields an explicit measure of spike timing precision. We applied this technique to study feature selectivity and spike timing precision in two types of sensory interneurons in the cricket cercal system. The dejittered estimates of the mean stimulus waveforms

preceding spikes were up to three times larger than estimates based on the standard techniques used in previous studies, and had power that extended into higher frequency ranges. Spike timing precision was approximately 5msec.

Introduction

Three questions often addressed in studies of neural coding include the following: What is the optimal stimulus waveform for eliciting a spike in a neuron? What is the nature of the distribution of the waveforms around this optimal feature that can elicit a spike? What is the temporal precision with which a spike is linked to the occurrence of a stimulus feature? One general approach toward answering these questions involves a) presenting a long-duration stimulus waveform capturing the natural stimulus regime of the neuron under study, b) recording the train of spikes elicited by that stimulus, and c) estimating the average stimulus waveform that precedes each spike (or multiple-spike pattern) in the elicited spike train. Many different algorithms have been used to obtain such estimates, ranging from spike-triggered averaging (STA) of stimuli to correlation-based extraction of ‘stimulus-reconstruction’ kernels (Bryant and Segundo, 1976) and spatio-temporal receptive fields (Theunissen et al., 2001). These approaches yield estimates that differ mainly in the manner through which they are normalized and decorrelated from biases in the stimulus set.

As we demonstrate here, these methods all lead to entanglement of the three questions listed above, and may result in significant errors with respect to each

question. These errors arise from the manner in which the stimulus waveforms are aligned to one another during the averaging or cross-correlation operations. Specifically, these algorithms register the waveform segments to one another based on the precise time of spike occurrence. We know, however, that the biophysical processes underlying sensory transduction, synaptic integration, spike initiation and synaptic transmission are not perfectly deterministic, and some significant degree of 'jitter' in stimulus-to-spike latency is always observable upon repeated presentation of identical stimuli (see, for example, (Bryant et al., 1973; Marsalek et al., 1997; Berry et al., 1997; Liu et al., 2001; Zoccolan et al., 2002; Uzzell and Chichilnisky, 2004; Hsu et al., 2004)). By ignoring this intrinsic 'jitter,' these analytical algorithms all yield distorted estimates of the relevant stimulus waveform and of the variance around that waveform.

We present an algorithm that takes this stimulus-to-spike-latency jitter into account, and enables the partial disentanglement of the three questions listed above. The 'dejittered' estimates of a neuron's feature selectivity provide better estimates of the mean waveform eliciting a spike, and have smaller variance around that waveform than estimates obtained using the standard techniques. This procedure disambiguates the uncertainty about the *time of occurrence* of the stimulus feature from the uncertainty about its *waveform*, and also provides insight into the intrinsic temporal precision with which information from a nerve cell can be decoded.

We applied this technique to study feature selectivity and spike timing precision of two types of identified sensory interneurons in the cricket cercal system, designated as IN10-3a and IN10-2a. The feature selectivity of these cell types was studied in previous experiments using first-order Volterra kernel analysis (Theunissen et al., 1996). Application of the dejittering procedure yields significantly different estimates of the stimulus feature selectivity of these cells. Furthermore, calculations of the lower bound of information encoding rates by these cells, using the 'direct method' (Strong et al., 1998) yield values that are substantially greater than those obtained through the earlier kernel-based estimates.

Materials and Methods

Preparation

Experiments were performed on 14 adult female crickets (*Acheta domesticus*) obtained from a commercial supplier (Bassett's Cricket Ranch, Visalia CA). Each specimen was selected within four hours following the final molt, and anesthetized on ice for 3-5 minutes. The legs, ovipositor and wings were removed, and a window was cut into the dorsal cuticle. Digestive, reproductive, and fat tissues were removed. The abdominal cavity was filled with hypotonic saline solution (O'Shea and Adams, 1981). The preparation was pinned to a plate of silicone elastomer, and a stainless steel platform was inserted beneath the terminal abdominal ganglion and elevated to provide tension on the cercal

nerves to facilitate electrode penetration. The mounted preparation was placed within a multidirectional air current stimulator. The stimulator consisted of a central chamber linked to four sets of loudspeakers through enclosed channels (Dimitrov et al., 2003). Movements of the speakers were controlled by power-amplified, computer-generated waveforms, such that the coordinated movement of the speakers generated controlled movements of air across the preparation, thereby stimulating the filiform mechanosensory hairs on the cerci.

Electrophysiology

Neural activity was monitored from the axon of each interneuron in the abdominal nerve cord, near its exit from the terminal abdominal ganglion, using a sharp intracellular microelectrode containing 3M KCl. Activity was elicited by the presentation of Gaussian noise (GN) air current stimuli that were band-passed between 5-300 Hz and had an RMS speed of 35mm/sec, as calibrated with a low-velocity air current sensor (MicroFlown Technologies, Zevenaar, Netherlands). The stimulus waveforms and neural responses were digitally sampled at 10kHz (NI PCI-6070E and LabWindows-based proprietary data logging system, National Instruments, Austin TX) and stored for subsequent analysis.

Calculation of a 'Dejittered' Mean Stimulus Waveform

The algorithm used to dejitter the mean waveform was as follows:

1. We collected a set of stimuli x from the stimulus-response data set,

conditioned on isolated spikes (*i.e.*, spikes that were preceded by a period of at least 30msec segments devoid of any other spikes, and followed by a spike-free interval of at least 30msec.) Note that this restriction of the analysis to isolated spikes is not essential in general, but is done here for the sake of simplicity in illustrating the method. In fact, the procedure could be conditioned on any arbitrary single- or multiple-spike pattern with any arbitrary bounding intervals.

2. We calculated the mean m_{x0} of this stimulus set [*i.e.*, the spike-triggered average (STA) for isolated single spikes]. This became our initial model for the mean stimulus waveform preceding a spike. In any association between stimuli and spiking responses of single cells, the STA is equivalent to the stimulus-response correlation. In the case discussed here, m_{x0} can be obtained from the STA by normalizing the latter by the response power spectrum, which makes m_{x0} equivalent to the first-order Volterra reconstruction kernel (Rieke et al., 1997)

3. We assumed an initial model for the jitter, equivalent to a truncated Gaussian distribution:

   a) The core assumption was that the latencies of the recorded spikes had been jittered with respect to the time of the occurrence of the stimulus feature that had elicited those spikes, according to a Gaussian distribution with some variance σ_t. Note that making this assumption is equivalent to assuming that the temporal resolution of this particular neural response is

limited by this variance; i.e., that the time of occurrence of the stimulus feature eliciting a spike would not be resolvable from this cell's spike train with precision greater than σ_t. For the particular cell under study, the initial value we assumed for this variance (σ_{t0}) was 3 msec. (As will be shown below, the technique is robust under a fairly wide range of initial assumed values for the temporal jitter, as long as the value falls within the physiologically realistic range.)

b) We also defined a minimum stimulus-response latency l_{min}. In the subsequent re-alignment procedure, l_{min} served as a lower bound for shifting the stimuli with respect to the mean. Shifts in time which were more negative than l_{min} were assumed to violate causality, in the sense that the spike occurrence time would have occurred before the significant part of the stimulus feature.

4. For each individual stimulus waveform sample in the set:

a) we formed all possible time-shifts of that waveform in the range l_{min} to $3\sigma_{t0}$;

b) for each of the time-shift values for this waveform sample, we calculated the distance between the time-shifted waveform and the mean stimulus waveform calculated in the previous iteration. The distance measure we used was the weighted squared difference between the shifted waveform and the mean waveform, penalized by the weighted square of the shift time (details are presented below).

c) we chose the value of the time-shift for this waveform sample that yielded

the smallest distance;

d) we replaced the original waveform sample with this new time-shifted sample.

5. After all stimulus waveforms in the set were shifted to minimize their distance from the mean waveform, we calculated a new mean m_{x1} of this time-shifted stimulus set. This became the seed value of the mean for the next iteration of dejittering.

6. We assessed the temporal variance of the output distribution as the standard deviation of the shift times across the entire data set. This value (σ_{ti}) became the penalty term for the next iteration of dejittering.

7. We looped to step 4 and repeated the subsequent processing steps until the convergence criterion was attained (described in more detail below). The convergence condition results in a minimization of the variance of the dejittered stimulus waveforms around their dejittered mean.

The final mean waveform (m_{xf}) was assumed to be the best approximation of the dejittered mean waveform preceding a spike, and the distribution of the shift times was likewise taken as our best approximation of the distribution of spike jitter times.

Calculation of Shift Times from a Distance Measure

The shift time *t* for a stimulus segment during one iteration of the dejittering procedure was calculated by minimization of a Gaussian distance *d* between that segment and the mean of all segments calculated from the previous iteration:

$$d \equiv \frac{1}{2}\left(xC^{-1}x + \frac{t^2}{\sigma_t^2} \right) \tag{3.1}$$

where x is the residual between the stimulus segment sample and the mean stimulus from the previous iteration, C is the covariance matrix of the stimulus ensemble, σ_t is the assumed variance of the jitter distribution, and t is the specific shift time being tested. This distance can be seen as the negative log likelihood of a joint Gaussian model of stimulus and time shifts. Here for simplicity we use a diagonal approximation of C, which assumes that individual time samples are independent. This distance d was calculated for a range of t values between l_{min} and $+3\sigma_t$ at a sampling resolution of 0.1msec, and the value of t that minimized d was selected as the shift time for that stimulus segment. A shift time was calculated for each different stimulus sample independently, and all segments were realigned according to these relative shift times. The mean of these re-aligned segments was then calculated, and used as the basis for calculating the convergence criterion (see next section) and, if convergence was not achieved, for calculating the residuals x during the next iteration cycle of the procedure. A justification for this distance is presented in (Dimitrov and Gedeon, 2006). A further simplification of the covariance matrix to a multiple of the identity matrix will turn the stimulus distance into a Euclidean distance (sum of squares). Such distance and the iterative re-estimation of features are typically used in standard clustering algorithms, like the *k*-means (Duda et al., 2000).

Convergence Criteria

Convergence of the dejittering procedure was achieved through the minimization of an error function Err_i. The error function corresponded to the percentage change in the square of the residual of the dejittered mean waveforms (Fig. 4*F*) calculated between successive iterations:

$$Err_i \equiv \frac{\left\langle Var\left(stim_{i-1}'\right)\right\rangle - \left\langle Var\left(stim_i'\right)\right\rangle}{\left\langle Var\left(stim_{i-1}'\right)\right\rangle} \tag{3.2}$$

where $\langle . \rangle$ denotes the average of the values of the sample waveforms at each time point across all time points, Var(.) denotes the variance vector at each time point across all time points in all samples, $stim$ is the ensemble of dejittered stimulus waveform samples, and the subscript i denotes the i^{th} iteration of the dejittering process. Iteration was stopped when $Err_i \leq 10^{-6}$, *i.e.,* when the relative change between iterations fell below 0.0001%. In general, convergence was achieved in 10-50 iterations.

Calculation of Information Rates

Estimates of information encoding rates were calculated from the stimulus-response measurements via two different approaches. The first approach yielded a linear estimate, obtained through the use of stimulus reconstruction techniques (Theunissen et al., 1996; Rieke et al., 1997). The coherence between the air-current stimulus waveform and the spike train response was calculated (equation 8 in (Theunissen et al., 1996)). Information per frequency was calculated as the negative of the logarithm base 2 of (1 – coherence), and the total information rate

was then estimated as the integral of this quantity from 0 Hz up to the highest frequency at which there is significant power in the stimulus (equation 11 in (Theunissen et al., 1996)).

A second estimate of information rate was obtained using the 'direct method' (Strong et al., 1998). Briefly, the unconditional and stimulus-conditioned response probabilities were estimated from data for several different 'word lengths'. De-biased estimates of mutual information rates between the stimuli and associated responses were then obtained using Paninski's 'best upper bound' estimator (Paninski, 2003) for each word length. The best estimate for the information rate was obtained by extrapolating to infinite word length. Note that by using de-biased estimates for the information rates, the problem of extrapolation becomes essentially trivial, as rate estimate vs. word length becomes essentially a straight line (Kennel et al., 2005).

Results

Illustration of the Problem Using a Thought Experiment, Formulated as a Simulation

Imagine that we are studying a sensory interneuron that is known to operate as a feature detector, that the 'optimal stimulus feature' for eliciting a spike has been determined, and that this optimal feature has been presented repeatedly to the cell in the absence of significant background noise (Figure 3.1*A*). We know that the biophysical processes of sensory transduction, synaptic integration, spike initiation and synaptic transmission at all stages of the nervous system

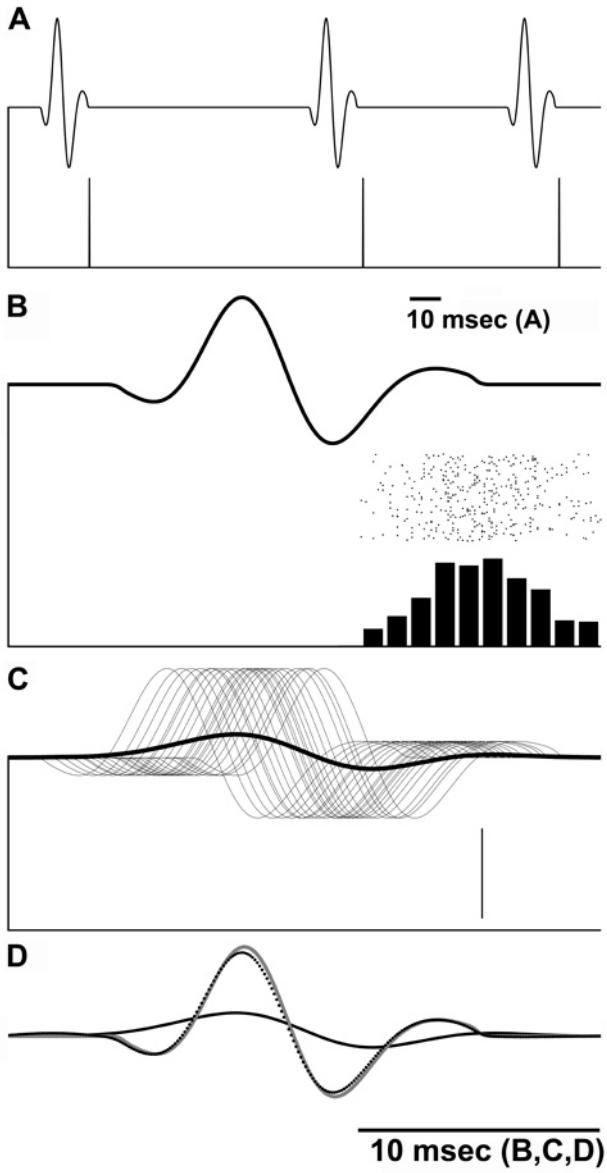

Figure 3.1. A thought experiment to define the jitter problem, using simulated recordings. *A*, Upper trace: a segment of simulated stimulus consisting of three identical 'optimal features' presented at random intervals, with no background noise; lower trace: three spikes elicited by those stimulus features. *B*, Superposition of 500 examples of the stimulus waveform at an expanded timescale, with a raster plot of the 'jittered' occurrence times of spikes elicited by those 500 repetitions, and a histogram of those times, immediately below. *C*, 24 randomly-selected samples of the stimulus waveform, out of the total dataset of 500. These stimulus segments have been shifted with respect to one another so as to bring all of their elicited spikes into alignment (*i.e.*, the vertical line to the lower right of the set of waveforms is the realigned spike raster). The mean of all re-aligned waveforms (*i.e.*, the spike-triggered-average, or STA) is shown with the heavy solid line. *D*, Comparison of the STA from *C* (solid line) with the actual stimulus waveform from *B* (gray line) and the 'dejittered' mean (dotted trace).

providing input to this interneuron are not perfectly deterministic (Berry et al., 1997; Marsalek et al., 1997; Hsu et al., 2004), and so we expect that the observed ensemble of stimulus-to-spike latencies in our experiment will have some observable variability around a mean latency. If we create a histogram of spike occurrence times relative to the repeated presentation of a stimulus waveform (Figure 3.1*B*), that distribution will not be a perfect delta function, but will have some observable jitter around the mean. Consider the error that will occur in our estimation of the stimulus waveform that we had presented, if we calculate a spike-triggered average (STA) of the stimulus waveforms preceding the spikes. The procedure starts with the alignment of all instances of the presented waveforms relative to the time of occurrence of the spike elicited by each waveform (Figure 3.1*C*). The *observed* distribution of spike times in panel *B* is translated into a jittering of the actual presented waveforms with respect to one another in panel *C*. The subsequent averaging of the waveforms with this imposed jitter (bold trace, Figure 3.1*C*) yields an estimated stimulus waveform that is distorted with respect to the true waveform. Figure 3.1*D* shows a comparison of this jittered mean (solid black trace) with the original waveform (solid gray trace). This distortion is equivalent to a blurring of the true waveform with a point spread function identical to the actual spike train jitter distribution, similar to the manner in which an image is blurred by the point spread function of an optical system. We note that calculation of a Volterra or Wiener ‘stimulus reconstruction’ kernel (Bryant and Segundo, 1976; Rieke et al., 1997), a spatio-

temporal receptive field (STRF) (Theunissen et al., 2001), or any other method based on the cross correlation between each spike in the ensemble and the stimulus waveforms preceding those spikes, would also result in such a blurring of the estimated waveform.

A much-improved estimate of the true mean stimulus waveform can be obtained by taking the spike-timing jitter into account. This ‘dejittering’ is achieved by shifting the ensemble of sample waveforms with respect to one another in a manner that minimizes the variance around the subsequent mean, while penalizing large shifts (see Methods). The application of this procedure to the simulated data in Figure 3.1*C* yielded the dotted black trace in Figure 3.1*D*, which is a much better estimate of the actual waveform (solid gray trace) than the STA (solid black trace).

We note that it is possible, in principle, to employ an approach to dejittering that is the inverse of the approach presented here, i.e., to shift spike train segments that code for the stimulus features in a manner that maximizes the correlation between those spike train segments. This would require different measures of closeness, specific to the neuron’s response space, such as the metric space approach developed by Victor and colleagues (Victor and Purpura, 1996).

Time Scale of the Stimulus-to-Spike Latency Jitter in a Sensory Interneuron

We applied this algorithm to study the stimulus-response properties of two

pairs of mirror-symmetric primary sensory interneurons in the cercal sensory system of the cricket *Acheta domesticus*. This mechanosensory system mediates the detection and analysis of low velocity air currents, and can be thought of as a low-frequency, near-field extension of the animal's auditory system (Palka et al., 1977; Bacon and Murphey, 1984; Kämper and Kleindienst, 1990; Miller et al., 1991; Theunissen et al., 1996). The inerneurons receive direct excitatory synaptic input from filiform mechanosensory hairs on the animal's two antenna-like cerci at the rear of the abdomen. The sensory stimuli we used to drive the interneurons were dynamic air currents with velocity waveforms characterized by Gaussian noise (GN), band-passed between 5 and 300Hz. Figure 3.2 shows one typical segment from an experiment in which a 10 second stimulus was repeated 100 times. Figure 3.2 *A3* shows a 500msec segment of this GN stimulus waveform, and *A1* shows the corresponding raster plot of the spike trains elicited by the 100 repeated presentations of that waveform segment. Figure 3.2 A2 is the histogram of these spike occurrence times (PSTH). This segment of data demonstrates the wide range of stimulus-to-spike latency distributions that are typically elicited by GN stimuli. The three panels in Figure 3.2 *B* show the central 60msec segment of the data shown in Figure 3.2*A* at an expanded time-scale, which captures the sharpest distribution of spike times from that segment.

Figure 3.2 *C* illustrates the result of calculating the STA of the stimulus waveform segments from the subset of data shown in Figure 3.2 *B*. Figure 3.2

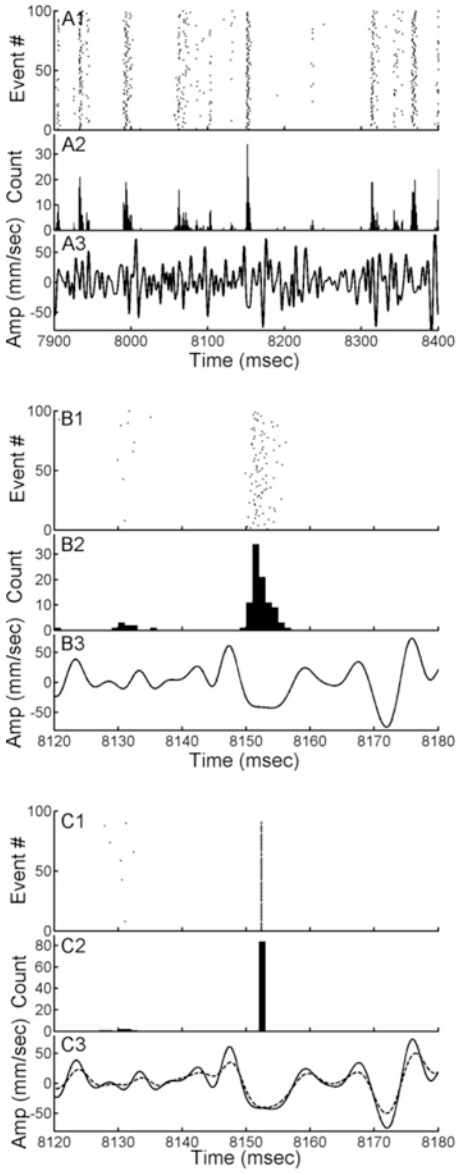

Figure 3.2. An experiment to illustrate the jitter problem, using a mechanosensory interneuron. *A3*, a 0.5 sec segment of the Gaussian noise stimulus waveform. *A1*, Raster of the spike times elicited by 100 repetitions of this waveform. *A2*, Histogram of this raster plot using 1 msec time bins. *B*, The central 60 msec segment of the data panels shown in *A* at an expanded time-scale. *C*1, Spike time raster plot after realignment of the spikes in the distribution shown in *B*. *C3*, Dashed line: mean of all stimulus segments re-aligned to the evoked spikes (*i.e.*, the STA). *C3*, Solid line: the actual stimulus waveform (as in *B*).

C1 is the raster plot of spikes after their realignment into precise registration. Figure 3.2 *C2* is the histogram of these spikes (*i.e.*, all fall into a single bin), and the dashed trace in *C3* is the average of all 100 stimulus segments following their realignment (*i.e.*, the STA for these spikes). For comparison, the solid line in that bottom panel is the actual stimulus waveform that had been repeatedly presented to the animal (and was, therefore, also the *real* mean waveform leading up to any spikes). Clearly, the STA yields a distorted image of the true waveform.

Dejittering a Sample of Spike-Conditioned Stimulus Waveforms

Although the thought experiment (Figure 3.1) and the demonstration of spike jitter (Figure 3.2) were based on repeated presentations of identical stimulus waveforms for the sake of illustration, the dejittering protocol we introduce below does not require such repeated stimulus presentations, nor does it require *a priori* knowledge about the optimal stimulus. Rather, we used a single non-repeating, long-duration, band-passed Gaussian noise waveform. Figure 3.3*A* shows a 500 msec segment of the air current stimulus waveform. The corresponding spike train response (containing five spikes) elicited by this segment is shown directly above the stimulus trace. The times of spike occurrence are indicated on the stimulus waveform (Figure 3.3*A*) with small colored circles. Figure 3.3*B* shows the superposition of the stimulus waveform segments preceding all five spikes, aligned with respect to the times of spike

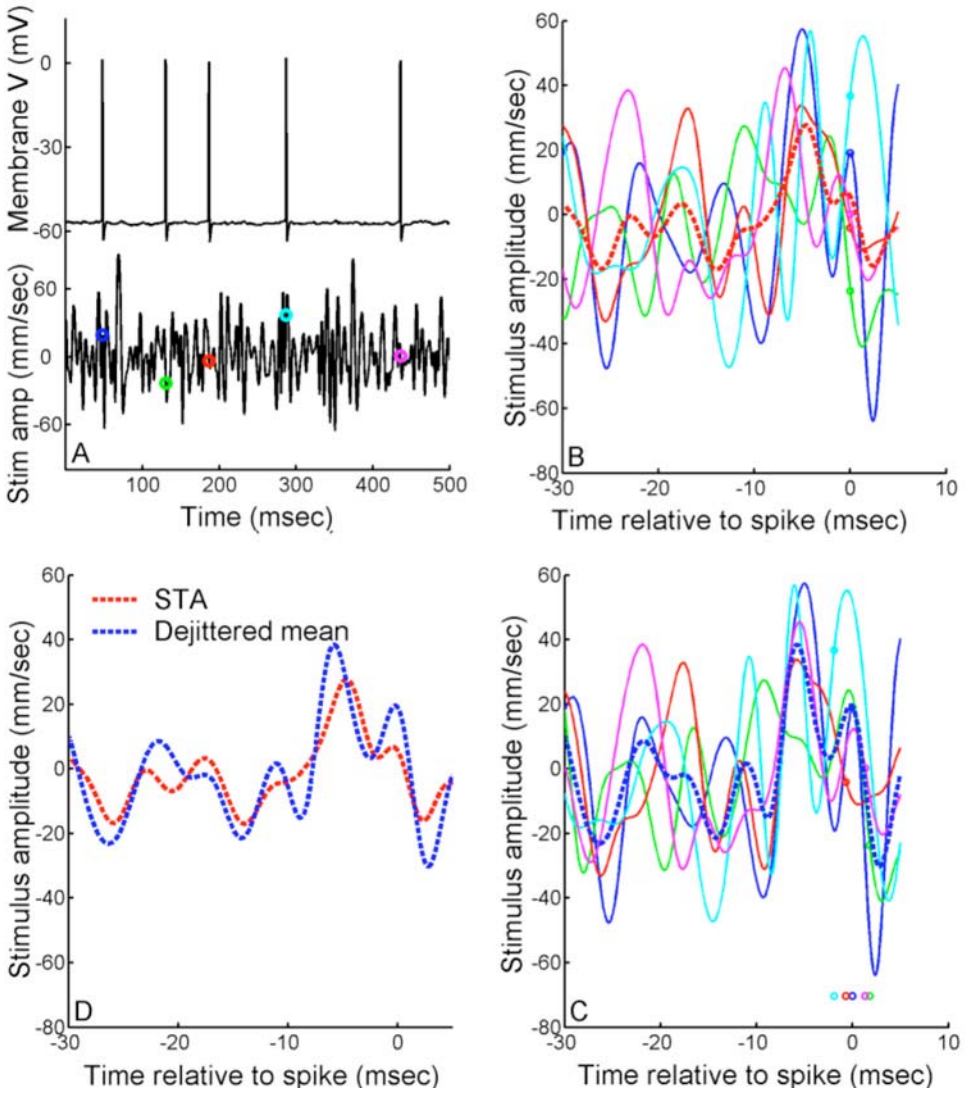

Figure 3.3. Illustration of the dejittering algorithm. *A*, a 500 msec segment of stimulus (lower trace) and corresponding intracellular membrane potential with five spikes elicited by that stimulus (upper trace). The time of spike occurrences are marked on the stimulus waveform with colored circles. *B*, Five 35 msec segments of the stimulus waveforms preceding each of the five spikes in panel *A*, locked to the times of spike occurrence at t=0 msec. The color of each stimulus waveform matches the colored markers in *A*. The mean (i.e., spike-triggered-average) waveform is shown with the heavy dashed red line. *C*, The same five 35 msec segments as shown in *B*, but now 'dejittered'. The time-shifted spike times are shown by the markers under the waveforms. The mean is shown with the heavy dashed blue line. *D*, Comparison of dejittered mean (blue dashed trace) with STA (red dashed trace) for the data.

occurrence (defined as t=0; note that panels *B* - *D* are at an expanded timescale). The bold dashed red curve is the STA of all stimulus segments. Figure 3.3*C* shows the results of shifting this set of stimulus segments with respect to one another, to recover an estimate of the stimulus waveform that minimizes the distortion due to spike timing jitter. The extent to which each of the five waveforms was shifted in time is indicated by the small colored circles. The mean of the set of shifted waveforms is shown as the bold blue curve. Figure 3.3*D* compares the pre-shifted STA from panel *B* with the 'dejittered' mean from panel *C*. The dejittered mean clearly has larger amplitude than the standard STA, with the frequency composition of the increased component biased toward the higher frequency range of the waveform.

The results of a complete analysis of this IN10-3a stimulus-response dataset are shown in Figure 3.4. All instances of isolated single spikes (preceded and followed by spike-free intervals of at least 30msec) were extracted from a 33 minute recording, yielding a sample size of approximately 13,600 stimulus segments. Figure 3.4*A* shows raster plots of a random representative subset of 100 of the sample segments of stimulus-response data. Each horizontal raster line is color-coded to indicate the stimulus velocity *vs.* time, with colors toward red indicating positive velocity and colors toward blue representing negative velocity. The black dot at time 0 indicates the time of occurrence of the spike elicited by the waveform within that particular sample. All of the stimulus waveforms in Figure 3.4*A* are locked in their alignment to the spike occurrence

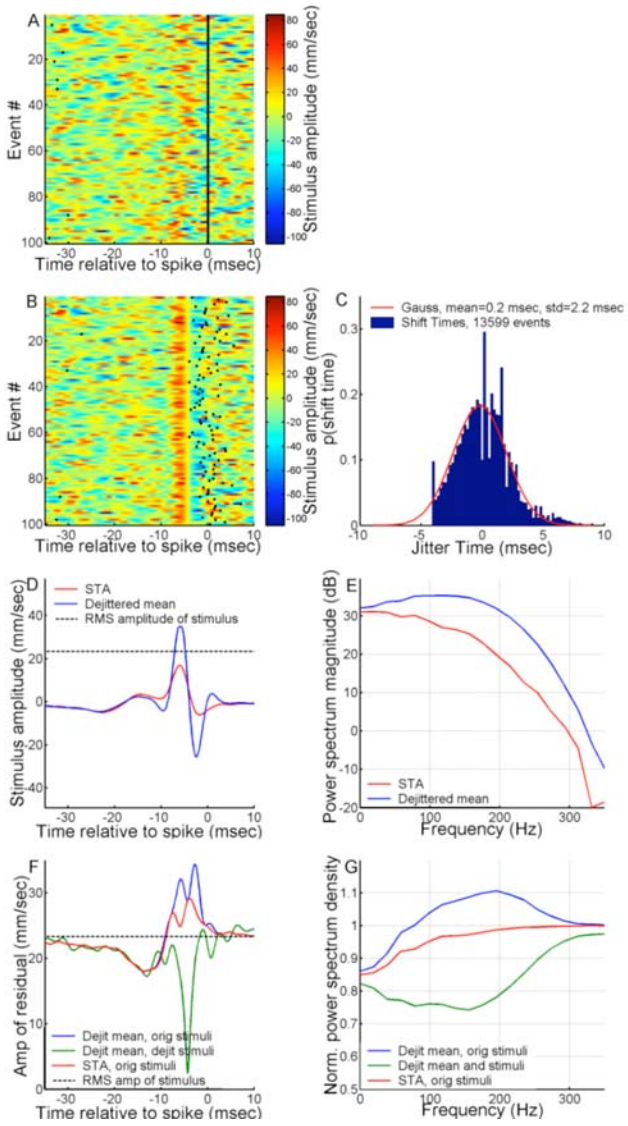

Figure 3.4. Characteristics of a dejittered mean stimulus. *A*, Random representative subset of 100 sample segments of stimulus-response data aligned to time of spike occurrence. The vertical black line at t=0 is the raster plot of spikes superimposed on the color-coded traces of air current velocity *vs.* time. *B*, The same random subset of 100 segments of stimulus-response data from *A*, but now 'dejittered' so that their alignment is based on minimal variance of the stimuli. *C*, Shift times for all 13,600 samples (blue histogram), compared with a Gaussian having a STD of 2.2 msec (red line). *D*, Spike-triggered-average (STA, red trace) and dejittered mean (blue trace) The RMS amplitude of the stimulus is indicated with the dashed black line. *E*, Power spectra of the STA (red trace) and dejittered mean stimulus (blue trace). *F,* Red trace: mean-square residual between the STA and the original stimulus segments. Blue trace: mean-square residual between the dejittered mean and the original stimulus segments. Green trace: mean-square residual between the dejittered mean and the dejittered stimulus segments. The RMS amplitude of the stimulus is indicated with the dashed black line. *G*, Power spectra of the residuals, normalized by power spectra of stimulus segments. Colors are the same as in *F*.

times. Figure 3.4*B* shows the result of dejittering these waveforms, assuming a value of 3msec for σ_{t0} during the procedure. The redistribution of the stimulus/response raster lines resulting from this dejittering procedure results in a visibly sharpened registration of the stimulus waveforms across the raster set, and a visibly scattered de-registration of the spike occurrence times. The distribution of shift times to achieve the optimal dejittered mean had a σ_t of 2.2msec (Figure 3.4*C*). Figure 3.4*D* compares the uncorrected spike-conditioned mean (*i.e.*, the STA: red trace) with the dejittered mean (blue trace) across all 13,600 samples in the dataset. The dejittered mean stimulus had a peak amplitude 2.6 times higher than that of the STA. The dejittered mean also had a greater relative proportion of its power extending into the higher frequency range than did the STA, as can be seen from a comparison of the power spectral densities of the STA and dejittered mean waveforms (Figure 3.4*E*). Note that, as discussed earlier, the STA is equivalent to the first order Volterra kernel calculated with the same data in this particular case, since the correlation time of the mean was less than the interspike interval.

Functional Significance of the Dejittered Mean Waveforms

The dejittered mean waveform is visibly different than the STA. However, it is somewhat problematic to assess the functional significance of this difference. It is not meaningful, for instance, to simply carry out a ‘stimulus reconstruction’ using the different types of waveforms (*e.g.* dejittered mean and STA or Volterra

kernel), calculate the mean-squared error between the estimated and actual stimulus in all cases, and compare the results. The STA (equivalent to the Volterra kernel for this case) will always give a lower mean-squared error than a dejittered mean, since the Volterra kernel is derived precisely to minimize the mean-squared error (without taking the jitter into account). The animal *could not*, of course, take the jitter into account, *i.e.*, it could not carry out the dejitter operation *a priori,* since it can't recover the precise times at which the dejittered estimates occurred before the spike. Within this context, the jitter σ_t can be interpreted as *the degree of uncertainty about the timing of the feature that elicited the spike*, i.e., the limiting temporal resolution of the cell.

The experimentor *can*, however, carry out an informative calculation that takes jitter into account, and illustrates how the use of dejittered mean stimuli can help to disambiguate the uncertainty about the time of occurrence of a stimulus feature from the uncertainty about its waveform. The red trace in Figure 3.4*F* is the standard deviation between the stimulus and the STA at each time sample in the experimental ensemble, with the STA and sample *both* aligned to the time of spike occurrence. This residual reflects the combination of all factors which contribute to error in the estimation, including temporal jitter of the spikes, coarseness in the tuning of the cell to a distribution of sub-optimal waveforms around the 'optimal' mean waveform, any correlation structure in the stimulus set, and all other biological factors that contribute to 'noisiness' in the neural processing stream. The corresponding red trace in Figure 3.4*G* is the power

spectrum of that residual, normalized by the power spectrum of the stimulus. This shows the fraction of the power in the signal which is *not explained* by the STA, and is analogous to the mean-squared error of a reconstruction (Roddey et al., 2000).

In contrast, the green traces in Figures 3.4*F* and 3.4*G* were calculated using the dejittered mean waveform *and* dejittered stimulus segments. That is, before subtracting the dejittered mean waveform from each stimulus segment sample in the test ensemble, that stimulus segment was time-shifted to the alignment with respect to the dejittered mean that had been determined to yield the minimal residual for that specific segment. This procedure specifically excluded the contribution of the temporal uncertainty to the residual error, leaving only the uncertainty about the stimulus waveform. The gap between the red and green traces in both panels corresponds to the error introduced by the STA (or Volterra kernel) in estimating the waveform of the mean stimulus: the higher the red trace above the green, the greater is the relative error of the STA as compared to that of the dejittered mean. It is clear that the dejittered mean yields a much lower residual error than the STA over the most significant segment of the stimulus waveform preceding the spikes. The spike jitter contributed a significant amount of residual error to the STA-based estimate of the stimulus waveform, and this error is biased toward the high-frequency end of the cell's sensitivity range.

Note that the red and green traces in Figure 3.4*F* are equivalent to the standard deviations across all of the spike-locked and dejittered stimulus traces,

respectively. Consideration of these different estimates of variance leads to substantially different interpretations of the cell's feature selectivity and stimulus-response dynamics. The variance across all of the de-jittered stimulus signals around the dejittered mean waveform (green trace) is lower than the signal RMS throughout the entire duration of the segment shown here, with the lowest point (*i.e.*, the greatest significance) associated with the period between 3 and 5msec before the spike. The residual decreases nearly to zero at about 4msec before the spike, indicating an extremely high degree of significance near this time point in the stimulus waveform, i.e., a very high degree of stimulus waveform selectivity.

Consideration of the variance around the STA (red trace, Figure 3.4*F*) is problematic: within the critical time segment leading up to the spike, the variance across all stimulus signals around the STA residual actually climbs to a maximum value that is larger than the RMS signal amplitude itself, and would indicate that the shape of the STA has no significance during that period. Interpretation of that red curve would lead to the conclusion that the significant part of the waveform was the segment between 10msec and 20msec preceding the spike, where the amplitude of the STA is negligible. Thus, interpretation of the feature selectivity and stimulus-to-spike latency on the basis of an STA is problematic. Here again, a conventional Volterra kernel or STRF would also yield the same problematic results.

The blue traces in Figures 3.4*F* and 3.4*G* were calculated by subtracting the

dejittered mean waveform directly from each of the stimulus segments, locked to the spike time rather than shifting the dejittered mean to the position yielding the smallest residual. (This is equivalent to carrying out a 'stimulus reconstruction' using the dejittered mean instead of the Volterra kernel.) As expected, the residual and its power spectrum are both greater (*i.e.*, worse) than those obtained with the STA. This is a corollary to the fact that the STA was constructed to give the minimum least-squared fit to the un-shifted set of stimulus segments: even though the dejittered kernel is a more accurate and precise estimate of the actual mean waveform that elicited each spike, it results in a poorer estimate of the stimulus if the jitter is not taken into account.

Sensitivity of the Technique to the Value of σ_{t0} Used for the Calculations

In general, the dejittering procedure is robust over a broad range of values for the assumed spike jitter penalty term σ_{t0}, as long as that value is kept within a physiologically reasonable range. Figure 3.5*A* is a surface plot comparing the dejittered mean waveforms obtained from several independent dejittering procedures, run on the same data set, using different values for σ_{t0} (y axis). The STA corresponds to the first horizontal color band at the top of the plot (σ_{t0} = 0). Each successive color band below that first one was calculated with a σ_{t0} increased by 0.2msec. Calculations initiated with all values of σ_{t0} converged to essentially identical estimates. Figure 3.5*B* is a surface plot of the distributions of shift times for each value of the penalty term σ_{t0}. Each horizontal color band

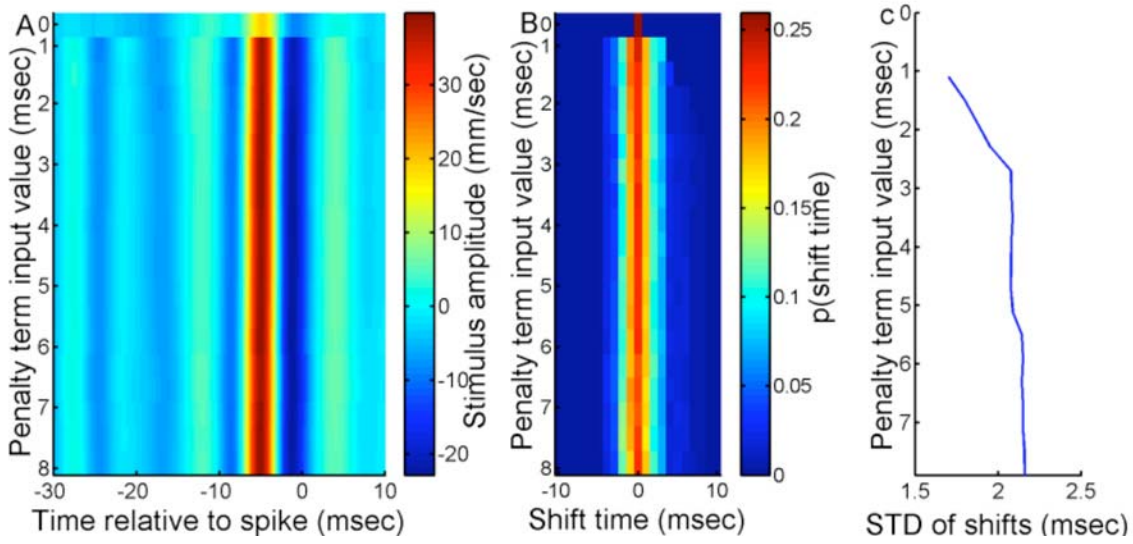

Figure 3.5. Dependence of the dejittered mean shape and σ_{tf} on σ_{t0}. *A*, Mean output stimulus, for each value of input penalty term σ_{t0}. The top row (σ_{t0}=0) shows the original STA. *B*, Probability distributions of the output shift times at 1msec resolution, for each value of the penalty term σ_{t0}. The top row (σ_{t0}=0) shows the spike times prior to dejittering. The color scale has been truncated from a maximum value of p(shift time)=1 at σ_{t0}=0, shift time=0. *C*, STD of dejitter shift times (σ_{tf}), for each value of input penalty term σ_{t0}.

represents the output distribution of shift times for a different value of the penalty term. The probability of a specific shift time is shown by color, with blue colors indicating a low probability of that shift time, red colors indicating a high probability. The curve in Figure 3.5*C* shows the standard deviations of the final shift distributions (σ_{tf}). The standard deviations stop increasing for values of σ_{t0} greater than about 4msec, demonstrating that the dejittered mean is insensitive to variation of the penalty term beyond that value.

Inter-Animal Variability of the Dejittered Mean Stimuli and σ_t for This Type of Interneuron

The data presented in the preceding sections were all recorded from a single

identified interneuron designated as a Left IN10-3a (the 10-3a interneurons exist as mirror-symmetric pairs in the terminal abdominal ganglion, with one 'Right' and one 'Left' IN10-3a). In order to assess the inter-animal and inter-pair variability in the dynamic response characteristics of this cell type, we repeated the experimental analysis and extracted de-jittered mean stimuli for a sample of seven R and L IN10-3as from different animals. The results are shown in Figure 3.6. The uncorrected STAs are shown in Figure 3.6*A*, and the dejittered means are shown in Figure 3.6*B*. The dejittered means were very similar to one another in duration, amplitude and waveform. Each dejittered mean was significantly larger in amplitude than its corresponding uncorrected STA, by a factor ranging from 2 to 3. Figure 3.6C shows the jitter distributions for these seven cells on an expanded time scale. The mean σ_t for this sample of seven IN10-3a cells was 2.08 +/- 0.26 msec.

Every terminal abdominal ganglion in each cricket also contains another mirror-symmetric pair of interneurons designated as 'Right' and 'Left' IN10-2a (Jacobs and Murphey, 1987). The four 10-3a and 10-2a INs comprise a functionally discrete subunit of the cercal system: they have the lowest stimulus threshold of all of the cercal interneurons, and are the only cells that encode information about the *direction* of air current stimuli in the horizontal plane in this low stimulus velocity range (Miller et al., 1991). Their directional sensitivities are mutually orthogonal: each has a selectivity for stimuli originating primarily from within one quadrant, and their peak directional selectivities are distributed at 90

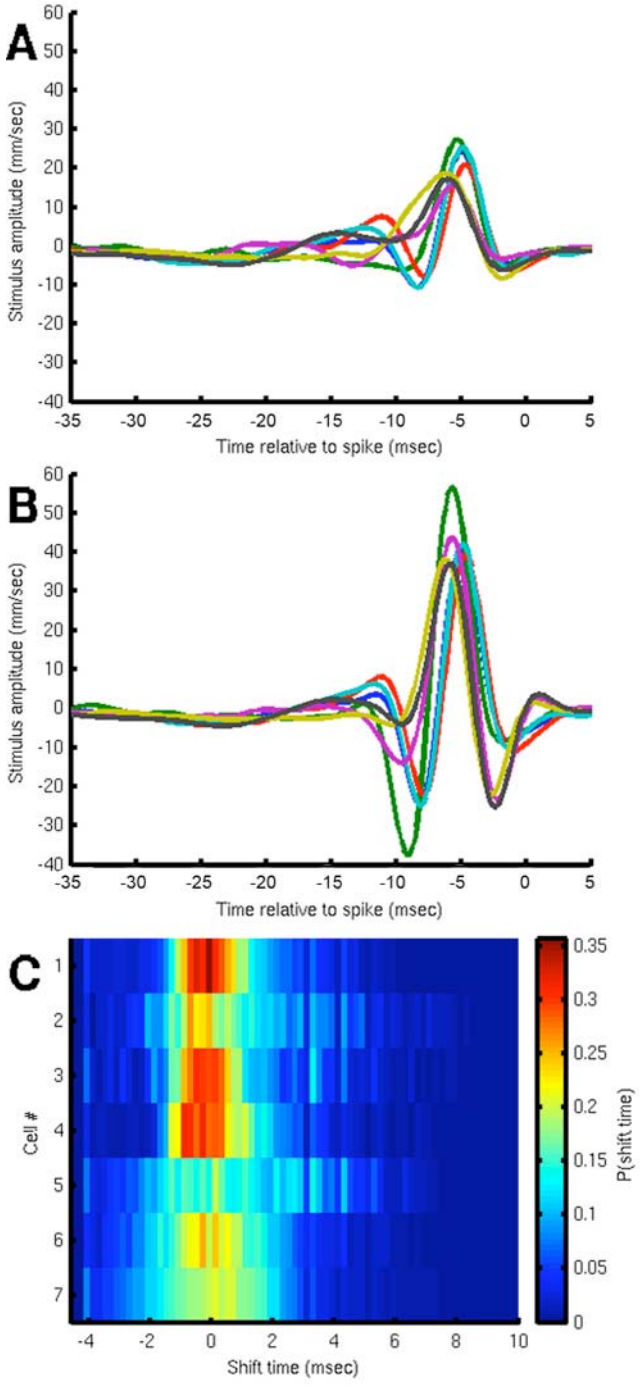

Figure 3.6. Composite average stimulus waveforms for a sample of seven cells from class 10-3a. *A*, Standard STAs. *B*, Dejittered means. *C*, Histograms of the shift times for the seven IN10-3a cells at an expanded time scale, with color coding for the fraction of samples shifted by the indicated time.

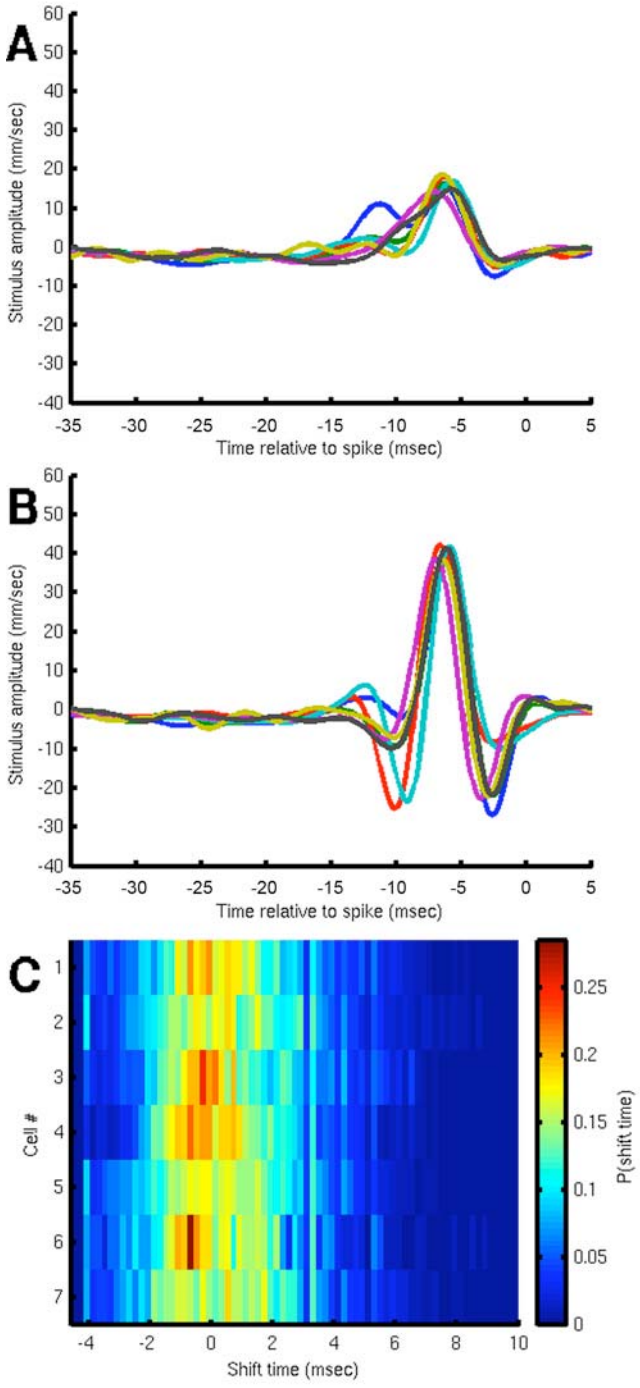

Figure 3.7. Composite average stimulus waveforms for a sample of seven cells from class 10-2a. *A*, Standard STAs. *B*, Dejittered means. *C*, Histograms of the shift times for the seven IN10-2a cells at an expanded time scale, with color coding for the fraction of samples shifted by the indicated time.

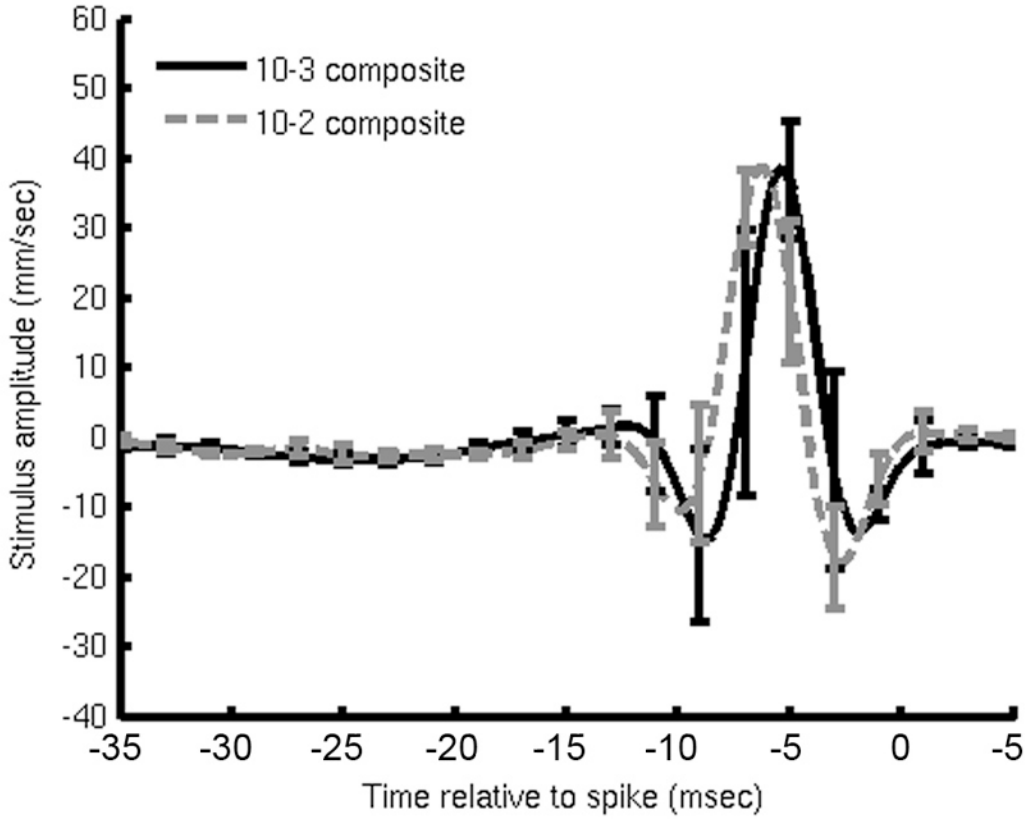

Figure 3.8. Comparison of the composite average dejittered mean stimulus waveforms for seven examples of each of the cell classes 10-3a (solid black curve) and 10-2a (dashed gray curve). Error bars on each curve represent one standard deviation across the corresponding sample.

degree intervals around the horizontal plane. Previous studies using Volterra analysis suggested that the 10-2a and 10-3a cells have indistinguishable dynamical sensitivities (Theunissen et al., 1996). In order to assess the dynamic response characteristics of IN10-2a, we repeated the experimental analysis and extracted de-jittered mean stimuli for a sample of seven R and L IN10-2as from different animals. The results are shown in Figure 3.7. The uncorrected STAs are shown in Figure 3.7*A*, and the dejittered means are shown in Figure 3.7*B*. The dejittered means were very similar to one another in duration, amplitude and

waveform. Each dejittered mean was significantly larger in amplitude than its corresponding uncorrected STA, by a factor ranging from 2 to 2.5. Figure 3.7*C* shows the jitter distributions for these seven cells on an expanded time scale. The mean σ_t for this sample of seven IN10-2a cells was 2.33 +/- 0.12 msec.

Figure 3.8 shows a comparison of the composite averages of the dejittered mean stimulus waveforms for the IN10-3a (solid black trace) and IN10-2a (dashed gray trace) sample sets. There is no significant difference between the two composite means, nor was there any significant difference between the two values for σ_t. This indicates that all four cells have functionally equivalent dynamic stimulus-response selectivities and characteristics within the stimulus regime tested here.

Calculation of the Information Rate for IN10-3a Using a Direct Method

In previous studies, the information encoding rates for a sample of 10-2a and 10-3a interneurons were calculated on the basis of a Volterra kernel-based analysis (Theunissen et al., 1996). Considering the extent to which the Volterra kernels were shown above to misrepresent these cells' stimulus selectivities, we wished to recalculate the encoding rate for an IN10-3a using a method that was independent of assumptions about stimulus selectivity (Buracas et al., 1998; Borst and Theunissen, 1999). This was done using a version of the 'direct method' (Strong et al., 1998; Paninski, 2003). The calculation was based on stimulus-response data from the same IN10-3a preparation used for Figures 2

through 5, within a regime where the mean spike rate was 10.8 spikes/sec. The information rate for this cell was calculated to be 27.2 +/- 0.4 bits/sec using the direct method. In contrast, the kernel-based calculation identical to that used in our previous studies, applied to the same data, yielded a rate of 20.3 +/- 1.5 bits/sec. This represents an upward revision of the calculated encoding rate by a factor of 1.34.

Discussion

Refinement of Conventional Techniques

Jitter happens. Although spike jitter has been characterized and considered in many studies (Bryant et al., 1973; Marsalek et al., Proc Natl Acad Sci U S A, 94, 735-40}; Berry et al., 1997; Mainen and Sejnowski, 1995; Victor and Purpura, 1996; Reich et al., 1997; Reinagel and Reid, 2000; Keat et al., 2001; Liu et al., 2001; Zoccolan et al., 2002; Uzzell and Chichilnisky, 2004; Hsu et al., 2004), it is not taken fully into account when analyzing feature selectivity with standard analysis techniques. Conventional methods for the derivation of the STA, STRF, or Volterra and Wiener kernels misrepresent the class of stimulus waveforms that elicit spikes in a cell: those techniques *underestimate* the amplitude and bandwidth of the mean stimulus waveform, and *overestimate* the variance of the waveforms around that mean. Application of this dejittering algorithm to cercal sensory interneurons 10-2a and 10-3a yielded estimates of the mean waveforms preceding isolated spikes that were up to 3 times larger in amplitude than the

STAs extracted from the same data sets, and also had greater relative power extending into a higher frequency range. Further, the dejittered estimates of IN10-3a's feature selectivity were more accurate and more precise than estimates obtained using the STA: the variance of the dejittered stimuli around the mean stimulus was substantially lower than the variance around the STA.

Conventional techniques also obscure the statistical structure of the stimulus-response latency relationship. Dejittered estimates disambiguate the uncertainty about the *time of occurrence* of the stimulus feature from the uncertainty about its *waveform*. Further, and perhaps more important, the variance σ_t of the jitter distribution provides an explicit metric for assessing the temporal precision with which a spike is linked to the occurrence of a specific stimulus feature. An implicit assumption is that the sensory system '*knows'* its own feature selectivity, as well as its intrinsic temporal uncertainty, and does not need such tools to obtain that information. The cell's output provides information about the stimulus waveform *and* its time of occurrence, but that information has some irreducible degree of uncertainty.

It is important to emphasize that dejittering cannot violate the data processing inequality. Information rates cannot be 'improved' by dejittering; rather, the *model of stimulus selectivity* is improved, enabling a better estimation of stimulus-response properties than other similar models that do not take explicit account of uncertainties in spike timing and/or feature waveform.

Implications for the Assessment of Temporal Precision

A consideration of the magnitude of σ_t is informative with respect to assessments of the time scale for neural coding. Many analyses of neural coding require an explicit determination (or assumption) of the precision with which a cell's spike train must be decoded (*i.e.*, its 'intrinsic' or 'natural' time scale). The width of the jitter distribution provides a rough estimate for the lower bound on that precision, assuming a linear encoding scheme (Theunissen and Miller, 1995). Regardless of the precision with which an upstream decoder could resolve the time of occurrence of a PSP from one of the interneurons we studied, the time of occurrence of the stimulus event that triggered the corresponding spike in that interneuron could not be resolved in time with more precision than the jitter distribution we observed. In the cells we studied here, the temporal uncertainty of the occurrence time for isolated spikes (calculated as $\pm 2\sigma_t$ of the jitter distribution) was approximately 5msec, which was approximately 20% of the duration of the significant portion of the dejittered waveform. This jitter in the stimulus-to-spike latency therefore appears to impose a significant constraint on the temporal accuracy of any linear decoding operation that could be carried out on the individual spike train from this cell. We note, however, that overall system-level temporal precision could be improved beyond this limit at a subsequent stage, through ensemble processing of this cell's spike train along with spike trains from additional cells carrying redundant and/or complimentary information (Chichilnisky and Kalmar, 2003). From this perspective, an essential role of

ensemble averaging of multiple redundant inputs might be to improve temporal precision, rather than (or in addition to) improving stimulus waveform recognition.

Note that information about other independent stimulus features cannot, in principle, be extracted from the distribution of spike latencies, even if latencies correlate with such features. This is because the *absolute* latencies are not available to later stages of the nervous system. However, additional information about feature identity is potentially obtainable from *relative* latencies in population responses. In this case, the response of a single cell should not be considered in isolation, but as part of a multi-cell response pattern.

Factors Contributing to Stimulus-to-Spike Timing Jitter

Although the dejittered mean yields a more accurate estimate of a cell's feature and frequency selectivity, this approach still cannot completely disambiguate the different intrinsic and extrinsic factors which contribute to the observed spike-timing variance. The GN waveforms we used for our determination of the dejittered means and σ_t values contained a broad range of stimulus waveforms. As shown in Figure 3.2, some waveform segments elicited spikes with relatively high timing precision (*i.e.*, low jitter σ_t). Such segments are very similar to the dejittered mean waveforms, and we might surmise that these are near-optimal stimuli. However, the long-duration GN stimuli *also* contained many more segments that were significantly different from the dejittered mean waveform, but were still similar enough that they elicited spikes. The inclusion of the responses from these sub-optimal stimulus segments in the dejittering

procedure would be expected to *increase* the value calculated for σ_t relative to the value that would be derived for spikes elicited by near-optimal stimuli. This is because the net blurring function can be conceptualized as a convolution of the 'minimal jitter' distribution (*e.g.*, resulting from presentation of a truly optimal stimulus, due to all lumped factors contributing to biophysical noise) with the distribution emerging from the responsiveness of the cell to a range of stimuli around the mean. Although the *shape* of the dejittered mean will not necessarily be effected by the inclusion of these less-than-optimal stimulus-response samples (*i.e.*, if their deviation from the mean waveform is symmetric), the estimated σ_t will depend on the specific dataset used for the calculation, and will always overestimate the minimal jitter due to biophysical noise alone.

Other Related Measures of Spike Jitter

There have been many previous characterizations of spike latency jitter. In most cases, the experimental paradigms have involved the repeated presentation of a specific stimulus waveform to a cell, and the analyses have been based on observations of the variation in spike timing in the corresponding set of elicited spike trains. Researchers in one of the most rigorous studies (Berry et al., 1997) calculated a quantity τ that is somewhat similar to our measure σ_t. However, this τ measure does not take the variability in spike latency between events into account. Specifically, by using the median value of the standard deviation of spike times to assess total variation, all information about the mean value of spike times (indicating spike latency) is lost from the calculation. If

different events have different mean stimulus-to-spike latencies (which is certainly the case in our data set), then τ will significantly underestimate the total variability of spike timing. To illustrate the extent to which this quantity τ underestimates the actual spike jitter, we calculated τ using stimulus-response data from the IN10-3a used for figures 2-5. We found τ calculated in this manner to have a value of 1.5msec, compared with σ_{tf} of 2.2msec for this same cell using the dejittering approach.

Implications for Kernel-Based Analyses of Information Encoding Rates

To the extent that the timescale of spike jitter is significant with respect to the correlation time of the mean waveform, and to the extent that the dejittered mean differs in shape from a kernel, we lose confidence in the relevance of the 'stimulus reconstruction' approach and the measure of 'gain' as a means for characterizing information coding rates. The use of a distorted kernel to generate an estimate of the stimulus waveform leads to a severely low-passed underestimate of that stimulus. The subsequent use of this distorted stimulus estimate to derive a lower bound to the encoding rate results in a bound that is lower than we had imagined, to a degree that is difficult to quantify. To borrow a term from the realm of political science, we would *misunderestimate* the true coding rate (see (Hsu et al., 2004) for an excellent discussion).

There are alternate approaches for estimating encoding rates which make no explicit assumptions about details of stimulus representation, such as the 'direct

method' (Strong et al., 1998; Paninski, 2003). Although these methods provide no explicit information about a cell's feature selectivity, they can provide accurate estimates of the total information available to potential downstream decoders that are insensitive to spike jitter. Our application of the direct method to stimulus-response data from IN10-3a yielded an estimate for the information encoding rate that was a factor of 1.3 higher than the rate estimated using the conventional kernel-based stimulus reconstruction method we had used in earlier studies. Thus, even in the case of this IN10-3a, which appears to be well-approximated as having a nearly linear encoding scheme, calculation of the lower bound on information encoding rate by integration under the 'gain' curve had lead to a substantial underestimate of its channel capacity.

Reappraisal of Encoding by This Four-Cell Group of Cricket Cercal Interneurons

Beyond this upward revision of the estimate of IN10-3a's coding capacity, the results of this analysis also lead us to a refinement of our understanding of the feature sensitivity of this set of interneurons. These four interneurons appear to have much higher feature selectivity than was realized previously, and the mean stimulus waveform eliciting a spike differs significantly from kernel-based estimates with respect to amplitude and frequency composition. Previous estimates indicated a stimulus frequency selectivity limited to the range between 5 and 80 Hz, with peak sensitivity at 15 Hz (Theunissen et al., 1996). The new estimates, based on the dejittered means, indicate that stimulus frequency

selectivity extends to at least 200 Hz, with peak sensitivity ranging between 100 and 150 Hz.

This range brackets the wing-beat frequencies of predatory wasps (Gnatzy and Heusslein, 1986) and other signals of neuroethological significance that had previously been considered as undetectable by these cells. One possible role for this group of low-threshold, directionally-selective cells is as an ‘early warning’ system for detecting the approach and direction of such flying predators.

TEMPORAL CODING

Abstract

The possibility of temporal coding in single neurons of an invertebrate sensory system is examined. We study the elicitation of temporally precise patterns of two spikes ('doublets') by repeated Gaussian white noise stimuli. We find that the timing of spikes occurring within 30 msec of each other covary significantly: spike doublets with ISIs of 5 msec and less have correlation coefficients of 0.5 or greater, exceeding the correlation expected from consideration of a hard refractory period alone. We then develop linear and non-linear models for decoding these doublets, and compare the capabilities of these two types of decoding schemes in representing the stimuli which elicited the doublets. We find that doublets with ISIs of 2-4 msec are elicited by stimuli which cannot be predicted as well by a linear model (such as the kernels from linear reconstruction) as by models which consider second-order, non-linear interactions between spikes.

Introduction

The question of whether or not individual neurons can use temporal patterns of spiking activity to represent stimuli has generated a large amount of controversy over the last three decades (e.g. Richmond et al., 1987; Shadlen and Newsome, 1994; Laurent and Davidowitz, 1994). While it has been shown that

neurons can respond to temporally-varying stimuli with high precision (Bryant and Segundo, 1976; Mainen and Sejnowski, 1995; Bair and Koch, 1996; de Ruyter van Steveninck et al., 1997), it is not known to what (if any) extent this precision is used to represent aspects of the stimulus beyond its own temporal modulation. This has led to the suggestion that temporal coding, as defined in (Theunissen and Miller, 1995), is not implemented in individual neurons, and rather that the temporal precision of neuronal responses to stimuli is used only to represent high-frequency components of the stimulus, a form of rate coding (Buracas et al., 1998; Borst and Theunissen, 1999).

In this article we examine whether or not temporal coding may be operative in the cercal system of the house cricket, *Acheta domesticus*, by first determining whether stimuli can reliably elicit precise temporal patterns of spikes in the presence of known jitter in stimulus-response timing, and second by determining whether the stimuli associated with temporal patterns of spikes are significantly different than what is predicted by linear reconstruction theory.

Materials and Methods

Preparation

Experiments were conducted on 32 female crickets of the species *Acheta domesticus*, obtained from a commercial supplier (Basset's Cricket Ranch, Visalia California). Animals were fed water and dry cat food *ad libitum*, and were kept on a 12 H:12 H light-dark cycle (experiments were performed at all phases

of this cycle). Specimens were selected which had undergone their imaginal molt within the last 48 hours.

Crickets were anaesthetized by placing them on ice for 5-10 minutes. The legs, ovipositor, and wings were all removed, along with a small flap of the dorsal abdominal cuticle. The gut, reproductive organs, and fatty tissue were all removed and the abdominal cavity was connected to a perfusion system containing hypotonic cricket saline (O'Shea and Adams, 1981). The preparation was pinned to a disk of silicone elastomer, and all incisions from removing the legs and ovipositor were sealed with petroleum jelly. A small steel platform was inserted under the terminal abdominal ganglion, which was then gently lifted from the surface of the abdominal cavity. Care was taken so as not to disturb the trachea.

Stimulation

Experiments were performed in a custom-designed stimulation system described previously in (Dimitrov et al., 2003). Briefly, air movement was generated with a bank of 8 speakers, subdivided into two groups of four. Within each group of four speakers were two pairs located on opposite sides of the cricket. The two pairs of speakers were driven with inverted versions of the same computer-generated, power-amplified waveform, forming a push-pull mechanism for creating airflow from both sides of the body. The two groups of four speakers were oriented perpendicularly to each other, allowing stimulation from any arbitrary angle within the horizontal plane. Calibration of the stimulus

system was performed with a low-velocity air current sensor (MicroFlown Technologies, Zevenaar, Netherlands). Air particle displacement caused by the movement of the speakers stimulated the filiform hairs on the crickets' cerci.

All stimuli consisted of single-dimensional, 10-200 Hz band-passed (BP) Gaussian White Noise (GWN) air movement with an RMS amplitude of 72-76 mm/sec. Stimuli were either long-term, non-repeating stimuli of approximately 33 minutes length for the stimulus codeword analysis, or else 30 to 100 repeats of a short, 10 second segment for the analysis of temporal variability of the doublet spiking pattern.

Electrophysiology

Intracellular recordings were made from neurons 10-2a (n=19) and 10-3a (n=21), two pairs of giant projecting interneurons in the terminal abdominal ganglion of the cricket (Jacobs and Murphey, 1987). Sharp intracellular electrodes were pulled from glass capillary tubes using a model P-97 Flaming/Brown Micropipette Puller (Sutter Instruments Co., Novato, CA). Electrode penetration was facilitated by applying a small piece of kimwipe paper soaked in an approximately 2% protease solution (Sigma-Aldritch, P5147, St Louis, MO) for 2-3 minutes. Electrodes were backfilled with 2% Neurobiotin (Vector Laboratories, SP1120, Burlingame, CA) in ddH_20 and then filled with 3M KCl. Electrode resistances were between 2 and 10 MΩ. During recordings the Neurobiotin passively entered the neuron, allowing for later morphological identification. Membrane potential and amplified stimulus voltage were sampled

at 10 kHz and recorded on a Windows XP computer running custom-built Labview software.

Histology

Following electrophysiology, neurons filled with neurobiotin were prepared with a ABC-DAB reaction for morphological identification (full protocol at http://cns.montana.edu/lab-private/recipes/StaudacherNeurobiotin.pdf). Briefly, the abdominal nerve cord was dissected out of the animal, fixed overnight in paraformaldahyde (5% mixed with 0.1 M millonigs tween buffer), stored for at least two days in millonigs tween, incubated first for 40 hours with a Streptavidin-biotin complex (DAKOCytomation, K0377, Glostrup, Denmark), then for 1 hour with a DAB solution (Vector Laboratories, SK4100), reacted with H_20_2 solution in millonigs buffer, put through an ascending alcohol series, cleared with xylene and mounted in DPX for morphological identification. 29 of the 40 cells used in the study were identified by morphological characteristics (the remaining 11 were identified by their physiological responses).

Identification of Doublet Events

Doublet events that were consistently elicited by repeated presentations of the stimulus were identified with a modified version of the event identification protocol from (Yen et al., 2007). First, in order to avoid results due to including data in which the cell was adapting, we excluded repetitions of the stimulus where the average firing rate differed by more than 20% from the average firing

rate across all trials. The adapted responses to repeating trials of the stimulus were then binned into histograms at 1 msec resolution, and thresheld at thirty times the mean firing rate in order to define firing boundaries of events. From the collections of all events in the data set it was determined which ones consisted of doublets with no contaminating spikes in a 70 msec window around the event for at least 20% of the trials (varying between 10-90% of the trials did not greatly effect the results of the correlation analysis). For each doublet event, the timing of the first and second spikes of the doublet on each trial was then extracted. For analysis of the population data (figure 4.2 E), all of the events with a specified ISI were pooled across data from the 40 cells.

Response-Conditioned Stimulus Models

Two distinct doublet-conditioned stimulus models were developed. For the first model, all of the well-isolated doublets of a given inter-spike-interval, which were neither preceded nor followed by other spikes, were located. The stimulus from 40 msec prior to the doublet event and extending to 1 msec before the second spike of the doublet were collected to form the doublet-triggered stimulus ensemble (DTSE). 10% of these stimuli were held out for later testing as the test doublet-triggered stimulus ensemble (tDTSE), while the remaining 90% of the ensemble was used to build the data-based, or doublet-triggered stimulus model (DTSM). This consisted only of the mean, μ_{doub}, and the covariance matrix of the ensemble, C_{doub}, both sampled at 1 kHz.

For the second model all of the single spikes (isolated by the same criteria

used for the doublets) were found. Again all of the stimuli were collected, this time extending from 40 msec plus the length of doublet ISI to be modeled prior the spike to the ISI-1 msec after the spike. The entire singlet-triggered stimulus ensemble (STSE) was then used to build a Gaussian model (with mean and covariance specified). In order to form a model of the stimulus for the doublet, the Gaussian model of the single spike-triggered stimulus was replicated, shifted in time by the amount of the desired ISI, and finally summed to form the synthetic doublet-triggered stimulus model (sDTSM), composed of the synthetic mean, μ_{sd}, and covariance matrix, C_{sd}.

To ensure that the variance of the synthetic model did not bias our likelihood estimates, we normalized the diagonal of the covariance matrix of the synthetic model to match that of the isolated singlet model.

Likelihood Test

The relative ability of the sDTSM and the DTSM to predict the stimuli preceding a doublet response was tested with a simple log likelihood test. The log likelihood L for each sample x of the tDTSE coming from each model is calculated by:

$$L = -\frac{1}{2}\sum_{j=1}^{n}\left[(x-\mu)\left(C^{-1}\right)_j(x-\mu)\right] - \log(2\pi) * \frac{n}{2} - \log\left(|C|^{\frac{1}{2}}\right) \qquad (4.1)$$

where n is the dimensionality of the model, μ and C are the mean and covariance of the model being tested (either the DTSM or sDTSM), and |•| represents the determinant of the matrix. The ratio of these two log likelihood values,

L_{DTSM}/L_{sDTSM}, was then calculated. Samples with log likelihood ratios greater than zero were more likely to have been elicited by the data-based model, while samples with log likelihood ratios less than zero were more likely to have been elicited by the synthetic model.

iSTAC Analysis

In order to compactly describe the difference between the DTS and the sDTS models, we borrow from the "information-theoretic spike-triggered average and covariance" (iSTAC) analysis of (Pillow and Simoncelli, 2006), which is intended to describe the difference between a spike-triggered ensemble and an unconditional GWN stimulus. We briefly summarize their method here:

Since our DTSM is Gaussian, we can denote the probability of a stimulus x given that a doublet occurred as:

$$P(x) = \frac{1}{(2\pi)^{\frac{n}{2}} |C_{doub}|^{\frac{1}{2}}} e^{-\frac{1}{2}\left[(x-\mu_{doub})^T C_{doub}^{-1} (x-\mu_{doub})\right]} \tag{4.2}$$

We can take advantage of this probabilistic description to describe the difference between our two models using the Kullback-Leibler distance:

$$D(P,P') = \int_{R^n} P(x) \log \frac{P(x)}{P'(x)} dx \tag{4.3}$$

where $P'(x)$ is the probability of a stimulus x given that a doublet occurred according to the sDTSM. $D(P,P')$ is an information-theoretic quantity describing the difference between the two distribution in bits.

In order to effectively make our sDTSM zero mean with unity covariance, we can de-mean and 'whiten' our DTSM according to:

$$\mu_W = C_{sd}^{-\frac{1}{2}}\left(\mu_{doub} - \mu_{sd}\right) \tag{4.4}$$

and

$$C_W = C_{sd}^{-\frac{1}{2}} C_{doub} C_{sd}^{-\frac{1}{2}} \tag{4.5}$$

where μ_W and C_W are the whitened DTSM mean and covariance, respectively. This allows us to simplify equation 4.3 to:

$$D(P,P') = \frac{1}{2}\left(Tr(C_W) - \log|C_W| + {\mu_W}^T \mu_W - n\right) \tag{4.6}$$

where $Tr(\bullet)$ represents the matrix. We can then specify an m-dimensional subspace of $D(P,P')$ with orthonormal basis B:

$$D_{[B]}(P,P') = \frac{1}{2}\left(Tr\left[B^T\left(C_W + \mu_W {\mu_W}^T\right)B\right] - \log\left|B^T C_W B\right| - m\right) \tag{4.7}$$

The most informative such subspace is described by the B which maximizes equation 4.7.

We repeat this procedure for a variety of dimensionalities m, ranging from single dimensional to the full dimensionality of the DTSM.

Results

Simulation of Distinct Stimulus-Conditioned Spike Interactions

Our goals in this study were two-fold. First, we wished to find out if temporally-precise patterns of stimulus-evoked spiking activity could persist in

the presence of the observed level of variability in stimulus-response latency. Second, we wished to determine whether or not a non-linear decoding operation on such doublet spike patterns could represent stimuli with greater accuracy than would be obtainable through linear-reconstruction decoding.

In order to address the temporal precision question, we first consider three very simple models of how spikes in repeatable patterns of doublets could interact with each other. For each model, two parameters were held constant. The first parameter was the jitter in spike timing across trials, defined as the standard deviation of the normal distribution used to draw the event times. This was set at 1.3 ms (equal to the across-trial jitter of isolated single spikes in 40 recordings from cells 10-2a and 10-3a). The second parameter held constant was the inter-spike interval averaged across trials. This parameter was set to a value of 3 msec.

For the first of the three models, the timing of the two spikes in the doublet in each trial were drawn from two independent normal distributions (distribution for time of first spike mean=0 msec, standard deviation=1.3 msec; distribution for time of second spike mean=3 msec, standard deviation=1.3 msec). This meant that on any given trial there was no correlation between the first and second spikes of the doublet. In practice the first observed spike was always attributed to the ‘first spike’ model, regardless of which model actually generated the spike. This induced a small correlation between first and second spike times across trials (figure 4.1 G, blue trace).

For the second of the three models, spike times were again drawn independently from the above-mentioned distributions, but correlation was then implicitly imposed through a hard refractory period. This was implemented by finding all trials in which the first and second spike occurred within 2 msec of each other (the minimum observed ISI in recordings from actual 10-2a and 10-3a cells), and then moving the arrival time of the second spike to 2 msec after the first.

For the third model, correlation was explicitly imposed by reducing the variance of the normal distribution of the second spike and conditioning it to the time of the first spike. The distribution of the first spike times remained as above, but the distribution of second spike times conditioned on the time of the first spike was drawn from a normal with mean 3 msec and standard deviation of 1.3 msec. Conditioning the time of the second spike on the time of the first spike in this way effectively produced ISIs with very narrow distributions relative to the first two models.

The results of running these simulations are shown in figure 4.1. Although all three models produced relatively equivalent-looking rasters and PSTHs (figure 4.1 A, C, and E, upper and lower plots, respectively), the distributions of both spikes minus the time of the first spike (effectively the ISI- figure 4.1 B, D, and F) are distinct between models, with each model showing a different amount of correlation due to the correlation put into them by design.

Figure 4.1 G shows how these correlations, as expressed by Pierson's

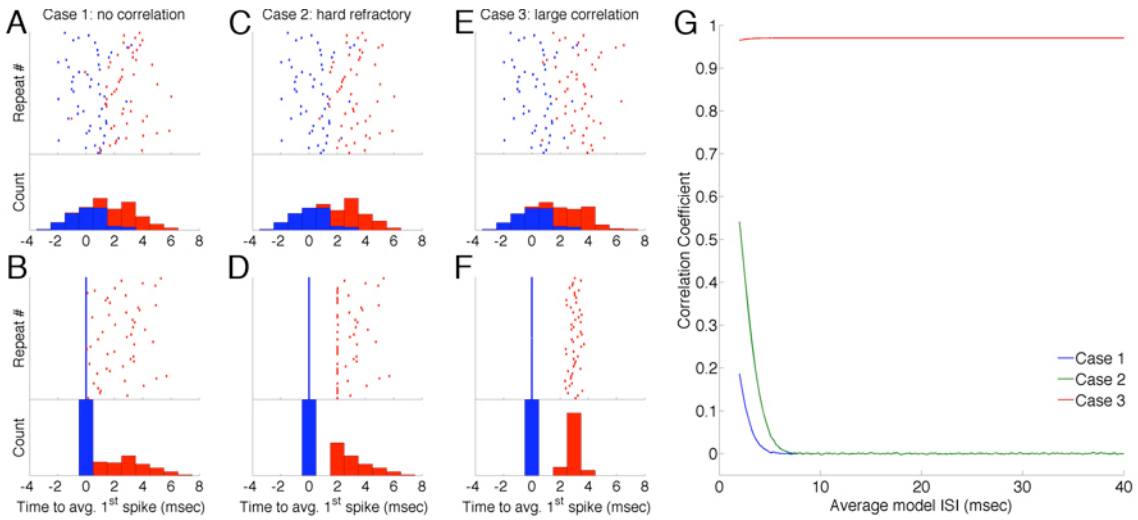

Figure 4.1. Three models of spike-spike interactions in a doublet pattern. A, Upper trace: simulated raster plot of a cell's response to repeated presentations of a stimulus which reliably elicits a doublet with mean ISI of 3 msec. Both the first (blue) and second (red) spikes in the doublet are drawn independently from normal distributions with means of 0 and 3 msec, respectively, and standard deviations of 1.25 msec. A, Lower trace: standard PSTH of raster from upper trace, color convention conserved. Timing is relative to the stimulus, with T=0 representing the average time of occurrence of the first spike in the doublet. B, Upper and lower traces: raster plot and PSTH showing same data from A with each row aligned to the time of occurrence of the first spike in the response on each presentation, rather than to the stimulus or average time of spike occurrence. C and D: same data presentation as in A and B for doublet spiking with mean ISI of 3 msec, however the simulation breaks the independence of the first and second spike by enforcing an absolute refractory period of 2 msec between spikes. E and F: (data presentation as in A and B) simulation of doublet spiking with mean ISI of 3 msec and first and second spikes subject to high degree of correlation. G: simulation showing how correlation coefficient between timing of first and second spikes of doublets drawn from the three previous models evolve for mean values of ISI ranging from 2 msec to 40 msec.

correlation coefficient, would evolve if the average ISI was varied between 2 msec and 40 msec. Note here that the correlation for the third model is explicitly kept high for all ISI values, which could be explained as a low frequency noise source which adds stimulus-to-response jitter, but also acts to correlate nearby spikes (Reinagel and Reid, 2000). The second and third models represent minimally and maximally precise doublet-spiking according to biophysically plausible mechanisms, while the first model shows doublet spiking as predicted by strict

interpretation of the assumptions of linear reconstruction analysis.

Measurement of Pattern Variability

We measured the variability of doublet spiking in giant interneurons 10-2a and 10-3a of the cricket cercal system to repeated presentation of white noise stimulation. Figure 4.2 summarizes the results for the 40 neurons from which recordings were obtained. 4.2 A shows the a portion of the response of an IN 10-2a to 80 presentations of a stimulus that elicited a doublet of 2.45 msec on average. The upper and lower plots show the raster and PSTH of the spiking, respectively. The temporal precision of the first and second spikes, as measured by the standard deviation of the distributions, were 0.58 and 0.57 msec, respecitively. Figure 4.2 B shows spiking from the same event, but now conditioned on the first spike of the event rather than the time of the stimulus. The precision of the ISI, as measured by the standard deviation of the difference between the second and first spike time, was 0.13 msec. It can be seen that while the individual spikes times elicited by the stimulus had a relatively large degree of variability, the overall ISI response to the stimulus could be extremely precise.

Figure 4.2 C-D shows raster data and a PSTH for a second event from the same recording as in figure 4.2 A-B. The mean ISI of this second event was larger than the first, 6.52 msec compared with 2.45 msec, while the precision of each spike within the doublet were similar to before (0.61 msec and 0.53 msec for the first and second spikes of the doublet, respectively). Here however, it is

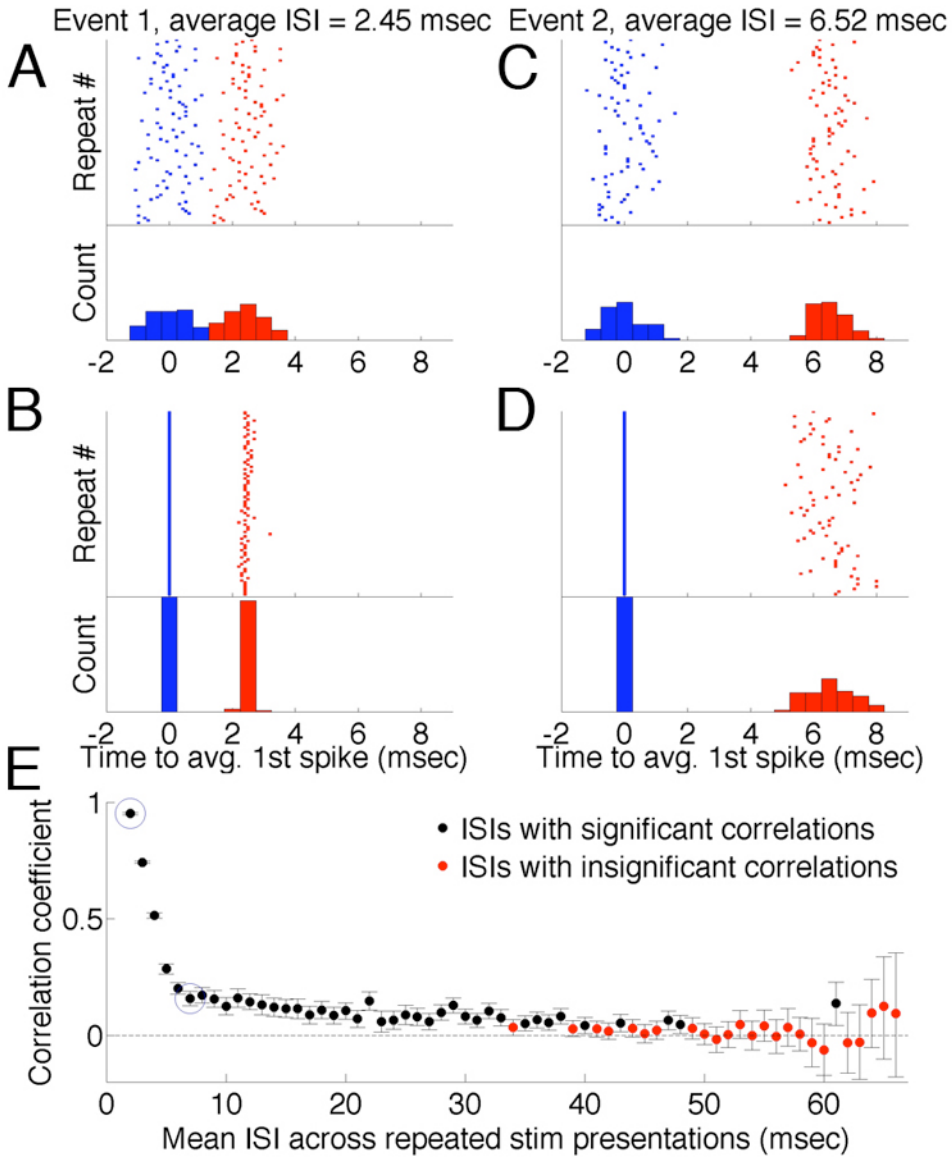

Figure 4.2. Spike-spike interactions in doublet patterns recorded in cricket interneurons. A, Upper trace: recording from a right interneuron 10-2a, showing a raster of 80 responses to repeated presentations of a GWN stimulus. The cell consistently responded to the stimulus by firing a doublet (first spike shown in blue, second spike in red) with average ISI of 2.45 msec. A, Lower trace: PSTH of data from raster upper trace, with the color convention conserved. B, upper and lower traces: raster plot and PSTH showing same data from A, here aligned to the time of the first spike in the doublet (t=0) rather than the timing of the stimulus. C and D, data from a second doublet event (mean ISI = 6.52 msec) from the same interneuron, data presentation conserved. E: estimate of correlation coefficient between first and second spikes in repeatable doublets recorded from 40 different cells in 32 animals, as a function of ISI (7753 events composed of 387,708 total spikes). Correlation coefficients which are significantly different from 0 at the 95% confidence level are shown in blue, correlation coefficients which are insignificantly different from 0 are shown in red. Error bars represent 95% confidence limits on estimation of correlation coefficient. Blue circles indicate ISIs exemplified in panels A-D.

shown that the distribution of the ISI itself is not reduced relative to the two spikes which compose it (precision = 0.71 msec).

In figure 4.2 E the data from 7753 events occurring in recordings from 40 cells is pooled to find the correlation between first and second spikes in a doublet as a function of the average ISI of the doublet. It can be seen here that there is significant correlation out to approximately 35 msec ISIs, and that for short ISIs (~<5 msec) the two spikes in doublets are tightly correlated. In principle this means that stimulus events which can elicit short doublet ISIs will almost always produce the same response pattern, while stimuli that produce average ISIs of 10 msec or greater will produce doublet responses with a high degree of noise across the ensemble. However, while short doublets can be reliably elicited, it is not clear whether or not they code for anything different than what could be predicted by linear reconstruction analysis.

Modeling of Pattern-Conditioned Stimuli

To determine whether or not these temporally-precise response patterns represented stimuli distinct from what is predicted by linear reconstruction analysis, we developed a novel model test. For a specific ISI, a model of the doublet-conditioned stimulus ensemble was generated by collecting 90% of the stimulus samples associated with that ISI, and then taking the mean and covariance across the sample. This was referred to as the data-based doublet-conditioned model. To build a model of the same ISI which was consistent with

the stimulus-reconstruction methodology, we first collected the stimulus associated with isolated single spike events, and took the Gaussian approximation of the ensemble as above. We then took two copies of the same model, offset them by the desired ISI, and summed the means while summing and conditioning the covariance matrix (see methods). This produced a model of the stimuli associated with a doublet consistent with the assumptions of linear reconstruction, which we denote as the synthetic doublet-conditioned model. To test which of these models explained the data better, we performed a likelihood ratio test between the two models and the 10% of the data which was not used to build the data-based model. We then took the log of the ratio test, so that models which were equally likely to explain the data had a log-likelihood ratio value of zero, cases in which the data-based model outperformed the synthetic model had values > 0, while in the reverse case the value was < 0. A schematic for building the models and the results of the likelihood test for the same cell as used in figure 4.2 are shown in figure 4.3. In this case, doublets with ISIs of 2 and 3 msec had stimuli preceding them that could not be predicted by the synthetic model. For ISIs greater than 6 msec the synthetic model actually outperformed the data-based model, which we attribute to overfitting of the data-based model in this spiking regime for which not many samples were produced by white noise.

Consistency of Measure Across Population of Animals

In order to show which ISIs across our population of cells had log-likelihood

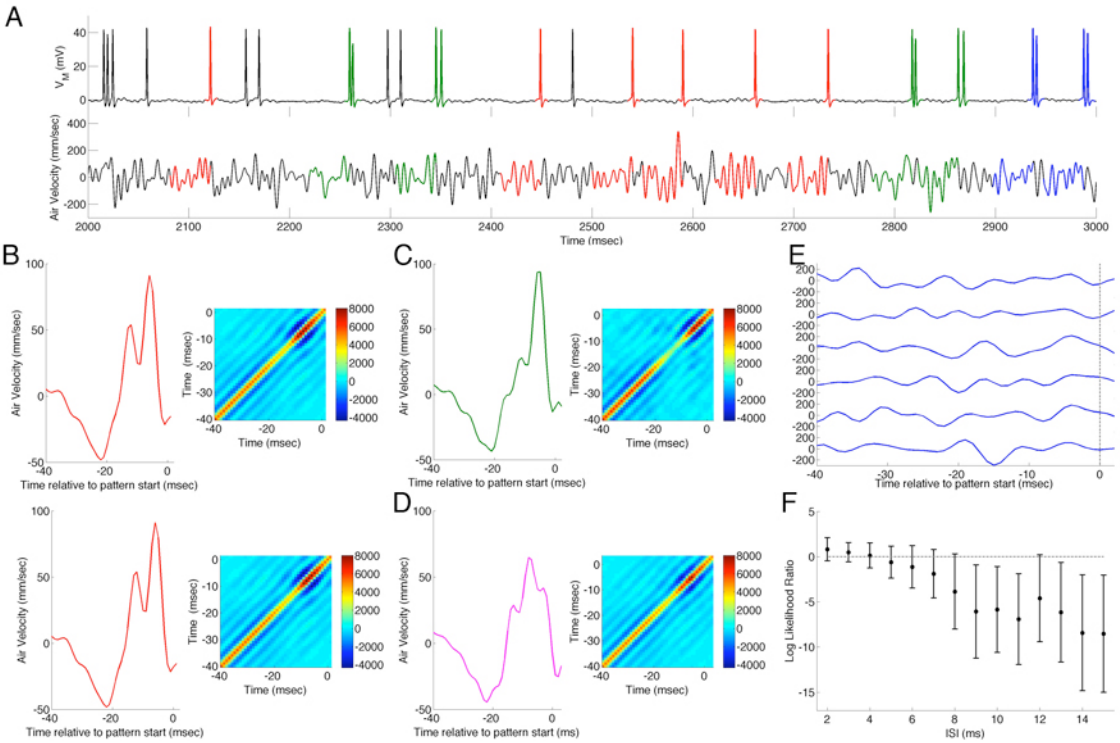

Figure 4.3. Building and testing of models of stimuli associated with doublet spiking patterns. A, simultaneous recording of 1 second of GWN wind stimulus (bottom trace) and intracellular response (upper trace) from same interneuron as in figure 4.2. Well-isolated response patterns are divided into two groups: isolated single spike responses (red) and short doublets of approximately 3 msec (green and blue). Response patterns which either are not sufficiently isolated or otherwise do not fall into one of the two groups are not considered in subsequent analysis (black). The 30 msec of the stimulus preceding the response pattern is highlighted in matching colors. B, Upper panel: Gaussian model of 30 msec of stimulus preceding an isolated single-spike response, consisting of a mean (left panel) and covariance (right panel) of the entire single-spike-conditioned stimulus ensemble (13,375 events from 30 minutes of recording). B, Lower panel: same Gaussian model as in upper panel, offset by 3 msec. C: Gaussian model (mean and covariance) of 30 msec of stimulus preceding isolated doublet response patterns with 3 msec ISIs, based on 90% of the doublet-conditioned stimulus ensemble (2,652 events from 30 minutes of recording). D: Synthetic Gaussian model of stimulus preceding 3 msec doublets, obtained by summing the means from panel B and summing and then constraining the covariances (see methods). E: Selection of 6 of the 294 stimulus samples which elicited a 3 msec doublet response which were not used to build the Gaussian model in panel C. These samples were used to probe the synthetic and data-based Gaussian models of the doublet-conditioned stimulus ensemble in a log-likelihood test. F: Log-likelihood ratio for data-based models to synthetic models for ISIs ranging from 2 to 15 msec, same interneuron as in panels A-E. Error bars represent standard deviation of the mean log-likelihood ratio obtained by randomly shuffling the model and test samples (10-fold validation).

ratios indicating a non-linear mapping of stimulus space, we performed a T-test

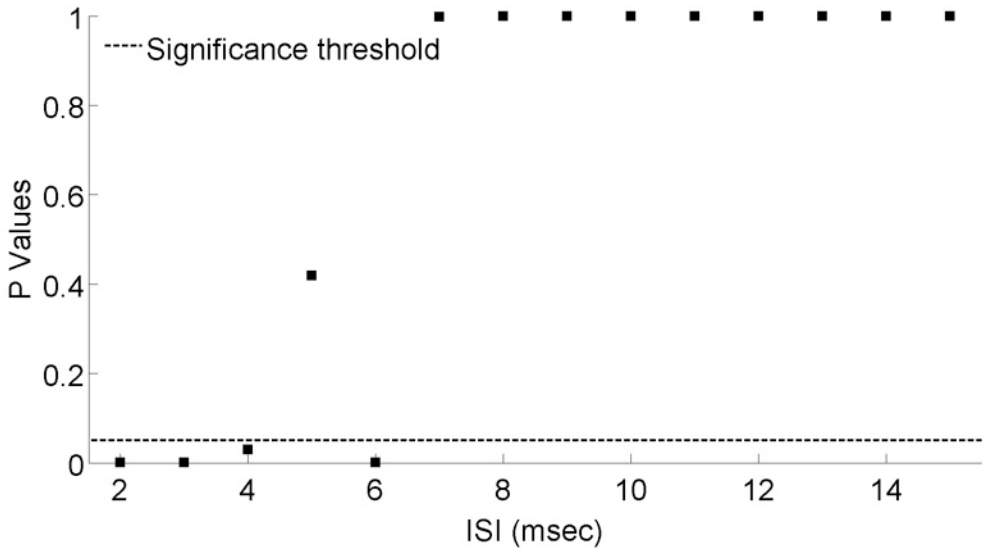

Figure 4.4. T-test for log-likelihood distributions. P values from t-test to determine if log-likelihood ratio data for each ISI (pooled across 10-fold validation sets and across 40 cells) could have randomly arisen from distributions with means less than 0. The null hypothesis is that the distributions *could* have arisen from means less than zero- P values greater than the significance threshold of 0.05 are insufficient to reject the null hypothesis.

against the null hypothesis that the log-likelihood values were drawn from a distribution with mean less than zero. To perform this test we first lumped together all of the log-likelihood values for a given ISI across our population of 40 cells. We then performed a right-tailed T-test on our sample of log-likelihood distributions at each ISI. We selected a significance threshold of 0.05, meaning we could reject the null hypothesis of linear mapping when our sample distribution of log-likelihood values had only a 5% or smaller chance of coming from an underlying distribution with mean less than or equal to zero simply by chance. Figure 4.4 shows the P values resulting from this test as a function of ISI.

For ISIs between 2 and 4 msec, the null hypothesis can clearly be

rejected. It is a little perplexing that for ISIs of 6 msec we could reject the null hypothesis, but for values of 5 msec we could not. We take the conservative approach to interpreting this and say that the stimulus preceding ISIs of up to 4 msec could not be predicted by linear reconstruction models.

Quantification of Difference in Synthetic and Data-Based Models

To quantify how our synthetic models differed from the data-based models of pattern-conditioned stimuli, we used the iSTAC form of dimensional reduction (Pillow and Simoncelli, 2006). This analysis attempts to find the most informative subspace between two multi-dimensional Gaussian spaces by finding the subspace which maximizes the Kullback-Leibler divergence between the two spaces, which reduces to equation 8 in (Pillow and Simoncelli, 2006). This dimensionality reduction can be performed to recover a maximally informative subspace of any dimensionality, from single-dimensional up to the full dimensionality of the original spaces. Along with the vectors specifying the coordinate axes of the subspace, the method also returns an estimate of the KL-divergence captured by each of the vectors in the subspace.

We use the iSTAC analysis to examine the difference between the synthetic and data-based models from the cell shown in figure 4.3 for three ISIs of interest: an ISI where the data-based model outperformed the synthetic model in describing the test data set; an ISI where the two models performed the same; and an ISI where the synthetic model outperformed the data-based model. These corresponded to ISIs of 2 msec, 4 msec, and 6 msec respectively, as

seen in figure 4.3 F. The results of the iSTAC analysis are shown in figure 4.5. In the case of the 2 msec model, most of the power in the first three maximally-informative dimensions lies between 17 and 7 msec prior to the onset of the pattern (figure 4.5 A1, bottom three traces). In contrast, for the 4 and 6 msec doublet-conditioned stimuli, the largest dimension has the most power in the time between ~0 and 2 msec after the first spike in the pattern, times which are probably too late for the stimulus to have a causal effect on spike generation, considering the latency of the cell (figure 4.5 A2 and A3, bottom three traces). Also note that repeated calculations of the iSTAC dimensions using different subsamples of the full data set repeatedly produce the same dimensions for the 2 and 4 msec doublet-triggered stimuli, while producing variable dimensions for the 6 msec model (figure 4.5 A3, bottom two traces).

In evaluating the K-L divergence between the different models, we see that for 4 msec ISIs, where both models perform equivalently in explaining data, that the total information recovered (the asymptote of the green curve in figure 4.5 D) is less than in the case of the other two models, as one would expect. Somewhat surprising is that the information recovered from the difference between the 6 msec models is larger than for the 2 msec model, but this could again reflect differences in the portions of the model that are not causally related to the spiking of the cell (see above). Finally, we note that a greater proportion of the difference between models can be described by a fixed number of dimensions for the 2 msec model compared with the others, as the cumulative

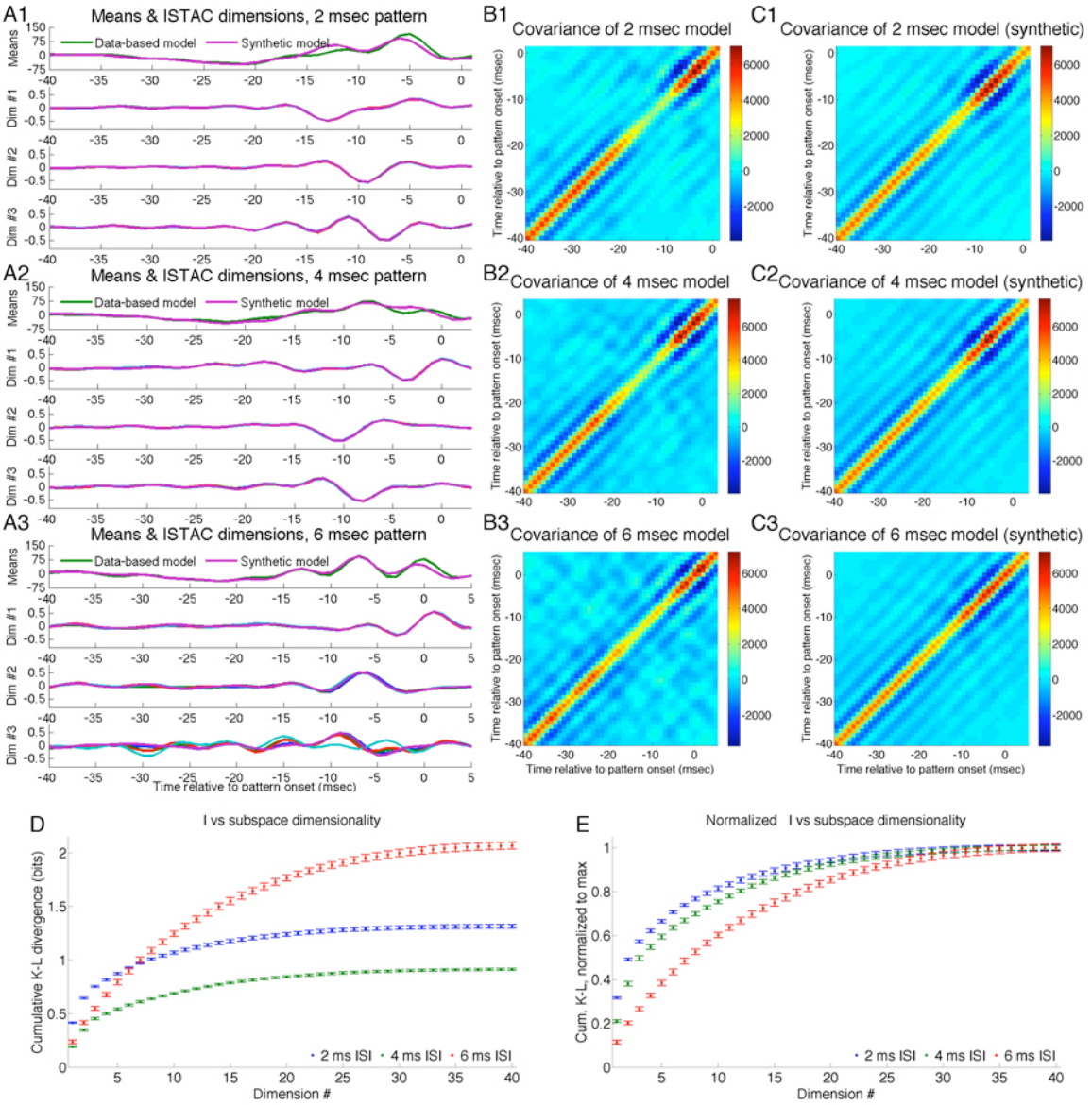

Figure 4.5. iSTAC analysis of difference between data-based and synthetic models of stimuli associated with doublet spiking patterns. A1, upper panel: Mean of data-based (green) and synthetic (magenta) Gaussian models for stimulus preceding a 2 msec doublet, from same cell as in figures 2-3. Covariance of data-based and synthetic models shown in panels B1 and C1, respectively. A1, second panel from top: 5 separate estimates of most informative iSTAC dimension, each obtained by performing dimensional reduction between different validation subsets of the data-based model with the synthetic model. A1, third and fourth panels from the top: 5 separate estimates of second and third most informative iSTAC dimensions, respectively, obtained as above. A2, B2, and C2: same analysis for difference between data-based and synthetic Gaussian models of 4 msec doublet-conditioned stimuli. A3, B3, and C3: same analysis as above for difference between data-based and synthetic Gaussian models of 6 msec doublet-conditioned stimuli. D: measure of total K-L divergence between data-based and synthetic models for 2 msec (blue), 4 msec (green), and 6 msec (red) doublet-conditioned stimuli, as a function of subspace dimensionality. E: measure of K-L divergence as in panel D, normalized to maximum K-L divergence = 1.

information for this model approaches its asymptotic value more quickly (figure 4.5, E).

Discussion

Temporal Coding Hypotheses

The nature of the neural code has long been debated. While early work such as that of Adrian showed that much of the information about the stimulus is contained in the firing rate of a neural response (Adrian and Zotterman, 1926), more sophisticated analyses have demonstrated that information about the stimulus can be extracted based on the timing of individual spikes in the neural response (Bialek et al., 1991; de Ruyter van Steveninck et al., 1988; Rieke et al., 1997). Additionally, it has been shown that neurons are capable of responding with responses as temporally precise as 1 msec to repeated presentations of dynamic stimuli across a variety of experimental animals as well as sensory modalities (Bair and Koch, 1996; Berry et al., 1997; Bryant and Segundo, 1976; Mainen and Sejnowski, 1995; Reinagel and Reid, 2002). This has led to the hypothesis that neurons might additionally utilize a temporal code, where patterns of spikes are used to represent stimuli distinct from that which could be predicted based on consideration of spikes that occur in isolation (Theunissen and Miller, 1995). However, several factors act to constrain the usefulness of such a code- temporal patterns are bounded from being too long by the biophysical realities of decoding as well as the eventual reaction time of the

animal, and they are bounded from being too short by the refractory period of the cell as well as the temporal uncertainty in the stimulus response relationship (Berry and Meister, 1998; de Ruyter van Steveninck et al., 1988; Oswald et al., 2007). Our results explicitly show not only the range in which precise temporal patterns of spikes are reliably elicited by repeated presentation of a stimulus, but also exactly where these patterns are used to represent stimuli distinct from simple summation of the STA. The analysis reported here also derives the approximate 'word length' of temporal patterns, and should be used as first step in determining parameters for analyses such as quantization (Dimitrov et al., 2003).

Burst vs Tonic Spiking

The results of the current study are in broad agreement with much work from the pyramidal cells of the electrosensory lateral line lobe (ELL) of weakly electric fish as well as the relay cells of the lateral geniculate nucleus (LGN) in the mammalian visual pathway, in both of which it has been shown that isolated single spikes and short ISI, 'bursty' events compose two separate channels for encoding information about the stimulus. At least in the case of the fish ELL it has been suggested that the tonic spiking is used to keep a 'running commentary' of the dynamics of the stimulus, while the burst events are used for feature detection of surprising or otherwise ethologically relevant stimulus events (Alitto et al., 2005; Gabbiani et al., 1996; Lesica and Stanley, 2004; Oswald et al., 2004; Oswald et al., 2007; Reinagel et al., 1999). The results that we present

here fit in nicely with this view of segregated tasks- in our case spikes belonging to ISIs of greater than 5 msec correspond with stimuli that essentially match the linear reconstruction kernels, while the stimuli associated with the shorter doublets are somewhat larger and sharper (e.g. figure 4.3 C and D).

ITERATIVE REFINEMENT

Abstract

An approach to querying the stimulus-response relationship of sensory systems is presented. The goals of this approach are twofold: first we seek to confirm that we can build accurate models of the stimulus-response relationship; and second we attempt to improve these models through an iterative refinement approach. We find that our models of response-conditioned stimuli are capable of eliciting responses far above the chance level for general white noise stimuli. Additionally, we find that through the iterative refinement algorithm the probability of eliciting a response improves over iterations.

Introduction

The general goal of studies in sensory coding is to understand the schemes through which information about sensory parameters are encoded and decoded in a neural system. Understanding the encoding and decoding schemes implemented within such a system can be reduced to two interconnected tasks. The *first task* is to determine the stimulus space monitored by the system, and to determine the behaviorally-relevant stimulus parameters or features within that space. The *second task* is to determine the mapping between features in the stimulus space and the different patterns of action potentials elicited by nerve cells in the corresponding response space. Although

linear rate-coding schemes have been shown to account for a substantial amount of information in many sensory systems (Bialek et al., 1991; Warland et al., 1991; Roddey and Jacobs, 1996; Theunissen et al., 1996; Rieke et al., 1997; Warland et al., 1997; Buracas et al., 1998; Reinagel et al., 1999; Chacron, 2006), more recent studies suggest that a significant amount of information is likely to be encoded through a non-linear, temporal code (de Ruyter van Steveninck et al., 1997; Haag and Borst, 1997; Buracas et al., 1998; Strong et al., 1998; Meister and Berry, 1999; Reinagel and Reid, 2000; Roddey et al., 2000; Dimitrov et al., 2003; Passaglia and Troy, 2004; Chacron, 2006).

A typical initiation point for system-identification studies of neural coding involve the presentation of Gaussian white noise stimuli (Marmarelis and Naka, 1972; de Ruyter van Steveninck et al., 1988; Chichilnisky, 2001). However, recent results indicate that sensory interneurons show sensitivity to higher-order statistical features that occur very infrequently in GWN stimuli (Dimitrov et al., 2003). Any characterization of the encoding scheme of a neural system that does not encompass the relevant stimulus regime would result in a flawed mapping from stimulus to response. Our approach seeks to avoid such a problem by effecting an iterative refinement of the stimulus set toward a more ‘natural’ stimulus regime.

We develop our approach and test it in interneurons from classes 10-2a and 10-3a in the cricket cercal system (Mendenhall and Murphey, 1974; Jacobs and Murphey, 1987). This is a mechanosensory system that functions as a near-field,

low-frequency extension of the animal's auditory system.

The procedure begins with the stimulation of the system with a band-limited Gaussian noise source. This broad, non-specific stimulus allowed us to explore a large portion of the input space, and provides sufficient stimulation for a coarse model of the system (see chapter 4). Such coarse analyses has yielded the preliminary set of response-conditioned mean stimuli leading up to the most frequently observed neural spike-pattern code words in these cells (e.g., single spikes and short-interval spike doublets). After the initial model is in place, we modify subsequent stimuli by adding samples of the response-conditioned stimulus classes derived from the coarse analysis into the GN stimulus waveforms, to increase the frequency of occurrence of the neural responses for that stimulus class. This allows us to sample this region of the stimulus space more finely, which in turn allows us to refine the stimulus-response model.

This refinement procedure is repeated, and the stimulus ensemble is thus iteratively refined from non-specific stimuli to the specific subset of stimuli which elicit a selection of the neural responses. In principle, this approach can be continued until the stimulus space is explored in sufficient detail that further refinements of the stimulus do not produce refinements of the response model. This approach should be generalizable to many other systems.

Materials and Methods

Preparation

Experiments were conducted on 8 female crickets of the species *Acheta domesticus*, obtained from a commercial supplier (Basset's Cricket Ranch, Visalia California). Animals were fed water and dry cat food *ad libitum*, and were kept on a 12 H:12 H light-dark cycle (experiments were performed at all phases of this cycle). Specimens were selected which had undergone their imaginal molt within the last 48 hours.

Crickets were anaesthetized by placing them on ice for 5-10 minutes. The legs, ovipositor, and wings were all removed, along with a small flap of the dorsal abdominal cuticle. The gut, reproductive organs, and fatty tissue were all removed and the abdominal cavity was perfused with hypotonic cricket saline (O'Shea and Adams, 1981). The preparation was pinned to a disk of silicone elastomer, and all incisions from removing the legs and ovipositor were sealed with petroleum jelly. A small steel platform was inserted under the terminal abdominal ganglion, which was then gently lifted from the surface of the abdominal cavity. Care was taken so as not to disturb the trachea.

Electrophysiology

Intracellular recordings were made from neurons 10-2a (n=5) and 10-3a (n=3), two pairs of giant projecting interneurons in the terminal abdominal ganglion of the cricket (Jacobs and Murphey, 1987). Sharp intracellular

electrodes were pulled from glass capillary tubes using a model P-97 Flaming/Brown Micropipette Puller (Sutter Instruments Co., Novato, CA). Electrode penetration was facilitated by applying a small piece of kimwipe paper soaked in an approximately 2% protease solution (Sigma-Aldritch, P5147, St Louis, MO) for 2-3 minutes. Electrodes were backfilled with 2% Neurobiotin (Vector Laboratories, SP1120, Burlingame, CA) in ddH_20 and then filled with 3M KCl. Electrode resistances were between 2 and 10 MΩ. During recordings the Neurobiotin passively entered the neuron, allowing for later morphological identification. Membrane potential and amplified stimulus voltage were sampled at 10 kHz and recorded on a Windows XP computer running custom-built Labview software.

Stimulation

Experiments were performed in a custom-designed stimulation system described previously in (Dimitrov et al., 2003). Briefly, air movement was generated with a bank of 8 speakers, subdivided into two groups of four. Within each group of four speakers were two pairs located on opposite sides of the cricket. The two pairs of speakers were driven with inverted versions of the same computer-generated, power-amplified waveform, forming a push-pull mechanism for creating airflow from both sides of the body. The two groups of four speakers were oriented perpendicularly to each other, allowing stimulation from any arbitrary angle within the horizontal plane. Calibration of the stimulus system was performed with a low-velocity air current sensor (MicroFlown

Technologies, Zevenaar, Netherlands). Air particle displacement caused by the movement of the speakers stimulated the filiform hairs on the crickets' cerci.

All initial stimuli were two-dimensional within the horizontal plane of the animal, with the separate banks of speakers acting quasi-independently. Stimuli were constructed from a convolution of an amplitude signal (10-150 Hz band passed Gaussian White Noise, RMS amplitude 44 mm/sec) and an angle signal (50 Hz low passed uniform noise). These two-dimensional stimuli were all 100 seconds long and identical to those used in chapter 3.

In addition to recording neural activity in response to air movement, recordings of 100 seconds of spontaneous activity were made for cells 3-8 in order to monitor whether or not the cell significantly changed its firing behavior over the course of the experiment.

Response-Conditioned Stimulus Ensembles

Two distinct pattern-conditioned stimulus models were constructed, one for the single spike pattern, and one for short doublets. For the first model all of the single spikes (isolated by at least 10 msec from any other spikes) were found. All of the stimuli associated with the singlet spikes were collected, extending from 30 msec prior to the spike to 15 msec after the spike. In previous work using this bandwidth of 2-dimensional white noise (see chapter 3), we have seen that the pattern-triggered average stimulus usually approaches zero approximately 20 msec prior to the first spike and 5 msec after the final spike. Here we use the 45 msec window length in order to allow us to smoothly imbed

the sample into a surrounding noise stimulus without deforming the portion of the model which is relevant to the neuron (see next section).

The entire singlet-triggered stimulus ensemble (STSE) was then dejittered (see chapter 3), and the mean and covariance of the dejittered ensemble were used to make a Gaussian model of the singlet-triggered stimulus. The same procedure was followed for the second model, excepting that well-isolated short doublets of 2-6 msec were used for the stimulus triggering instead of the singlets (see chapter 4 for justification of the division between single spikes and short doublets as separate coding units).

Refinement of Stimuli

Following construction of the Gaussian Model of the event-triggered (either short doublet or singlet) stimulus, new 'refined' stimulus were created, as represented schematically in figure 5.1. First, realizations were generated from the Gaussian models and were labeled according to which model they came from. This is shown schematically in the fourth trace from the top in figure 5.1 (realizations from the singlet model in red, from the short doublet model in green). The likelihood of drawing from each model was inverted relative to how many times that pattern had occurred in the recording (i.e, if singlets had composed 80% of the responses, then approximately 20% of the samples would be drawn fromt the singlet model). Next, these inserts were smoothly imbedded back into the original white noise stimulus (figure 5.1, fifth and sixth traces from top). To accomplish the smooth imbedding, the original stimulus was cross-

faded out simultaneous to the insert being cross-faded in by using a 50% Tukey window (Harris, 1978). This meant that the insert was completely represented from ~18 msec prior to a reference spike until ~5 msec after, matching the significant portions of the single spike- and short doublet-triggered averages (see above). This is attenuation of the edges of the samples is visible by comparing the fourth and sixth traces of figure 5.1. Samples from each model were randomly interleaved, and the time between inserts was drawn from a uniform random distribution over the interval 1 to 23 msec.

Once a stimulus was created in this way, it was presented to the animal. This process of building models, enriching the stimuli, playing the stimulus to the animal, and then building new models was iterated for as long as the physiological recording from the animal stayed viable.

During the period that the N+1 refinement stimulus was being prepared, the N^{th} stimulus was either played again, or, in some cases, spontaneous activity was recorded in order to monitor the health of the cell. Between the time required to identify the cell by physiological means and the time to build each subsequent iterative refinement stimulus, a series of ten 100-second iterations required a minimum of 45 minutes of recording time. Due to the difficulty of maintaining an intracellular recording for such a long time, refinement stimuli were only presented to 34 of the 63 INs 10-2a and 10-3a recorded from using this protocol, and only 8 of these were held long enough to obtain at least 10 iterations of the refinement.

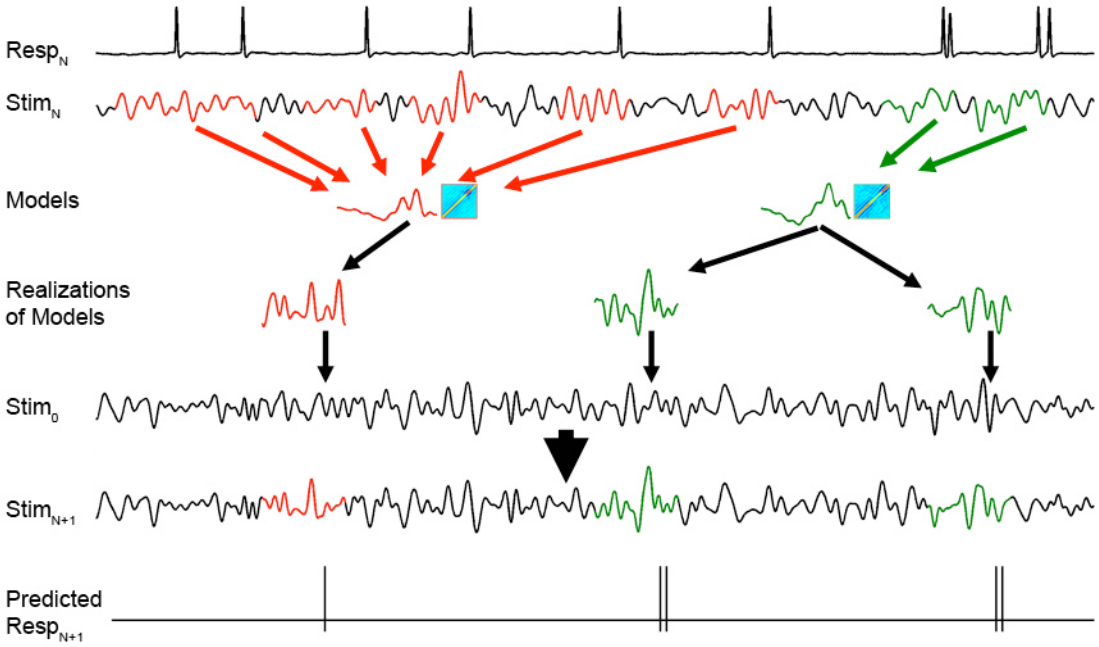

Figure 5.1. Schematic of iterative enrichment for a Gaussian white noise stimulus. From Nth joint stimulus-response recording (upper two traces), singlet-conditioned (red) and doublet-conditioned (green) stimuli are extracted and modeled as Gaussians (mean + covariance, third row from top). Realization are generated from these models (fourth row from the top), and then smoothly inserted into a GWN stimulus (third row from bottom) to form an enriched stimulus of GWN + inserts (second row from bottom). This enriched stimulus is then played to the cell for the N+1 iteration, where response times can be predicted based on the timing and class identity (singlet or doublet) of the inserts (bottom trace).

Discrimination Test

In order to ascertain how well the models described the data, we developed a simple discrimination test using information-theoretic tools. To do this we first found the logarithm of the posterior probability of each model y conditioned on each stimulus sample x, taking advantage of the fact that our models are gaussian:

$$P_{post}(y \mid x) = -\frac{1}{2}\sum_{j=1}^{n}\left[(x-\mu)\left(C^{-1}\right)_j\right]^2 - \log(2\pi) * \frac{n}{2} - \sum_{j=1}^{n}\log\left(C_{jj}\right) + \log\left(P_{prior}(y)\right) \quad (5.1)$$

In order to obtain an estimate of mutual information, we build an estimate of the joint probability of stimulus and response by assigning the stimulus category according to which model y produces the higher posterior probability in equation 5.1 (we already know which response was elicited by each stimulus sample from our experimental observation). From this joint probability matrix we then calculate the mutual information $I(R,S)$ and response entropy $H(R)$ according to:

$$I(R,S) = \sum_r \sum_s P(r,s)\log_2\left(\frac{P(r,s)}{P(r)P(s)}\right) \quad (5.2)$$

$$H(R) = \sum_r P(r)\log_2\left(P(r)\right) \quad (5.3)$$

see (Shannon, 1948; Cover and Thomas, 1991). We use Paninski's Best Upper Bound estimator to account for biases due to sample size (Paninski, 2003). In principal this test could be used for any number of stimulus-response classes. In the case of only two classes (as here), an equivalent discrimination analysis could be performed using ROC curves (Gabbiani et al., 1996).

In order to easily compare our information-theoretic quantities across our population of cells (which could potentially have different response entropies, and informations), we also estimate the coding efficiency (Rieke et al., 1997), Eff, of our models as:

$$Eff = \frac{I(R,S)}{H(R)} \quad (5.4)$$

We estimate these quantities not only for models built from the individual recordings from iterations of the refinement procedure, but also from a 'grand model' which is made by pooling the data from all iterations together. Note that the information from the grand model is probably biased upwards due to the fact that the model and test data set are the same. However, it is still useful to see how close to this information quantity we can get by using the models from single iterations which are built from 1/10 the number of data samples.

Results

Probability of Eliciting Responses

We have built models of the stimulus-response relationship in set of invertebrate sensory neurons by partitioning the neural response space into two classes (short doublets and single spikes), and modeling the stimulus space associated with each response class with a multi-dimensional Gaussian. We have attempted to test (and potentially improve) these models through a feedback procedure in which realizations from the stimulus models are imbedded in a white noise stimulus, which is then played back to the cell. To describe how good the models are in eliciting the spikes, we measure the probability of eliciting a response of class x, conditioned on having presented a stimulus from class x (where x is either singlet or doublet spiking responses and their associated stimulus classes). The resulting probabilities across ten iterations of this process from a single neuron are shown in figure 5.2 A. In addition to determining the

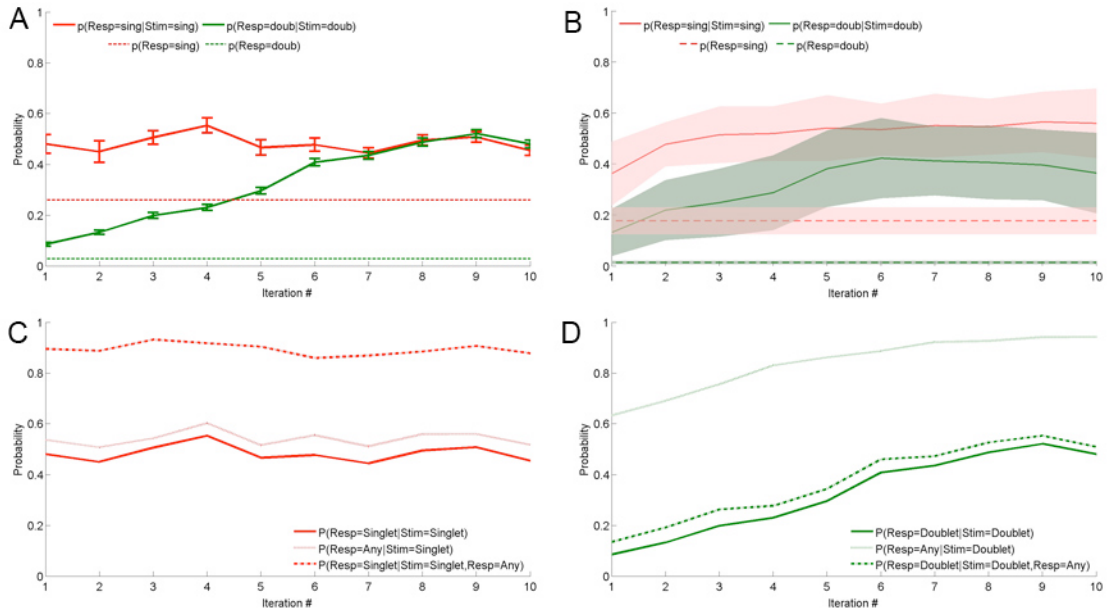

Figure 5.2. Probabilities of eliciting responses. A, ability of models to elicit responses compared with probability they will be elicited by white noise. Solid red and green curves show probabilities of singlets and doublets, respectively, for responses elicited by models. Dashed red and green curves show probabilities of singlets and doublets, respectively, for repsonses elicited by white noise. Error bars represent 95% confidence intervals on estimating probabilities. B, probabilities across population of 8 cells, coloring scheme same as in A. Shaded areas represent mean ± 1 standard deviation across 8 cells. C, conditional probabilities for singlet-conditioned model stimuli to elicit responses for 10 iterations of a single experiment. Solid curve shows probability a singlet stimulus elicits a singlet response, light curve shows probability a singlet stimulus will elicit *any* response, and dashed curve shows the probability that a singlet stimulus elicits a singlet stimulus, conditioned on that it elicits any response at all. Note that the probability of eliciting a singlet conditioned on a singlet stimulus having been presented is the product of the other two probabilities. D, conditional probabilities for doublet-conditioned model stimuli to elicit responses, same line-style convention as in C.

probability of response conditioned on stimulus ($P(R{=}x|S{=}x)$), we also determined the probability of these same responses occurring to white noise stimulation (figure 5.2 A, dashed lines). We use this probability as a chance probability with which to compare our probability of response conditioned on the stimulus. As can be seen in Figure 5.2 A, both our single spike-conditioned stimulus model (red) and our doublet-conditioned model (green) produce the corresponding responses well beyond chance level. Additionally, we are able to improve our

doublet-conditioned models over iterations of the procedure, such that the probability of eliciting the correct response in the tenth iteration is nearly five times the probability of doing so in the first iteration. the probability of eliciting a single spike with the single spike-conditioned stimulus model remains relatively constant across iterations. These general trends are consistent across all eight cells in our data set (see figure 5.2 B).

Distinction in Selectivity of Responses to Imbedded Stimuli

In order to more closely examine the difference in the probability of eliciting a response between the single spike- and short doublet-conditioned stimulus models, we looked at the two marginal probability distributions conditioned on presenting a stimulus of class x: $P(R{=}any|S{=}x)$ and $P(R{=}x|S{=}x,R{=}any)$. These two probabilities show how good our stimulus models are at eliciting *any* response, and how good they are at eliciting the intended response, respectively. Results for the cell from figure 5.2 A are shown in figures 5.2 C (x = singlets) and 5.2 D (x = short doublets).

From this it is clear that while our singlet-conditioned stimulus models are only moderately successful at generating any response ($P(R{=}any|S{=}singlet) \approx 0.55$ across all iterations), they are highly successful at generating the desired response ($P(R{=}singlet|S{=}singlet,R{=}any) \approx 0.9$ across all iterations). In contrast, the doublet-conditioned stimulus models show the exact opposite trend. They reach a value of $P(R{=}any|S{=}doublet)$ of near unity after several iterations, while the

probability $P(R=doublet|S=doublet,R=any)$ starts out at values less than 0.2 for early iterations, and only achieves a value greater than 0.5 for the last few iterations of the refinement. These tendencies were consistent across all eight cells in the data set (data not shown).

Temporal Precision of Models

In addition to measuring the ability of the models to elicit responses, we also looked at the temporal precision of the responses which occurred. The results of these measurements, pooled across all eight cells in the data set, are shown in figure 5.3. In both cases the precision of the elicited patterns, as measured by the standard deviation of the shift times of the responses, improves over iterations. In the case of the single spikes the precision improves from 2.0 msec in the first iteration to 1.6 msec in the tenth iteration, while in the case of the short doublets the precision improves from 1.7 msec in the first iteration to 1.1 msec in the eight iteration (precision was 1.2 msec in the tenth iteration). These numbers can be compared with the temporal precision of responses due to white noise measured with the dejittering technique in chapter chapter 3, where the precision for single spikes was measured to be 2.2 msec across a population of 14 cells of class 10-2a and 10-3a. Note that in the dejittering analysis cells from class 10-2a seemed to be slightly less precise than cells from class 10-3a (precisions of 2.3 and 2.1 msec, respectively). Since the population reported here consisted of five cells of class 10-2a and three cells of class 10-3a, the difference in precision between white noise stimulation and the refinement stimulation could be larger

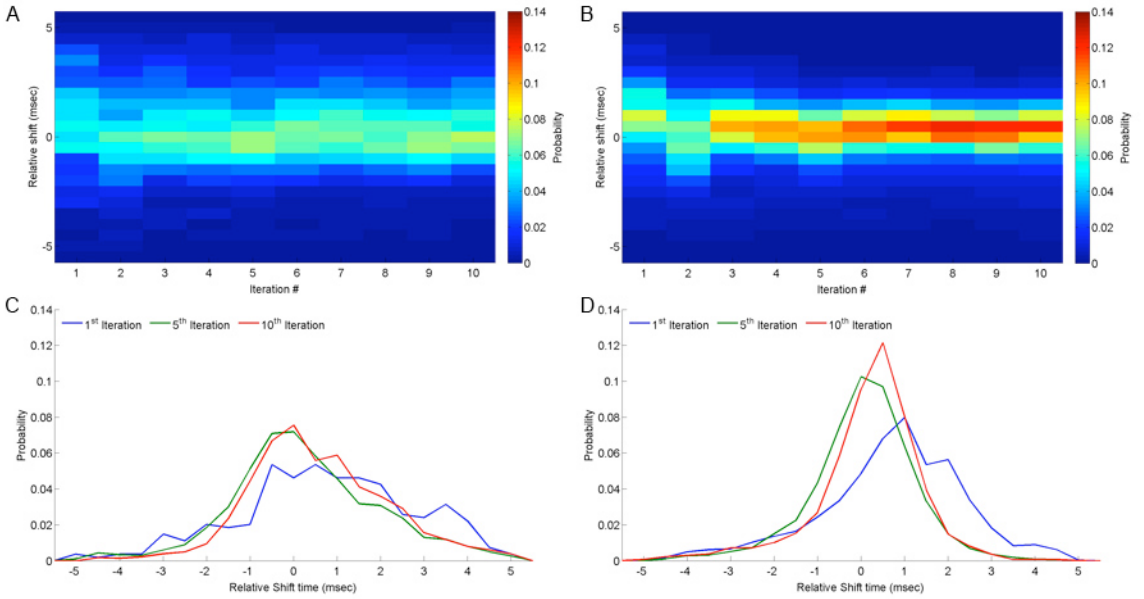

Figure 5.3. Temporal jitter of elicited responses. A, histogram of shift times of singlet patterns elicited by realizations from single-conditioned stimulus model, as a function of iterations. For each iteration, color denotes probability of an elicited response having occurred at a specific shift time. Negative shifts represent responses which occurred closer to the stimulus which elicited them. Data pooled across all eight cells, columns sum to probability=1. B, histogram of shift times of doublet patterns elicited by realizations from the doublet-conditioned stimulus model. Same conventions as A. C, plot of singlet shift times from 1st, 5th, and 10th iterations, in order to emphasize the modal latency and relative standard deviations of the distributions. D, plot of doublet shift times, same plotting conventions as in C.

than we are reporting here.

Changes in Models Over Iterations

In order to determine how the models were changing over iterations of refinement, we performed PCA on the covariance matrices of the pattern-conditioned stimulus models (de Ruyter van Steveninck et al., 1988). For the single spike-conditioned stimulus model, we found that the total variance of the models, as measured by the sum of the eigenvalues from the PCA analysis, remained relatively constant across iterations (figure 5.4 A, red trace). In contrast, the total variance of the doublet-conditioned stimulus model decreased

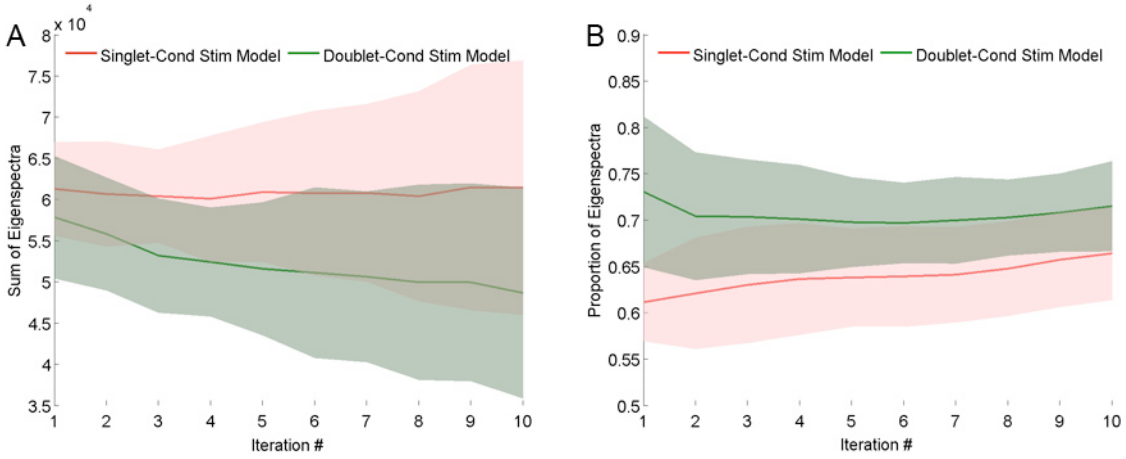

Figure 5.4. Change to eigenspectra of models. A, change to total eigenspectra, corresponding with total variance, of singlet-stimulus conditioned model (red) and doublet)stimulus conditioned model (green). B, change to proportion of the total eigenspectra of the two models explained by the ten largest eigenvalues, corresponding with the dimensional complexity of the models.

slightly across iterations, although the trend was small relative to the variability across the population (figure 5.4 A, green trace).

In addition to the total variability of the models, we also attempted to measure the relative complexity of the models. We did this by examining the proportion of the total variability of the models explained by the ten largest eigenvalues from the PCA analysis (corresponding to the ten most variable dimensions within the models). Models in which this quantity is large are not very complex, as their variance can be explained using just a few dimensions, while models in which this quantity is small are relatively more complex, as a greater number of stimulus dimensions are needed to explain their variance.

For the single spike-conditioned stimulus, we found that the complexity decreased (i.e. the proportion of the variance increased) over iterations of the refinement, while for the short doublet-conditioned model the complexity

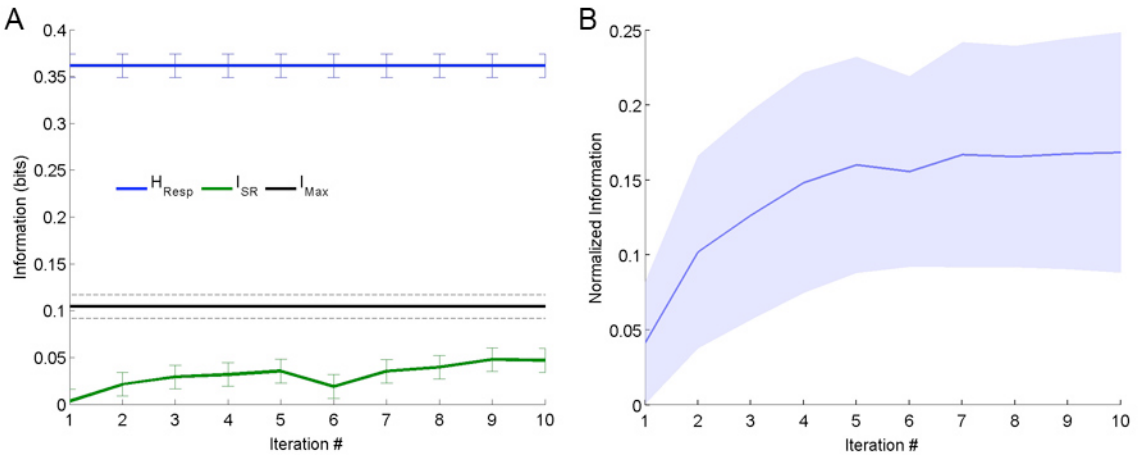

Figure 5.5. Discrimination ability of models. A, discrimination test for data shown in figure 5.2 panels A,C-D. Green curve shows mutual information recovered from discrimination of singlet vs. doublet data pooled across all iterations (see materials and methods for details of test). Black curve shows information recovered from a 'super model' built from all the data pooled across iterations. Blue curve represents response entropy of pooled data, the theoretical maximum mutual information attainable. Error bars represent confidence from Best Upper Bounds entropy estimation. B, plot showing normalized mean ± 1 STD of information returned from for each iteration, averaged across experiments. The data for the discrimination tests were pooled across all iterations. Mean is normalized to response entropy per experiment. Response entropy across all experiments was 0.47 ± 0.13 bits (mean ± 1 STD) Data from one of the eight experiments was excluded from this figure as it attained an anomalously high normalized value (0.8 normalized units)- it followed the same basic trend of low values for early iterations and reaching a plateau by iteration 7.

remained constant after the second iteration (figure 5.4 B, red and green traces, respectively).

Refinement Improves Discrimination Ability of Stimulus Models

The measurements of the probabilities and precisions of responses to our models are reflective of an encoding task, where we try to predict a response conditioned on a stimulus. We also sought to examine how good our models performed in the inverse problem of decoding, in which we try to predict a stimulus by observation of a response. In order to do this we developed a discrimination test which provided an answer in the information-theoretic quantity

of bits (see methods).

The results of such an analysis on the same experiment as in figure 5.2 A is shown in figure 5.5 A. While the decoding ability of the individual models remain low (~0.05 bits even at later iterations compared with ~0.36 bits of entropy in the response, or about 14% efficiency), it performs quite favorably with a model built from ten times as much data, and which is built from and tested on the same data set to boot (black trace in figure 5.5 A, see methods). The trend from this single experiment was reflective of the discriminability of the stimuli using our models across the entire data set (figure 5.5 B).

Changes to Global Structure of Stimuli

In order to examine how our manipulation of during the refinement process effected the global structure of the stimulus, we looked at the distribution of amplitudes and frequency content across iterations. The distribution of amplitude of the stimulus changed relatively little, broadening only slightly toward the later iterations, reflecting a higher proportion of large amplitude stimuli (figure 5.6 A).

The changes in the global spectral composition were much more interesting. For later iterations, the spectral content became more concentrated in frequencies below 150 Hz (figure 5.6 B). Additionally, sharp peaks become visible in later iterations at approximately 25 and 50 Hz. These peaks could not be accounted for by looking at power spectra of the start times of the inserts, power spectra of the end times of the inserts, or power spectra of the intervals between inserts, which in any case were statistically identical across all

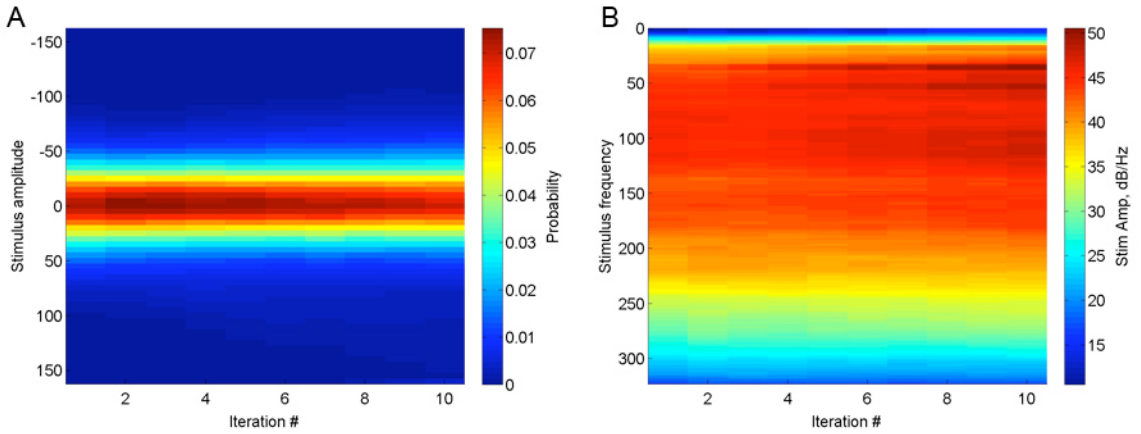

Figure 5.6. Changes to global statistics of stimuli. A, change of amplitude of stimulus over iterations. Y axis shows amplitude, X axis shows iteration number, color axis shows probability (columns sum to 1). B, change of frequency distribution over iterations of refinement. Y axis shows frequency, color axis shows spectral density.

iterations. Intriguingly, the peak at 25 Hz corresponds well with the syllable repetition rate of the calling song for this species of cricket (see chapter 1 and figure 1.11 D).

Discussion

Refinement of Models

We have confirmed that models of the stimulus associated with distinct temporal patterns of neural responses obtained through reverse correlation can be used to drive the firing activity of neurons in the cricket cercal sensory system. Additionally, we have shown that these models can be improved over the course of iteratively building the models and playing them back to the nervous system in the following two senses: the probability of eliciting a desired output from stimulation with the model increased over iterations; the temporal precision with which these responses were elicited increased over iterations. This improvement

was correlated with a reduction of the total variance of the models, consistent with the idea that the iterative refinement serves to pare away portions of the model which do not reliably elicit a response.

Models refined in this way maintained their general utility. In addition to being better at eliciting the correct response through stimulation, these models were also able to perform as well at a discrimination task on test data sets as models built from those test data sets. This is suggestive that the cell is not adapting as we refine our stimulus, as this would lead to models with reduced discriminatory ability with respect to earlier data.

Finally, we see that refinement in this case leads to stimulus with global stimulus statistics reminiscent of the statistical structure of ‘natural’ stimuli for this system. This result is consistent with a model of sensory processing in which neural systems are driven through evolutionary processes to optimally encode stimuli which match the statistical structure of their natural environment (Atick and Redlich, 1990; Atick and Redlich, 1992; Atick, 1992; Rieke et al., 1995; Olshausen and Field, 1996; Olshausen and Field, 2004).

BIBLIOGRAPHY

Adrian, E. D., and Zotterman, Y. (1926). The impulses produced by sensory nerve-endings: Part II. The response of a Single End-Organ. J Physiol *61*, 151-171.

Alitto, H. J., Weyand, T. G., and Usrey, W. M. (2005). Distinct properties of stimulus-evoked bursts in the lateral geniculate nucleus. J Neurosci *25*, 514-523.

Anjum, F., Turni, H., Mulder, P. G., van der Burg, J., and Brecht, M. (2006). Tactile guidance of prey capture in Etruscan shrews. Proc Natl Acad Sci U S A

Atick, JJ (1992) Could information theory provide an ecological theory of sensory processing? Network, 3:213–251.

Atick, JJ, Redlich, AN (1990) Towards a theory of early visual processing. Neural Comp., 2:308–320.

Atick, JJ, Redlich, AN (1992) What does the retina know about natural scenes? Neural Comp., 4:196–210.

Baba, Y., Hirota, K., and Yamaguchi, T. (1991). Morphology and response properties of wind-sensitive non-giant interneurons in the terminal abdominal ganglion of crickets. Zoolog Sci *8*, 437-445.

Baba, Y., Hirota, K., Yamaguchi, T., and Shimozawa, T. (1995). Differing afferent connections of spiking and nonspiking wind-sensitive local interneurons in the terminal abdominal ganglion of the cricket *Gryllus bimaculatus*. J Comp Physiol [A] *176*, 17-30.

Baba, Y., and Shimozawa, T. (1997). Diversity of Motor Responses Initiated by a Wind Stimulus in the Freely Moving Cricket, Gryllus bimaculatus. Zoological science *14*, 587-594.

Bacon, J. P., and Murphey, R. K. (1984). Receptive fields of cricket giant interneurones are related to their dendritic structure. J Physiol *352*, 601-623.

Bair, W., and Koch, C. (1996). Temporal precision of spike trains in extrastriate cortex of the behaving macaque monkey. Neural Comput *8*, 1185-1202.

Ball, E. E., and Stone, R. C. (1982). The cercal receptor system of the praying mantid, Archimantis brunneriana Sauss. I. Cercal morphology and receptor types. Cell Tissue Res *224*, 55-70.

Belosky, D. C., and Delcomyn, F. (1977). Information processing in a cricket ganglion: the response of giant fibres to sound pulses. J Insect Physiol *23*, 359-365.

Bennet-Clark, H. C. (1989). Songs and the Physics of Sound Production. In Cricket behavior and neurobiology, Huber, F., T. E. Moore, and W. Loher, eds. (Ithaca, N.Y.: Cornell University Press), pp. 227-261.

Bentley, D. (1975). Single gene cricket mutations: effects on behavior, sensilla, sensory neurons, and identified interneurons. Science *187*, 760-764.

Berry, M. J., 2nd, and Meister, M. (1998). Refractoriness and neural precision. J Neurosci *18*, 2200-2211.

Berry, M. J., 2nd, Warland, D. K., and Meister, M. (1997). The structure and precision of retinal spike trains. Proc Natl Acad Sci U S A *94*, 5411-5416.

Bialek, W., Rieke, F., de Ruyter van Steveninck, R. R., and Warland, D. (1991). Reading a neural code. Science *252*, 1854-1857.

Bodnar, D. A., Miller, J. P., and Jacobs, G. A. (1991). Anatomy and physiology of identified wind-sensitive local interneurons in the cricket cercal sensory system. J Comp Physiol [A] *168*, 553-564.

Borst, A., and Theunissen, F. E. (1999). Information theory and neural coding. Nat Neurosci *2*, 947-957.

Boyan, G. S., and Ball, E. E. (1986). Wind-sensitive interneurones in the terminal ganglion of praying mantids. J Comp Physiol [A] *159*, 773-789.

Boyan, G. S., and Ball, E. E. (1989). The wind-sensitive cercal receptor/giant interneurone system of the locust, *Locusta migratoria* III: Cercal activation of thoracic motor pathways. J Comp Physiol [A] *165*, 523-537.

Boyan, G. S., Williams, J. L. D., and Ball, E. E. (1989a). The wind-sensitive cercal receptor/giant interneurone system of the locust, *Locusta migratoria* I: Anatomy of the system. J Comp Physiol [A] *165*, 495-510.

Boyan, G. S., Williams, J. L. D., and Ball, E. E. (1989b). The wind-sensitive

cercal receptor/giant interneurone system of the locust, *Locusta migratoria* IV: The non-giant interneurones. J Comp Physiol [A] *165*, 539-552.

Bryant, H. L., and Segundo, J. P. (1976). Spike initiation by transmembrane current: a white-noise analysis. J Physiol *260*, 279-314.

Bryant, H. L. J., Marcos, A. R., and Segundo, J. P. (1973). Correlations of neuronal spike discharges produced by monosynaptic connections and by common inputs. J Neurophysiol *36*, 205-225.

Buracas, G. T., Zador, A. M., DeWeese, M. R., and Albright, T. D. (1998). Efficient discrimination of temporal patterns by motion-sensitive neurons in primate visual cortex. Neuron *20*, 959-969.

Burrows, M. (1996). Anatomy of the Nervous System. In The neurobiology of an insect brain, ed. (Oxford: Oxford University Press), pp. 12-36.

Butts, D. A., and Goldman, M. S. (2006). Tuning curves, neuronal variability, and sensory coding. PLoS Biol *4*, e92.

Camhi, J. M. (1969). Locust wind receptors. III. Contribution to flight initiation and lift control. J Exp Biol *50*, 363-373.

Camhi, J. M., and Nolen, T. G. (1981). Properties of the escape system of cockroaches during walking. J Comp Physiol [A] *142*, 339-346.

Camhi, J. M., and Tom, W. (1978). The escape behavior of the cockroach *Periplaneta americana* I: Turning response to wind puffs. J Comp Physiol [A] *128*, 193-201.

Camhi, J. M., Tom, W., and Volman, S. (1978). The escape behavior of the cockroach *Periplaneta americana* II: Detection of natural predators by air displacement. J Comp Physiol [A] *128*, 203-212.

Casagrand, J. L., and Ritzmann, R. E. (1991). Localization of ventral giant interneuron connections to the ventral median branch of thoracic interneurons in the cockroach. J Neurobiol *22*, 643-658.

Chacron, M. J. (2006). Nonlinear information processing in a model sensory system. J Neurophysiol *95*, 2933-2946.

Chichilnisky, E. J. (2001). A simple white noise analysis of neuronal light responses. Network *12*, 199-213.

Chichilnisky, E. J., and Kalmar, R. S. (2003). Temporal resolution of ensemble visual motion signals in primate retina. J Neurosci *23*, 6681-6689.

Clague, H., Theunissen, F. E., and Miller, J. P. (1997). Effects of adaptation on neural coding by primary sensory interneurons in the cricket cercal system. J Neurophysiol *77*, 207-220.

Collin, S. P. (1985). The central morphology of the giant interneurons and their spatial relationship with the thoracic motorneurons in the cockroach, Periplaneta americana (Insecta). J Neurobiol *16*, 249-267.

Coolen, I., Dangles, O., and Casas, J. (2005). Social learning in noncolonial insects? Curr Biol *15*, 1931-1935.

Cover, T. M., and Thomas, J. A. (1991). Elements of Information Theory (Wiley Series in Telecommunications and Signal Processing) (New York: Wiley-Interscience).

Cummins, G. I., Crook, S. M., Dimitrov, A. G., Ganje, T., Jacobs, G. A., and Miller, J. P. (2003). Structural and biophysical mechanisms underlying dynamic sensitivity of primary sensory interneurons in the cricket cercal sensory system. Neurocomputing *52-54*, 45-52.

Dagan, D., and Parnas, I. (1970). Giant Fibre and Small Fibre Pathways Involved in the Evasive Response of the Cockroach, Periplaneta Americana. J Exp Biol *52*, 313-324.

Daley, D. L., and Delcomyn, F. (1980). Modulation of the excitability of cockroach giant interneurons during walking. II. Central and peripheral components. J Comp Physiol [A] *138*, 241-251.

Dambach, M. (1989). Vibrational Responses. In Cricket behavior and neurobiology, Huber, F., T. E. Moore, and W. Loher, eds. (Ithaca, N.Y.: Cornell University Press), pp. 178-197.

Dambach, M., Rausche, H. G., and Wendler, G. (1983). Proprioceptive feedback influences the calling song of the field cricket. Naturwissenschaften *70*, 417-418.

Dangles, O., Casas, J., and Coolen, I. (2006). Textbook cricket goes to the field: the ecological scene of the neuroethological play. J Exp Biol *209*, 393-398.

de Ruyter van Steveninck, R., and Bialek, W. (1988). Real-Time Performance of a Movement-Sensitive Neuron in the Blowfly Visual System: Coding and

Information Transfer in Short Spike Sequences. Proceedings of the Royal Society of London. Series B, Biological Sciences *234*, 379-414.

de Ruyter van Steveninck, R. R., Lewen, G. D., Strong, S. P., Koberle, R., and Bialek, W. (1997). Reproducibility and variability in neural spike trains. Science *275*, 1805-1808.

Delcomyn, F. (1977). Corollary discharge to cockroach giant interneurones. Nature *269*, 160-162.

Dimitrov, A. G., and Gedeon, T. (2006). Effects of stimulus transformations on estimates of sensory neuron selectivity. J Comput Neurosci *20*, 265-283.

Dimitrov, A. G., and Miller, J. P. (2001). Neural coding and decoding: communication channels and quantization. Network *12*, 441-472.

Dimitrov, A. G., Miller, J. P., Aldworth, Z., and Gedeon, T. (2001). Non-uniform quantization of neural spike sequences through an information distortion measure. Neurocomputing *38-40*, 175-181.

Dimitrov, A. G., Miller, J. P., Gedeon, T., Aldworth, Z., and Parker, A. E. (2003). Analysis of neural coding through quantization with an information-based distortion measure. Network *14*, 151-176.

Doherty, J. A. (1985). Trade-off phenomena in calling song recognition and phonotaxis in the cricket, *Gryllus bimaculatus* (Orthoptera, Gryllidae). J Comp Physiol [A] *156*, 787-801.

Doiron, B., Oswald, A. M., and Maler, L. (2007). Interval Coding. II. Dendrite-Dependent Mechanisms. J Neurophysiol *97*, 2744-2757.

Duda, R. O., Hart, P. E., and Stork, D. G. (2000). Pattern Classification (2nd Edition) (New York: Wiley-Interscience).

Dumpert, K., and Gnatzy, W. (1977). Cricket combined mechanoreceptors and kicking response. J Comp Physiol [A] *122*, 9-25.

Edwards, J. S., and Palka, J. (1974). The cerci and abdominal giant fibres of the house cricket, *Acheta domesticus.* I. Anatomy and physiology of normal adults. Proc R Soc Lond B Biol Sci *185*, 83-103.

Edwards, J. S., and Reddy, G. R. (1986). Mechanosensory appendages and giant interneurons in the firebrat (Thermobia domestica, Thysanura): a prototype system for terrestrial predator evasion. J Comp Neurol *243*, 535-

546.

Ergun, A., Barbieri, R., Eden, U. T., Wilson, M. A., and Brown, E. N. (2007). Construction of point process adaptive filter algorithms for neural systems using sequential Monte Carlo methods. IEEE Trans Biomed Eng *54*, 419-428.

Fairhall, A. L., Burlingame, C. A., Narasimhan, R., Harris, R. A., Puchalla, J. L., and Berry, M. J. n. (2006). Selectivity for multiple stimulus features in retinal ganglion cells. J Neurophysiol *96*, 2724-2738.

Fraser, P. J. (1977). Cercal ablation modifies tethered flight behaviour of cockroach. Nature *268*, 523-524.

Friedman, N., Mosenzon, O., Slonim, N., and Tishby, N. (2001). Multivariate information bottleneck. Proceedings of UAI'01, 17th Conference on Uncertainty in Artificial Intelligence

Gabbiani, F., Metzner, W., Wessel, R., and Koch, C. (1996). From stimulus encoding to feature extraction in weakly electric fish. Nature *384*, 564-567.

Gedeon, T., Parker, A. E., and Dimitrov, A. G. (2003). Information distortion and neural coding. Can Math Q *10*, 33-70.

Gedeon, T., Parker, A. E., Campion, C., and Aldworth, Z. Annealing and the normalized N-cut. Pattern Recognition *In Press, Accepted Manuscript*,

Girish, B. Coding of Multiple Sensory Parameters in Neural Ensembles: Study of a Cartesian Projection Code for Wind Detection in Crickets. Berkeley, CA: University of California, Berkeley; 1998. p. Dissertation.

Gnatzy, W. (1978). Development of the filiform hairs on the cerci of *Gryllus bimaculatus* deg. (saltatoria, gryllidae). Cell Tissue Res *187*, 1-24.

Gnatzy, W., and Heusslein, R. (1986). Digger wasp against crickets I: Receptors involved in the antipredator strategies of the prey. Naturwissenschaften *73*, 212-215.

Gnatzy, W., and Kämper, G. (1990). Digger wasp against crickets II: An airborne signal produced by a running predator. J Comp Physiol [A] *167*, 551-556.

Gozani, S. N., and Miller, J. P. (1994). Optimal discrimination and classification of neuronal action potential waveforms from multiunit, multichannel recordings using software-based linear filters. IEEE Trans Biomed Eng *41*,

358-372.

Gras, H., and Bartels, A. (1999). Effects of spontaneous locomotion on the cricket's walking response to a wind stimulus. Naturwissenschaften *86*, 242-246.

Gras, H., and Hörner, M. (1992). Wind-Evoked Escape Running of the cricket Gryllus Bimaculatus: I. Behavioural Analysis. J Exp Biol *171*, 189-214.

Gras, H., Hörner, M., Runge, L., and Schürmann, F. W. (1990). Prothoracic DUM neurons of the cricket *Gryllus bimaculatus* - responses to natural stimuli and activity in walking behavior. J Comp Physiol [A] *166*, 901-914.

Gras, H., Hörner, M., and Schurmann, F. W. (1994). A comparison of spontaneous and wind-evoked running modes in crickets and cockroaches. Journal of Insect Physiology *40*, 373-384.

Haag, J., and Borst, A. (1997). Encoding of visual motion information and reliability in spiking and graded potential neurons. J Neurosci *17*, 4809-4819.

Harris, FJ (1978) On the use of windows for harmonic analysis with the discrete Fourier transform. Proceedings of the IEEE, 66:51–83.

Hedwig, B. (2000). Control of cricket stridulation by a command neuron: efficacy depends on the behavioral state. J Neurophysiol *83*, 712-722.

Heidelbac, J., Dambach, M., and Böhm, H. (1991). Processing wing flick-generated air-vortex signals in the African cave cricket *Phaeophilacris spectrum*. Naturwissenschaften *78*, 277-278.

Heinzel, H. G., and Dambach, M. (1987). Travelling air vortex rings as potential communication signals in a cricket. J Comp Physiol [A] *160*, 79-88.

Heusslein, R., and Gnatzy, W. (1987). Central projections of campaniform sensilla on the cerci of crickets and cockroaches. Cell and Tissue Research *247*, 591-598.

Hiraguchi, T., and Yamaguchi, T. (2000). Escape behavior in response to mechanical stimulation of hindwing in cricket, *Gryllus bimaculatus*. J Insect Physiol *46*, 1331-1340.

Hiraguchi, T., Yamaguchi, T., and Takahata, M. (2003). Mechanoreceptors involved in the hindwing-evoked escape behaviour in cricket, Gryllus

bimaculatus. J Exp Biol *206*, 523-534.

Hirota, K., Sonoda, Y., Baba, Y., and Yamaguchi, T. (1993). Distinction in morphology and behavioral role between dorsal and ventral groups of cricket giant interneurons. Zoolog Sci *10*, 705-709.

Hörner, M. (1992). Wind-Evoked Escape Running of the Cricket Gryllus Bimaculatus: II. Neurophysiological Analysis. J Exp Biol *171*, 215-245.

Hörner, M., and Gras, H. (1985). Physiological properties of some descending neurons in the cricket brain. Naturwissenschaften *72*, 603-604.

Hörner, M., Gras, H., and Schümann, F. (1989). Modulation of wind sensitivity in thoracic interneurons during cricket escape behavior. Naturwissenschaften *76*, 534-536.

Hsu, A., Borst, A., and Theunissen, F. E. (2004). Quantifying variability in neural responses and its application for the validation of model predictions. Network *15*, 91-109.

Jacobs, G. A., and Miller, J. P. (1985). Functional properties of individual neuronal branches isolated in situ by laser photoinactivation. Science *228*, 344-346.

Jacobs, G. A., and Miller, J. P. (1988). Analysis of synaptic integration using the laser photoinactivation technique. Cellular and Molecular Life Sciences (CMLS) *44*, 362-368.

Jacobs, G. A., Miller, J. P., and Murphey, R. K. (1986). Integrative mechanisms controlling directional sensitivity of an identified sensory interneuron. J Neurosci *6*, 2298-2311.

Jacobs, G. A., and Murphey, R. K. (1987). Segmental origins of the cricket giant interneuron system. J Comp Neurol *265*, 145-157.

Jacobs, G. A., and Nevin, R. (1991). Anatomical relationships between sensory afferent arborizations in the cricket cercal system. Anat Rec *231*, 563-572.

Jacobs, G. A., and Theunissen, F. E. (1996). Functional organization of a neural map in the cricket cercal sensory system. J Neurosci *16*, 769-784.

Kämper, G. (1984). Abdominal ascending interneurons in crickets: responses to sound at the 30-Hz calling-song frequency. J Comp Physiol [A] *155*, 507-520.

Kämper, G., and Dambach, M. (1979). Communication by infrasound in a non-stridulating cricket. Naturwissenschaften *66*, 530-530.

Kämper, G., and Dambach, M. (1981). Response of the cercus-to-giant interneuron system in crickets to species-specific song. J Comp Physiol [A] *141*, 311-317.

Kämper, G., and Dambach, M. (1985). Low-frequency airborne vibrations generated by crickets during singing and aggression. Journal of Insect Physiology *31*, 925-929.

Kämper, G., and Kleindienst, H.-U. (1990). Oscillation of cricket sensory hairs in a low-frequency sound field. J Comp Physiol [A] *167*, 193-200.

Kanou, M., Konishi, A., and Suenaga, R. (2006). Behavioral analyses of wind-evoked escape of the cricket, Gryllodes sigillatus. Zoolog Sci *23*, 359-364.

Kanou, M., Ohshima, M., and Inoue, J. (1999). The air-puff evoked escape response of the cricket *Gryllus bimaculatus* and its compensational recovery after cercal ablation. Zoolog Sci *16*, 71-79.

Kanou, M., and Shimozawa, T. (1985). Responses of Cricket Leg Motoneurons to Air-Current Stimuli : Velocity Dependent Inhibition and Acceleration Dependent Excitation(Physiology). Zoological science *2*, 629-639.

Keat, J., Reinagel, P., Reid, R. C., and Meister, M. (2001). Predicting every spike: a model for the responses of visual neurons. Neuron *30*, 803-817.

Keegan, A. P., and Comer, C. M. (1993). The wind-elicited escape response of cockroaches (*Periplaneta americana*) is influenced by lesions rostral to the escape circuit. Brain Res *620*, 310-316.

Kennel, M. B., Shlens, J., Abarbanel, H. D., and Chichilnisky, E. J. (2005). Estimating entropy rates with bayesian confidence intervals. Neural Comput *17*, 1531-1576.

Kohstall-Schnell, D., and Gras, H. (1994). Activity of giant interneurones and other wind-sensitive elements of the terminal ganglion in the walking cricket. J Exp Biol *193*, 157-181.

Kolton, L., and Camhi, J. M. (1995). Cartesian representation of stimulus direction: parallel processing by two sets of giant interneurons in the cockroach. J Comp Physiol [A] *176*, 691-702.

Kondoh, Y., Arima, T., Okuma, J., and Hasegawa, Y. (1991a). Filter characteristics of cercal afferents in the cockroach. J Comp Physiol [A] *169*, 653-662.

Kondoh, Y., Morishita, H., Arima, T., Okuma, J., and Hasegawa, Y. (1991b). White noise analysis of graded response in a wind-sensitive, nonspiking interneuron of the cockroach. J Comp Physiol [A] *168*, 429-443.

Landolfa, M. A. Response Properties of Filiform Hair Receptors of the Cricket Cercal Sensory System. Berkeley, CA: University of California, Berkeley; 1992. p. Dissertation.

Landolfa, M. A., and Jacobs, G. A. (1995). Direction sensitivity of the filiform hair population of the cricket cercal system. J Comp Physiol [A] *177*, 759-766.

Landolfa, M. A., and Miller, J. P. (1995). Stimulus-response properties of cricket cercal filiform receptors. J Comp Physiol [A] *177*, 749-757.

Laurent, G., and Davidowitz, H. (1994). Encoding of Olfactory Information with Oscillating Neural Assemblies. Science *265*, 1872-1875.

Lesica, N. A., and Stanley, G. B. (2004). Encoding of natural scene movies by tonic and burst spikes in the lateral geniculate nucleus. J Neurosci *24*, 10731-10740.

Levin, J. E., and Miller, J. P. (1996). Broadband neural encoding in the cricket cercal sensory system enhanced by stochastic resonance. Nature *380*, 165-168.

Levine, R. B., and Murphey, R. K. (1980). Pre- and postsynaptic inhibition of identified giant interneurons in the cricket (*Acheta domesticus*). J Comp Physiol [A] *135*, 269-282.

Libersat, F., Levy, A., and Camhi, J. M. (1989). Multiple feedback loops in the flying cockroach: excitation of the dorsal and inhibition of the ventral giant interneurons. J Comp Physiol [A] *165*, 651-668.

Liu, R. C., Tzonev, S., Rebrik, S., and Miller, K. D. (2001). Variability and information in a neural code of the cat lateral geniculate nucleus. J Neurophysiol *86*, 2789-2806.

Loher, W., and Dambach, M. (1989). Reproductive Behavior. In Cricket behavior and neurobiology, Huber, F., T. E. Moore, and W. Loher, eds. (Ithaca,

N.Y.: Cornell University Press), pp. 43-82.

Mainen, Z. F., and Sejnowski, T. J. (1995). Reliability of spike timing in neocortical neurons. Science *268*, 1503-1506.

Markl, H., and Tautz, J. (1975). The sensitivity of hair receptors in caterpillars ofBarathra brassicae L. (lepidoptera, noctuidae) to particle movement in a sound field. J Comp Physiol [A] *99*, 79-87.

Marmarelis, P. Z., and Naka, K. (1972). White-noise analysis of a neuron chain: an application of the Wiener theory. Science *175*, 1276-1278.

Marsalek, P., Koch, C., and Maunsell, J. (1997). On the relationship between synaptic input and spike output jitter in individual neurons. Proc Natl Acad Sci U S A *94*, 735-740.

Marsat, G., and Pollack, G. S. (2004). Differential temporal coding of rhythmically diverse acoustic signals by a single interneuron. J Neurophysiol *92*, 939-948.

Marsat, G., and Pollack, G. S. (2006). A Behavioral Role for Feature Detection by Sensory Bursts. Journal of Neuroscience J. Neurosci. *26*, 10542-10547.

Matsumoto, S. G., and Murphey, R. K. (1977). The cercus-to-giant interneuron system of crickets IV. Patterns of connectivity between receptors and the medial giant interneuron. J Comp Physiol [A] *119*, 319-330.

Meister, M., and Berry, M. J., 2nd (1999). The neural code of the retina. Neuron *22*, 435-450.

Mendenhall, B., and Murphey, R. K. (1974). The morphology of cricket giant interneurons. J Neurobiol *5*, 565-580.

Miller, J. P., Jacobs, G. A., and Theunissen, F. E. (1991). Representation of sensory information in the cricket cercal sensory system. I. Response properties of the primary interneurons. J Neurophysiol *66*, 1680-1689.

Miller, J. P., and Jacobs, G. A. (1984). Relationships between neuronal structure and function. J Exp Biol *112*, 129-145.

Mizrahi, A., and Libersat, F. (1997). Independent coding of wind direction in cockroach giant interneurons. J Neurophysiol *78*, 2655-2661.

Moiseff, A., and Hoy, R. (1983). Sensitivity to ultrasound in an identified auditory

interneuron in the cricket: a possible neural link to phonotactic behavior. J Comp Physiol [A] *152*, 155-167.

Moiseff, A., Pollack, G. S., and Hoy, R. R. (1978). Steering responses of flying crickets to sound and ultrasound: Mate attraction and predator avoidance. Proc Natl Acad Sci U S A *75*, 4052-4056.

Mumey, B., Sarkar, A., Gedeon, T., Dimitrov, A., and Miller, J. (2004). Finding neural codes using random projections. Neurocomputing *58-60*, 19-25.

Murphey, R. K. (1981). The structure and development of a somatotopic map in crickets: the cercal afferent projection. Dev Biol *88*, 236-246.

Murphey, R. K. (1985). A second cricket cercal sensory system: bristle hairs and the interneurons they activate. J Comp Physiol [A] *156*, 357-367.

Murphey, R. K., Jacklet, A., and Schuster, L. (1980). A topographic map of sensory cell terminal arborizations in the cricket CNS; correlation with birthday and position in a sensory array. J Comp Neurol *191*, 53-64.

Murphey, R. K., and Lemere, C. A. (1984). Competition controls the growth of an identified axonal arborization. Science *224*, 1352-1355.

Murphey, R. K., and Palka, J. (1974). Efferent control of cricket giant fibres. Nature *248*, 249-251.

Nemenman, I., Bialek, W., and de Ruyter van Steveninck, R. (2004). Entropy and information in neural spike trains: progress on the sampling problem. Phys Rev E Stat Nonlin Soft Matter Phys *69*, 056111.

Nolen, T. G., and Hoy, R. R. (1986). Phonotaxis in flying crickets. I. Attraction to the calling song and avoidance of bat-like ultrasound are discrete behaviors. J Comp Physiol [A] *159*, 423-439.

O'Shea, M., and Adams, M. E. (1981). Pentapeptide (proctolin) associated with an identified neuron. Science *213*, 567-569.

Olshausen, BA, Field, DJ (1996) Natural image statistics and efficient coding. Network, 7:333–339.

Olshausen, BA, Field, DJ (2004) Sparse coding of sensory inputs. Curr Opin Neurobiol, 14:481–487.

Orida, N., and Josephson, R. K. (1978). Peripheral control of responsiveness to

auditory stimuli in giant fibres of crickets and cockroaches. J Exp Biol *72*, 153-164.

Osborne, L. C. Biomechanical Properties Underlying Sensory Processing in Mechanosensory Hairs in the Cricket Cercal Sensory System. Berkeley, CA: University of California, Berkeley; 1997. p. Dissertation.

Oswald, A. M., Chacron, M. J., Doiron, B., Bastian, J., and Maler, L. (2004). Parallel processing of sensory input by bursts and isolated spikes. J Neurosci *24*, 4351-4362.

Oswald, A. M., Doiron, B., and Maler, L. (2007). Interval coding. I. Burst interspike intervals as indicators of stimulus intensity. J Neurophysiol *97*, 2731-2743.

Palka, J., Levine, R., and Schubiger, M. (1977). The cercus-to-giant interneuron system of crickets I: Some attributes of the sensory cells. J Comp Physiol [A] *119*, 267-283.

Palka, J., and Olberg, R. (1977). The cercus-to-giant interneuron system of crickets III: Receptive field organization. J Comp Physiol [A] *119*, 301-317.

Paninski, L., Pillow, J. W., and Simoncelli, E. P. (2004). Maximum likelihood estimation of a stochastic integrate-and-fire neural encoding model. Neural Comput *16*, 2533-2561.

Paninski, L. (2003). Estimation of Entropy and Mutual Information. Neural Comp. *15*, 1191-1253.

Parker, A. E. Symmetry Breaking Bifurcations of the Information Distortion. Bozeman, MT: MONTANA STATE UNIVERSITY Bozeman; 2003. p. Dissertation.

Passaglia, C. L., and Troy, J. B. (2004). Information transmission rates of cat retinal ganglion cells. J Neurophysiol *91*, 1217-1229.

Paydar, S., Doan, C. A., and Jacobs, G. A. (1999). Neural mapping of direction and frequency in the cricket cercal sensory system. J Neurosci *19*, 1771-1781.

Pfluger, H. J. (1984). The large fourth abdominal intersegmental interneuron: a new type of wind-sensitive ventral cord interneuron in locusts. J Comp Neurol *222*, 343-357.

Pillow, J., W., and Simoncelli, E., P. (2006). Dimensionality reduction in neural models: An information-theoretic generalization of spike-triggered average and covariance analysis. Journal of Vision J. Vis. *6*, 414-428.

Plummer, M. R., and Camhi, J. M. (1981). Discrimination of sensory signals from noise in the escape system of the cockroach: The role of wind acceleration. J Comp Physiol [A] *142*, 347-357.

Pollack, A. J., Ritzmann, R. E., and Watson, J. T. (1995). Dual pathways for tactile sensory information to thoracic interneurons in the cockroach. J Neurobiol *26*, 33-46.

Pollack, G. S., Givois, V., and Balakrishnan, R. (1998). Air-movement `signals' are not required for female mounting during courtship in the cricket *Teleogryllus oceanicus*. J Comp Physiol [A] *183*, 513-518.

Pollack, G. S., and Hoy, R. (1989). Evasive Acoustic Behavior and Its Neurbiological Basis. In Cricket behavior and neurobiology, Huber, F., T. E. Moore, and W. Loher, eds. (Ithaca, N.Y.: Cornell University Press), pp. 340-363.

Ponton, F., Lebarbenchon, C., Lefevre, T., Biron, D. G., Duneau, D., Hughes, D. P., and Thomas, F. (2006). Parasitology: parasite survives predation on its host. Nature *440*, 756.

Pumphrey, R. J., and Rawdon-Smith, A. F. (1936). Hearing in Insects: The Nature of the Response of Certain Receptors to Auditory Stimuli. Proc R Soc Lond B Biol Sci *121*, 18-27.

Pumphrey, R. J., and Rawdon-Smith, A. F. (1937). Synaptic Transmission of Nervous Impulses through the last Abdominal Ganglion of the Cockroach. Proc R Soc Lond B Biol Sci *122*, 106-118.

Reich, D. S., Victor, J. D., Knight, B. W., Ozaki, T., and Kaplan, E. (1997). Response variability and timing precision of neuronal spike trains in vivo. J Neurophysiol *77*, 2836-2841.

Reinagel, P., Godwin, D., Sherman, S. M., and Koch, C. (1999). Encoding of visual information by LGN bursts. J Neurophysiol *81*, 2558-2569.

Reinagel, P., and Reid, R. C. (2000). Temporal coding of visual information in the thalamus. J Neurosci *20*, 5392-5400.

Reinagel, P., and Reid, R. C. (2002). Precise firing events are conserved across

neurons. J Neurosci *22*, 6837-6841.

Reitze, M., and Nentwig, W. (1991). Comparative investigations into the feeding ecology of six Mantodea species. Oecologia *86*, 568-574.

Rice, M. J., and Webb, P. D. (1975). Giant axons in the central nervous system of Ctenomorphodes tessulatus (Gray), an Australian stick insect. Australian Journal of Entomology *14*, 277-282.

Richmond, B. J., Optican, L. M., Podell, M., and Spitzer, H. (1987). Temporal encoding of two-dimensional patterns by single units in primate inferior temporal cortex. I. Response characteristics. J Neurophysiol *57*, 132-146.

Rieke, F, Bodnar, DA, Bialek, W (1995) Naturalistic stimuli increase the rate and efficiency of information transmission by primary auditory afferents. Proc Biol Sci, 262:259–265.

Rieke, F., Warland, D., Bialek, W., and de Ruyter van Steveninck, R. (1997). Spikes : Exploring the Neural Code (Cambridge, Mass. ; London: MIT Press).

Ritzmann, R. E., and Camhi, J. M. (1978). Excitation of Leg motor neurons by giant interneurons in the cockroach *Periplaneta americana*. J Comp Physiol [A] *125*, 305-316.

Ritzmann, R. E., and Pollack, A. J. (1986). Identification of thoracic interneurons that mediate giant interneuron-to-motor pathways in the cockroach. J Comp Physiol [A] *159*, 639-654.

Ritzmann, R. E., and Pollack, A. J. (1988). Wind-activated thoracic interneurons of the cockroach: II. Patterns of connection from ventral giant interneurons. J Neurobiol *19*, 589-611.

Ritzmann, R. E., and Pollack, A. J. (1990). Parallel motor pathways from thoracic interneurons of the ventral giant interneuron system of the cockroach, Periplaneta americana. J Neurobiol *21*, 1219-1235.

Ritzmann, R. E., and Pollack, A. J. (1994). Responses of thoracic interneurons to tactile stimulation in cockroach, Periplaneta americana. J Neurobiol *25*, 1113-1128.

Ritzmann, R. E., Pollack, A. J., Hudson, S. E., and Hyvonen, A. (1991). Convergence of multi-modal sensory signals at thoracic interneurons of the escape system of the cockroach, Periplaneta americana. Brain Res

563, 175-183.

Ritzmann, R. E., Pollack, A. J., and Tobias, M. L. (1982). Flight activity mediated by intracellular stimulation of dorsal giant interneurons of the cockroach *Periplaneta americana*. J Comp Physiol [A] *147*, 313-322.

Ritzmann, R. E., Tobias, M. L., and Fourtner, C. R. (1980). Flight Activity Initiated Via Giant Interneurons of the Cockroach: Evidence for Bifunctional Trigger Interneurons. Science *210*, 443-445.

Robert, D., Amoroso, J., and Hoy, R. R. (1992). The evolutionary convergence of hearing in a parasitoid fly and its cricket host. Science *258*, 1135-1137.

Roddey, J. C., Girish, B., and Miller, J. P. (2000). Assessing the performance of neural encoding models in the presence of noise. J Comput Neurosci *8*, 95-112.

Roddey, J. C., and Jacobs, G. A. (1996). Information theoretic analysis of dynamical encoding by filiform mechanoreceptors in the cricket cercal system. J Neurophysiol *75*, 1365-1376.

Roeder, K. D. (1948). Organization of the ascending giant fiber system in the cockroach (*Periplaneta americana*). Journal of Experimental Zoology *108*, 243-261.

Rovner, J. S. (1980). Morphological and ethological adaptations for prey capture in wolf spiders (Araneae, Lycosidae). J. Arachnol *8*, 201-215.

Sakaguchi, D. S., and Murphey, R. K. (1983). The equilibrium detecting system of the cricket: Physiology and morphology of an identified interneuron. J Comp Physiol [A] *150*, 141-152.

Salinas, E., and Abbott, L. F. (1994). Vector reconstruction from firing rates. J Comput Neurosci *1*, 89-107.

Schaefer, P. L., and Ritzmann, R. E. (2001). Descending influences on escape behavior and motor pattern in the cockroach. J Neurobiol *49*, 9-28.

Schildberger, K. (1984a). Multimodal interneurons in the cricket brain: properties of identified extrinsic mushroom body cells. J Comp Physiol [A] *154*, 71-79.

Schildberger, K. (1984b). Temporal selectivity of identified auditory neurons in the cricket brain. J Comp Physiol [A] *155*, 171-185.

Schildberger, K., Huber, F., and Wohlers, D. W. (1989). Central Auditory Pathway: Neuronal Correlates of Phonotactic Behavior. In Cricket behavior and neurobiology, Huber, F., T. E. Moore, and W. Loher, eds. (Ithaca, N.Y.: Cornell University Press), pp. 423-458.

Schneidman, E., Slonim, N., Tishby, N., deRuyter, v. S., R, and Bialek, W. (2001). Analyzing neural codes using the information bottleneck method. Advances in Neural Information Processing Systems, NIPS

Schrader, S. (2000). The function of the cercal sensory system in escape behavior of the cave cricket Troglophilus neglectus Krauss. Pflugers Arch *439*, R187-9.

Schwartz, O., Pillow, J., W., Rust, N., C., and Simoncelli, E., P. (2006). Spike-triggered neural characterization. Journal of Vision J. Vis. *6*, 484-507.

Seabrook, W. D. (1970). The structure of the terminal ganglionic mass of the locust, *Schistocera gregaria* (Forskal). J Comp Neurol *138*, 63-85.

Shadlen, M. N., and Newsome, W. T. (1994). Noise, neural codes and cortical organization. Curr Opin Neurobiol *4*, 569-579.

Shannon, C. E. (1948). A mathematical theory of communication Bell Syst. Tech. J *27*, 379-423.

Sharpee, T., Rust, N. C., and Bialek, W. (2004). Analyzing neural responses to natural signals: maximally informative dimensions. Neural Comput *16*, 223-250.

Shen, J. X. (1983). The cercus-to-giant interneuron system in the bushcricket *Tettigonia cantans*: Morphology and response to low-frequency sound. J Comp Physiol [A] *151*, 449-459.

Shimozawa, T., and Kanou, M. (1984a). The aerodynamics and sensory physiology of range fractionation in the cercal filiform sensilla of the cricket *Gryllus bimaculatus*. J Comp Physiol [A] *155*, 495-505.

Shimozawa, T., and Kanou, M. (1984b). Varieties of filiform hairs: range fractionation by sensory afferents and cercal interneurons of a cricket. J Comp Physiol [A] *155*, 485-493.

Shlens, J., Kennel, M., B., Abarbanel, H., D. I., and Chichilnisky, E., J. (2007). Estimating Information Rates with Confidence Intervals in Neural Spike Trains. Neural Computation Neural Computation *19*, 1683-1719.

Simoncelli, E. P., Paninski, L., Pillow, J. W., and Schwartz, O. (2004). Characterization of Neural Responses with Stochastic Stimuli. In The Cognitive Neurosciences III, Gazzaniga, M. S., ed. (Center for Neural Science and Courant Institute of mathematical Sciences, New York University, New York, NY, 10003 The Salk Institute for Biological Studies, La Jolla, CA, 92037 Cambridge, MA: MIT Press), pp. 327-338.

Slonim, N., Friedman, N., and Tishby, N. (2002). Agglomerative multivariate information bottleneck. Advances in Neural Information Processing Systems *14*, 929-936.

Slonim, N., and Tishby, N. (2000). Agglomerative information bottleneck. Advances in Neural Information Processing Systems *12*, 617-623.

Staudacher, E. M. (2001). Sensory responses of descending brain neurons in the walking cricket, Gryllus bimaculatus. J Comp Physiol [A] *187*, 1-17.

Steiner, A. L. (1968). Behavioral interactions between *Liris nigra* van der linden (Hymenoptera: Sphecidae) and *Gryllus domesticus* L (Orthoptera: Gryllidae). Psyche *75*, 256-273.

Stout, J. F., DeHaan, C. H., and McGhee, R. W. (1983). Attractiveness of the male *Acheta domesticus* calling song to females I. Dependence on each of the calling song features. J Comp Physiol [A] *153*, 509-521.

Strong, S. P., Koberle, R., de Ruyter van Steveninck, R. R., and Bialek, W. (1998). Entropy and Information in Neural Spike Trains. Phys Rev Lett *80*, 197-200.

Tauber, E., and Camhi, J. (1995). The wind-evoked escape behavior of the cricket Gryllus bimaculatus: integration of behavioral elements. J Exp Biol *198*, 1895-1907.

Tautz, J., and Markl, H. (1978). Caterpillars detect flying wasps by hairs sensitive to airborne vibration. Behavioral Ecology and Sociobiology *4*, 101-110.

Theunissen, F., and Miller, J. P. (1995). Temporal encoding in nervous systems: a rigorous definition. J Comput Neurosci *2*, 149-162.

Theunissen, F. E., and Miller, J. P. (1991). Representation of sensory information in the cricket cercal sensory system. II. Information theoretic calculation of system accuracy and optimal tuning-curve widths of four primary interneurons. J Neurophysiol *66*, 1690-1703.

Theunissen, F. E., Roddey, J. C., Stufflebeam, S., Clague, H., and Miller, J. P. (1996). Information theoretic analysis of dynamical encoding by four identified primary sensory interneurons in the cricket cercal system. J Neurophysiol *75*, 1345-1364.

Theunissen, F. E., David, S. V., Singh, N. C., Hsu, A., Vinje, W. E., and Gallant, J. L. (2001). Estimating spatio-temporal receptive fields of auditory and visual neurons from their responses to natural stimuli. Network *12*, 289-316.

Thorson, J., Weber, T., and Huber, F. (1982). Auditory behavior of the cricket II: Simplicity of calling-song recognition in *Gryllus*, and anomalous phonotaxis at abnormal carrier frequencies. J Comp Physiol [A] *146*, 361-378.

Tishby, N., Pereira, F., and Bialek, W. (1999). The information bottleneck method. The 37th annual Allerton Conference on Communication, Control, and Computing

Tobias, M., and Murphey, R. K. (1979). The response of cercal receptors and identified interneurons in the cricket (*Acheta domesticus*) to airstreams. J Comp Physiol [A] *129*, 51-59.

Tokareva, V. S., and Rozhkova, G. I. (1973). Responses of the last abdominal ganglion units to air puffs and sounds of various directions in the cricket Gryllus domesticus. Zh. Evol. Biokhim. Fiziol *9*, 183-188.

Uzzell, V. J., and Chichilnisky, E. J. (2004). Precision of spike trains in primate retinal ganglion cells. J Neurophysiol *92*, 780-789.

van Rossum, M. C. (2001). A novel spike distance. Neural Comput *13*, 751-763.

Vedenina, V. Y., Rozhkova, G. I., Panjutin, A. K., Byzov, A. L., and Kämper, G. (1998). Frequency-intensity characteristics of cricket cercal interneurons: low-frequency-sensitive units. J Comp Physiol [A] *183*, 553-561.

Victor, J. D., and Purpura, K. P. (1996). Nature and precision of temporal coding in visual cortex: a metric-space analysis. J Neurophysiol *76*, 1310-1326.

Victor, J. D. (2002). Binless strategies for estimation of information from neural data. Phys Rev E Stat Nonlin Soft Matter Phys *66*, 051903.

Walker, T. J. (1964). Experimental Demonstration of a Cat Locating Orthopteran

Prey by the Prey's Calling Song. The Florida Entomologist *47*, 163-165.

Walker, T. J., and Masaki, S. (1989). Natural History. In Cricket behavior and neurobiology, Huber, F., T. E. Moore, and W. Loher, eds. (Ithaca, N.Y.: Cornell University Press), pp. 1-42.

Warland, D., Landolfa, M. A., Miller, J. P., and Bialek, W. (1991). Reading between the spikes in the cercal filiform hair receptors of the cricket. In Analysis and Modeling of Neural Systems, F, E., and B. J, eds. (Norwell, MA: Kluwer Academic Publishers), pp. 327-333.

Warland, D. K., Reinagel, P., and Meister, M. (1997). Decoding visual information from a population of retinal ganglion cells. J Neurophysiol *78*, 2336-2350.

Weber, T., and Thorson, J. (1989). Phonotactic Behavior of Walking Crickets. In Cricket behavior and neurobiology, Huber, F., T. E. Moore, and W. Loher, eds. (Ithaca, N.Y.: Cornell University Press), pp. 310-339.

Weber, T., Thorson, J., and Huber, F. (1981). Auditory behavior of the cricket I: Dynamic of compensated walking and discrimination paradigms on the Kramer treadmill. J Comp Physiol [A] *141*, 215-232.

Westin, J. (1979). Responses to wind recorded from the cercal nerve of the cockroach *Periplaneta americana.* I. Response properties of single sensory neurons. J Comp Physiol [A] *133*, 97-102.

Westin, J., Langberg, J. J., and Camhi, J. M. (1977). Responses of giant interneurons of the cockroach *Periplaneta americana* to wind puffs of different directions and velocities. J Comp Physiol [A] *121*, 307-324.

Westin, J., Ritzmann, R. E., and Goddard, D. J. (1988). Wind-activated thoracic interneurons of the cockroach: I. Responses to controlled wind stimulation. J Neurobiol *19*, 573-588.

Wiener, N. (1958). Nonlinear Problems in Random Theory (Cambridge, MA: MIT Press).

Yen, S. C., Baker, J., and Gray, C. M. (2007). Heterogeneity in the responses of adjacent neurons to natural stimuli in cat striate cortex. J Neurophysiol *97*, 1326-1341.

Zoccolan, D., Pinato, G., and Torre, V. (2002). Highly variable spike trains underlie reproducible sensorimotor responses in the medicinal leech. J Neurosci *22*, 10790-10800.